Optics of Marine Particles

Dariusz Stramski

Scripps Institution of Oceanography
University of California San Diego
Email: dstramski@ucsd.edu

IOCCG Summer Lecture Series
18 July - 31 July 2016, Villefranche-sur-Mer, France

What is ocean optics?

In principle it sounds straightforward, but in reality it's not...

Seawater is a highly complex medium containing a “witch's brew” of dissolved substances and suspended particles which strongly alter its optical properties.

Microscopic plankton

Because of this, ocean optics is a strongly interdisciplinary science combining physics, biology, chemistry, geology, and atmospheric sciences.

Seawater is a complex optical medium with a great variety of particle types and soluble species

- Molecular water
- Inorganic salts
- Dissolved organic matter

Suspended Particulate Matter

- Plankton microorganisms
- Organic detrital particles
- Mineral particles
- Colloidal particles
- Air bubbles

Diversity of biological and mineral particles

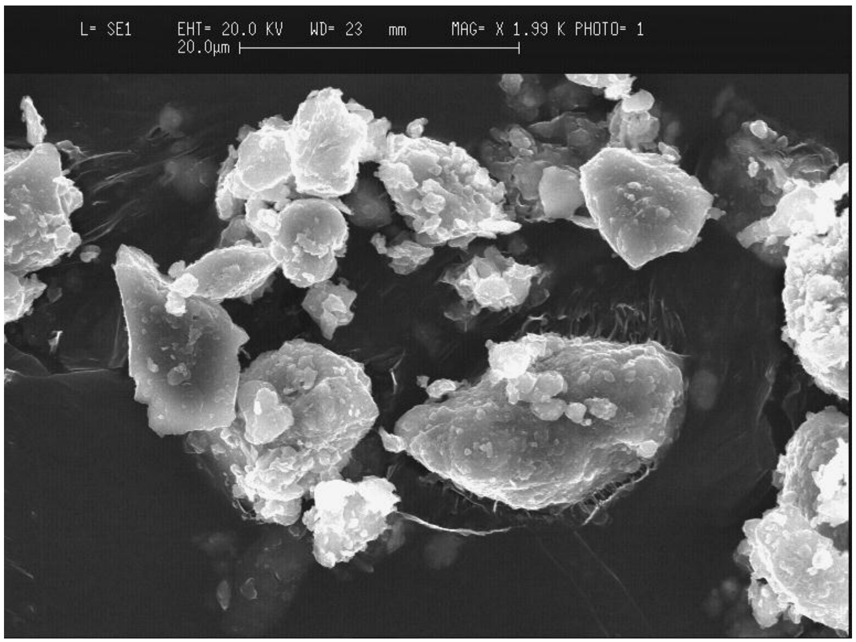

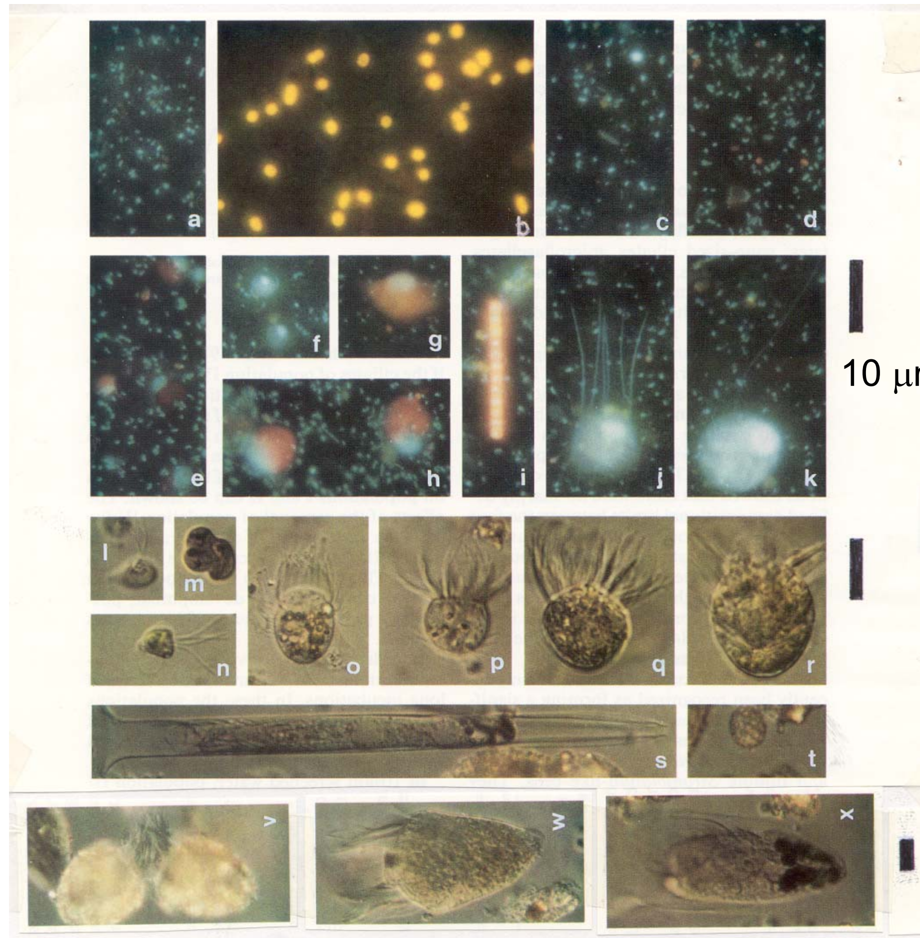

10 μm

Plankton microorganisms

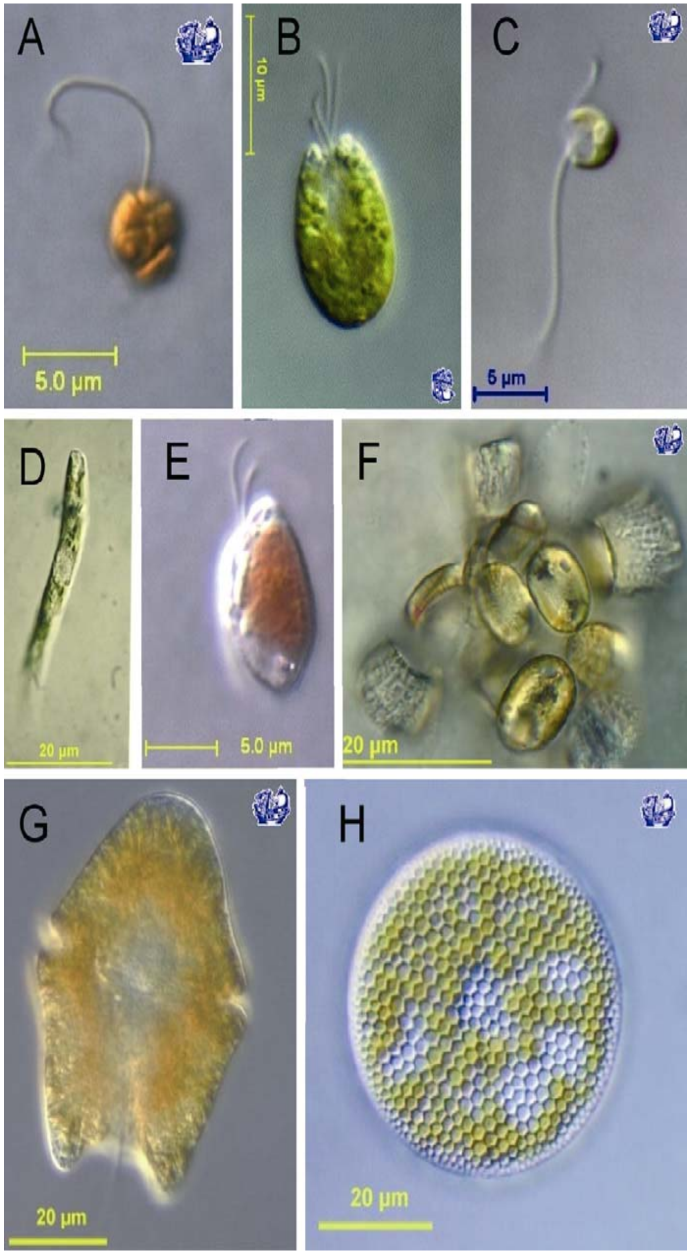

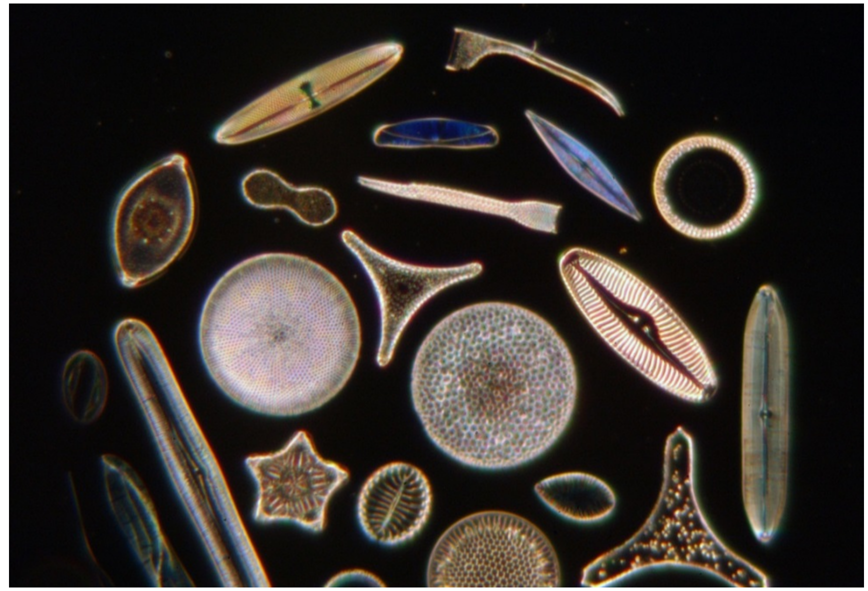

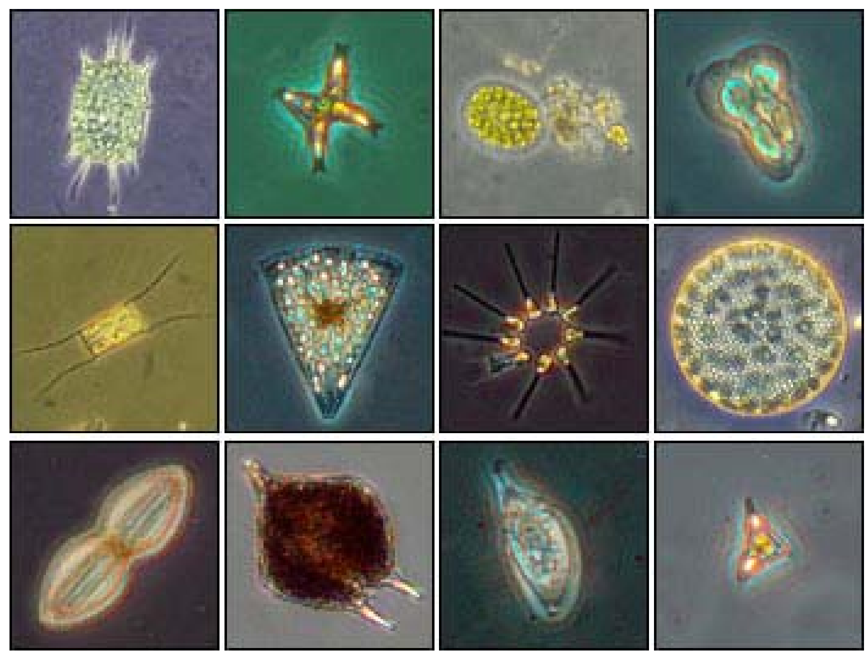

Example long-term goals

- Understand the magnitudes and variability of oceanic optical properties
- Predict ocean optical properties given the types and concentration of suspended particles (*forward problem*)
- Obtain bio-optical properties and biogeochemical information from optical in situ and remote-sensing measurements (*inverse problem*)

OCEAN COLOR

$$R_{rs}(\lambda) \equiv \frac{L_w(\lambda)_{z=0^+}}{E_d(\lambda)_{z=0^+}} \propto \frac{b_b(\lambda)}{a(\lambda)}$$

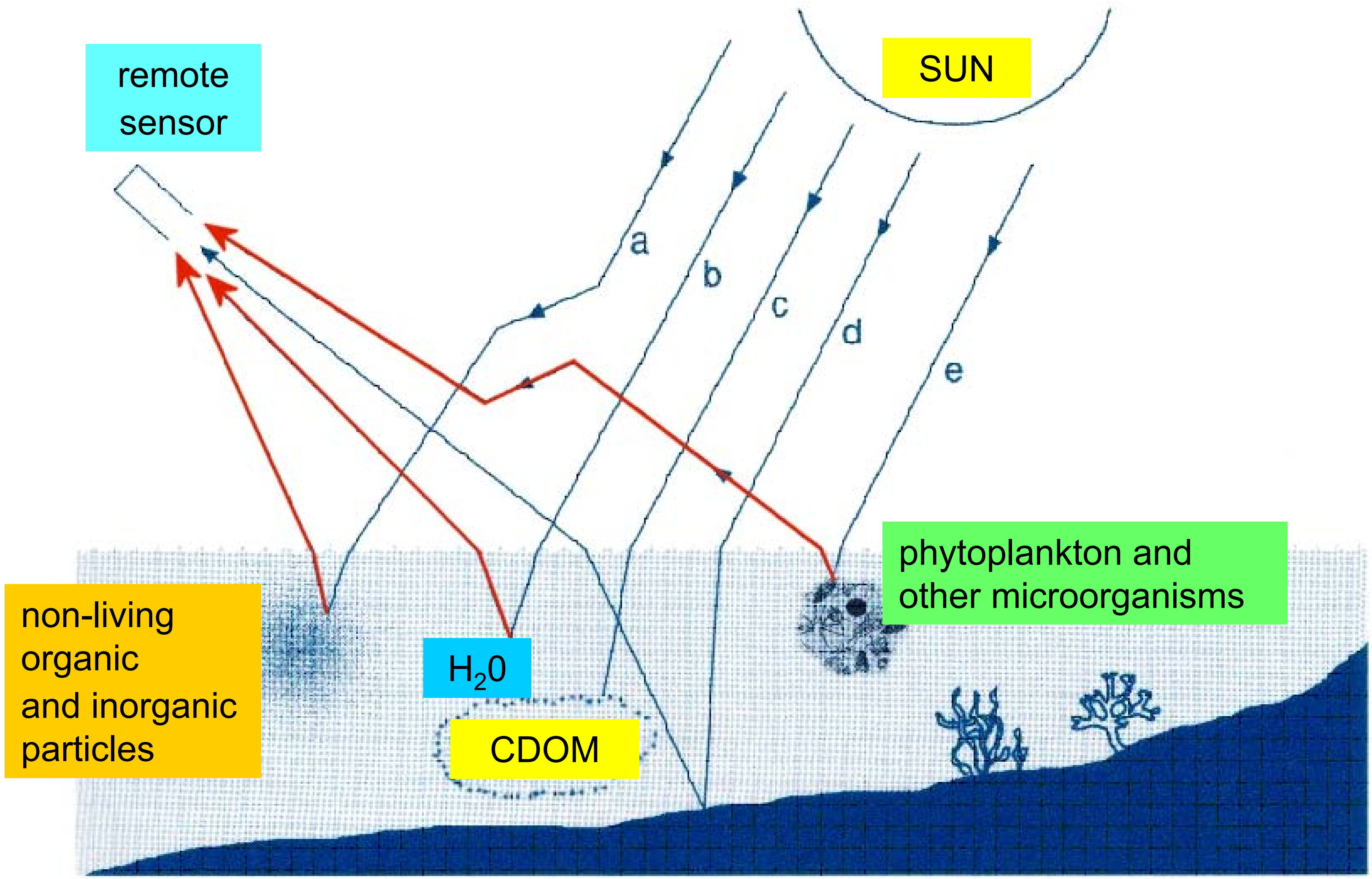

Direct problem

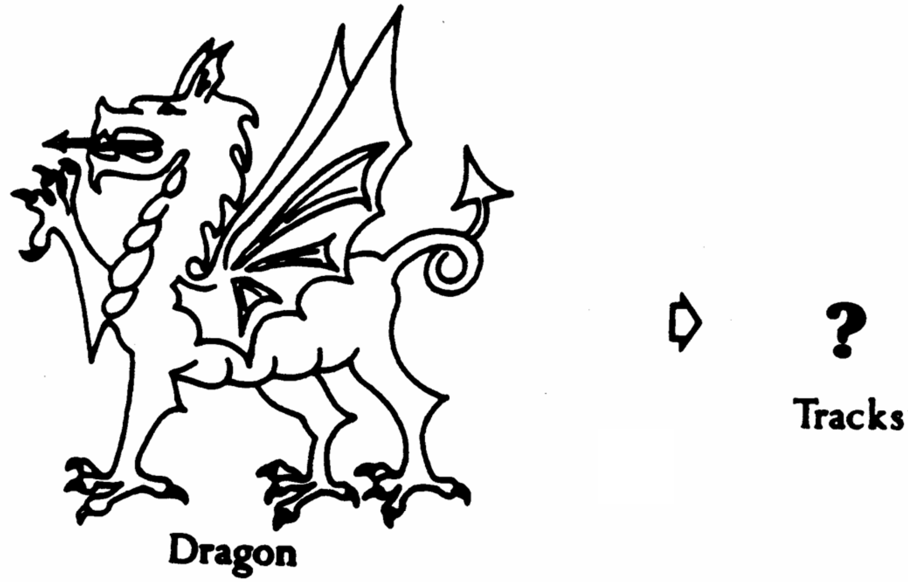

Inverse problem

(Bohren and Huffman 1983)

Absorption efficiency factor for particles

$Q_a(\lambda) = F_a(\lambda) / F_o(\lambda)$

particle in water

$$\rho' = 4\alpha n' = a_s D$$

$$\alpha = \frac{\pi \cdot D \cdot n_w}{\lambda}$$

$$n' = \frac{\lambda a_s}{4\pi n_w}$$

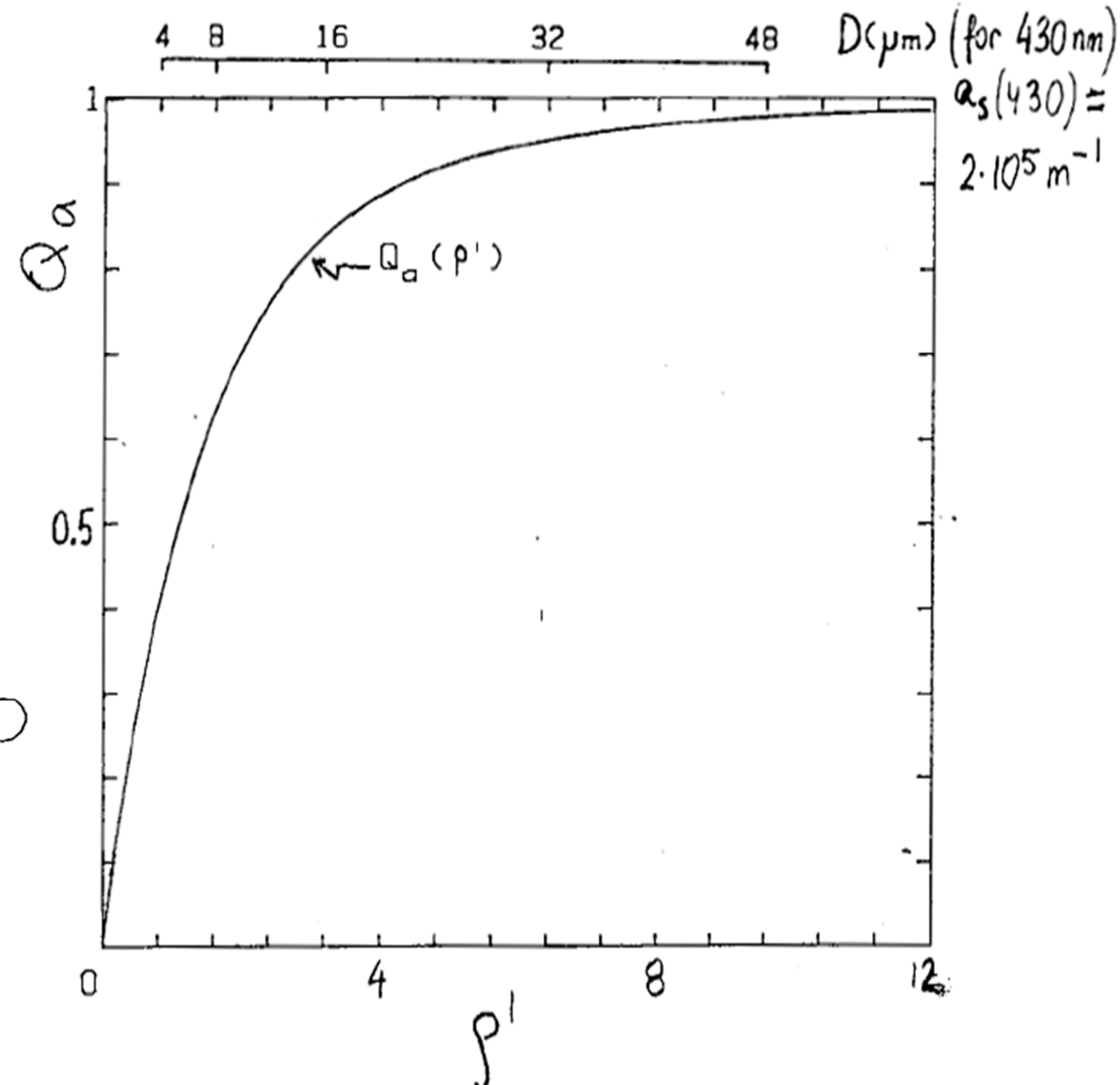

Note: Q_a, a_s, and n' are functions of λ

(Morel and Bricaud 1981)

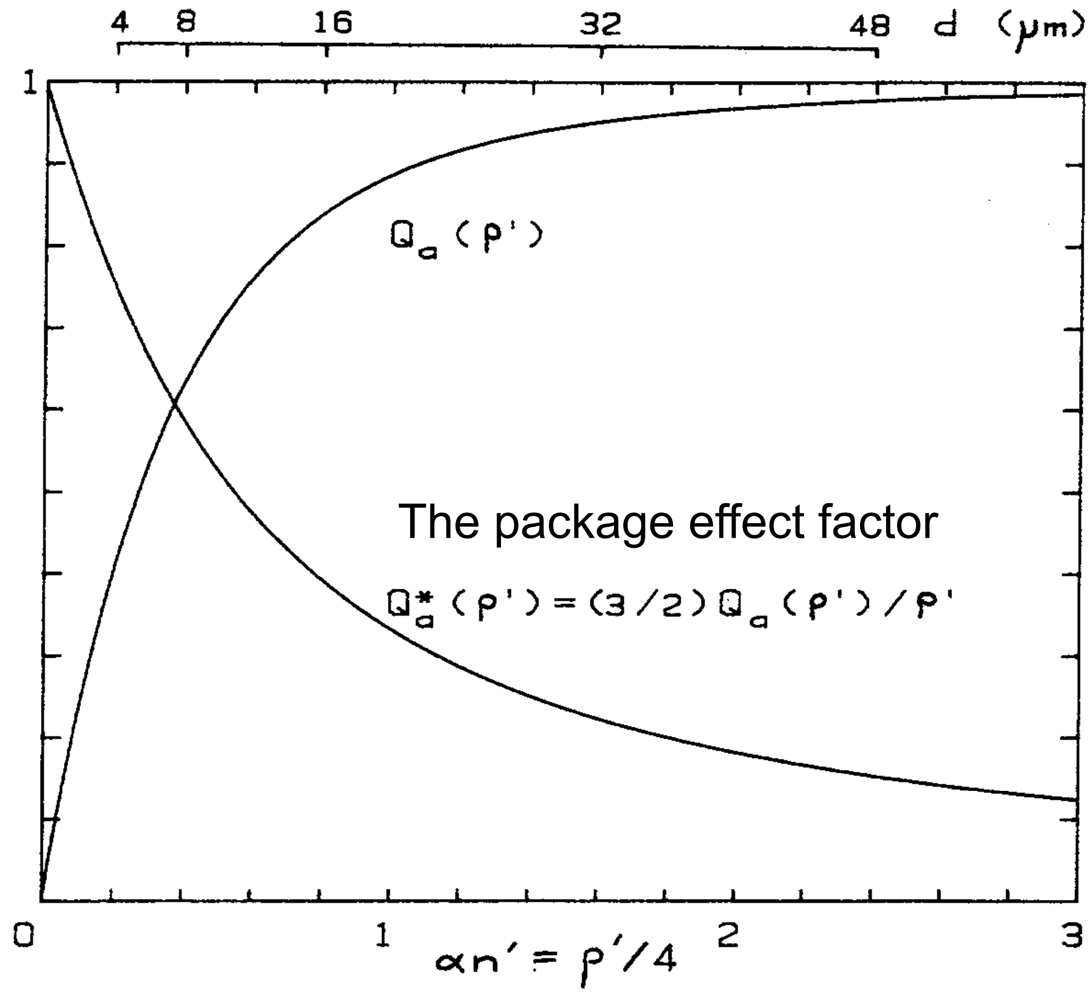

Fig. 1. Dimensionless functions Q_a and Q_a^* (equations 1 and 6) plotted vs $\alpha n'$. The corresponding scale in diameter d (μm) is obtained assuming that the absorption coefficient, a_{cm}, for the cellular material is equal to 2×10^5 m^{-1}, which is a representative mean value for many algal cells at $\lambda = 430$ nm (see text). Note that $\rho' = da_{cm} = 4\alpha n'$.

(Morel and Bricaud 1981)

Linkage between the single-particle optical properties and bulk optical properties of particle suspension

$$a = (N/V)\,Q_a\,G = (N/V)\,\sigma_a$$

a is the absorption coefficient of a collection of particles in aqueous suspension (units of m^{-1})

N/V is the number of particles per unit volume of water (units of m^{-3})

Q_a is the absorption efficiency factor (dimesionless)

G is the area of cross section of a particle (units of m^2). For spherical particles $G = (\pi/4)D^2$ where D is a diameter

σ_a (= $Q_a\,G$) is the absorption cross-section (units of m^2)

Note: a, Q_a, and σ_a are the spectral quantities (i.e., functions of light wavelength)

The package effect

$$a^* = a \,/\, Chl = a \,/\, [(Chl_{cell}/V_{cell})\ (\mathrm{N/V})V_{cell}] = a \,/\, [Chl_{\mathrm{i}}\ (\mathrm{N/V})V_{cell}]$$

For spherical particles:

$$a = (N/V)\ Q_{\mathrm{a}}\ (\pi/4)D^2 \quad \text{and} \quad V_{cell} = (\pi/6)D^3$$

$$a^* = (3/2)\ Q_{\mathrm{a}} \,/\, (Chl_{\mathrm{i}}\ D) = (3/2)\ (a_{\mathrm{s}} \,/\, Chl_i\ )\ [Q_{\mathrm{a}} \,/\, (a_{\mathrm{s}}\ D)] =$$

$$= (3/2)\ (a_{\mathrm{s}} \,/\, Chl_i\ )\ (Q_{\mathrm{a}} \,/\, \rho') = (a_{\mathrm{s}} \,/\, Chl_i\ )\ Q^*_{\mathrm{a}} = a^*_{\mathrm{sol}}\ Q^*_{\mathrm{a}}$$

where $a^*_{\mathrm{sol}} = a_{\mathrm{s}} \,/\, Chl_i$

$a^* = a^*_{\mathrm{sol}}$ if $\rho' \rightarrow 0$ and $Q^*_{\mathrm{a}} = 1$

The package effect factor:

$$Q^*_{\mathrm{a}} = a^* \,/\, a^*_{\mathrm{sol}} = (3/2)\ Q_{\mathrm{a}} \,/\, \rho' = (3/2)\ Q_{\mathrm{a}} \,/\, (a_{\mathrm{s}}\ D)$$

(Morel and Bricaud 1981)

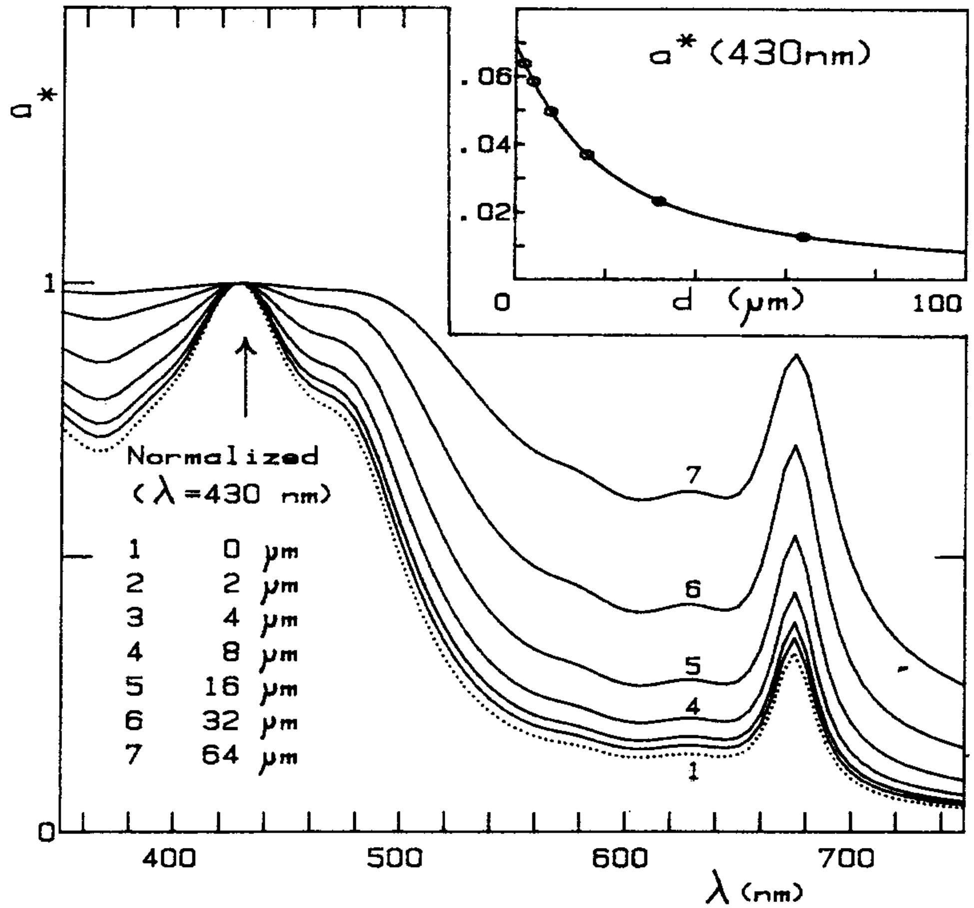

Fig. 2. Change in spectral absorption values with variable cell size (diameter, d, in μm) whereas the cell material forming the cells remains unchanged. The spectral absorption values of this material, somewhat arbitrarily adopted, are shown as the dotted curve. All curves are normalized, at $\lambda = 430$ nm, to evidence the progressive deformation. The variations with size of the specific absolute value at 430 nm ($m^2\ mg^{-1}$ Chl a) are shown in inset, under the same assumption of a constant absorption of the cell material ($a_{cm} = 2 \times 10^5\ m^{-1}$ at 430 nm) and with the additional assumption of a constant intracellular pigment concentration ($c_i = 2.86 \times 10^6$ mg Chl a m^{-3}).

(Morel and Bricaud 1981)

Solid lines: intact cells in cultures

Dotted lines: hypothetical aqueous solution of the material forming the cells

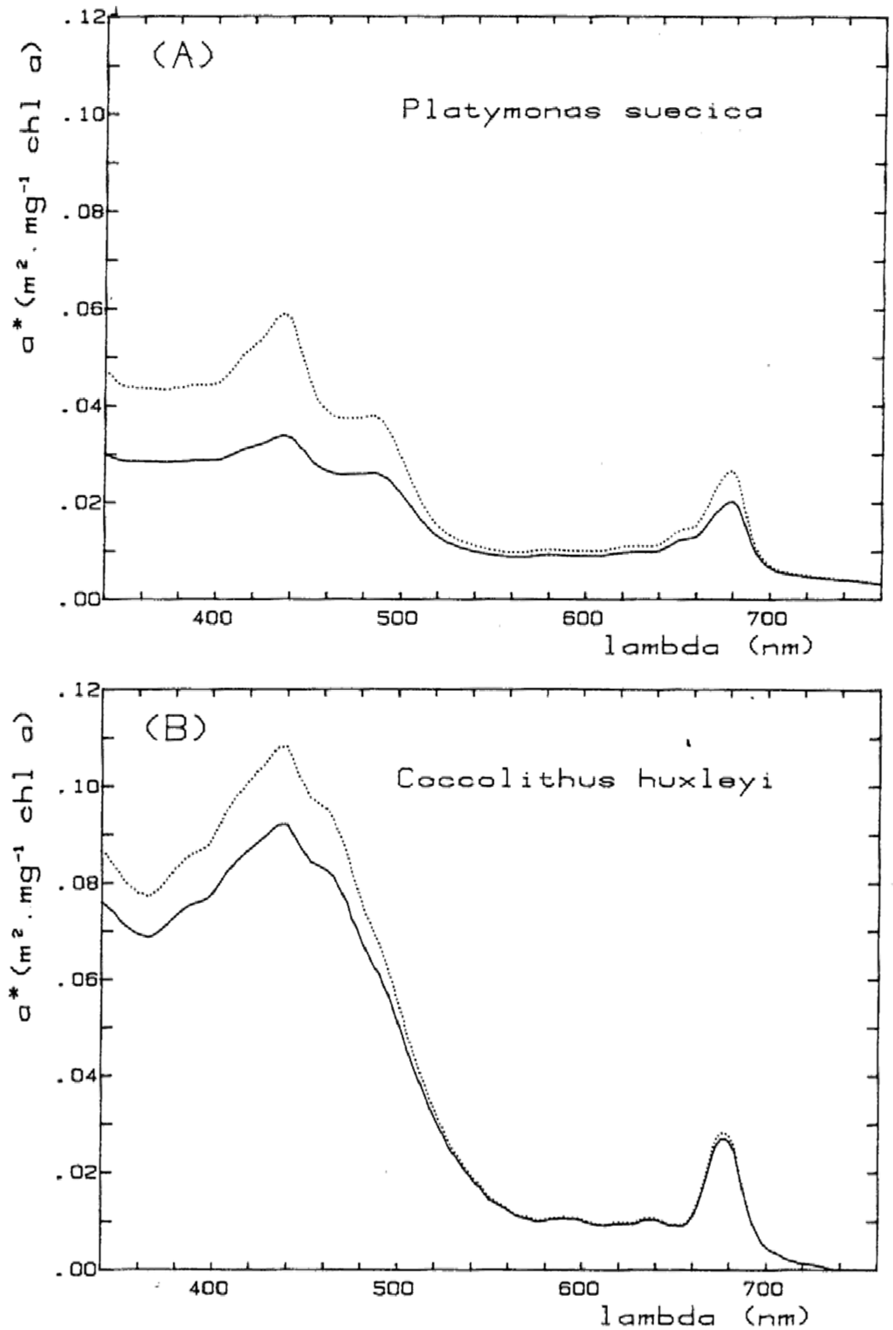

(Morel and Bricaud 1981)

Absorption efficiency for various phytoplankton and heterotrophic microorganisms

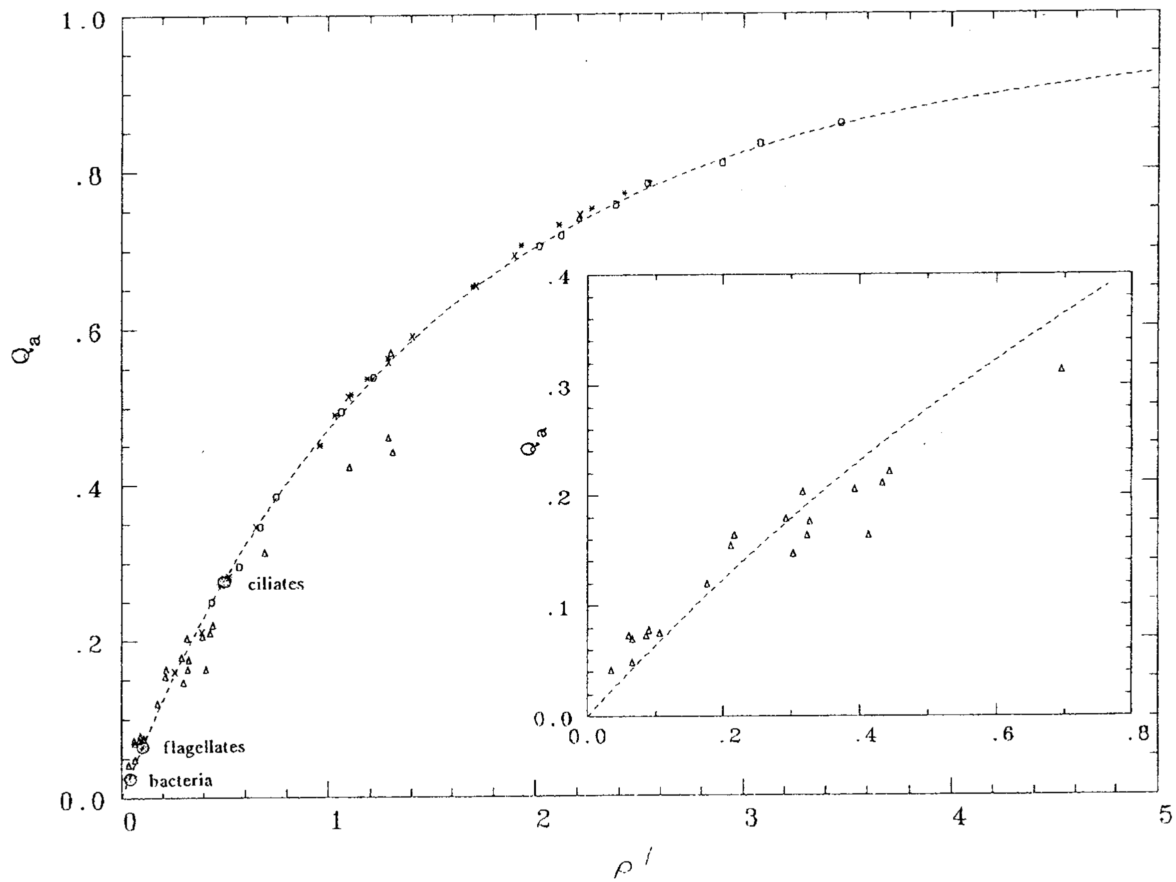

Figure 1. The theoretical variations of Q_a, the efficiency factor for absorption (dashed curves), as a function of the dimensionless parameter ρ',. The triangles are experimental determinations of Q_a (at 675 nm) for various algae (Morel and Bricaud, 1986; Ahn, 1990); other symbols are for determinations of 3 algal species studied by Sosik (1988). The values for heterotrophic organisms, as indicated, come from Morel and Ahn (1990, 1991). The inset is an enlargment of the initial part of the curve.

(Morel 1991)

Example spectra of absorption efficiency factor

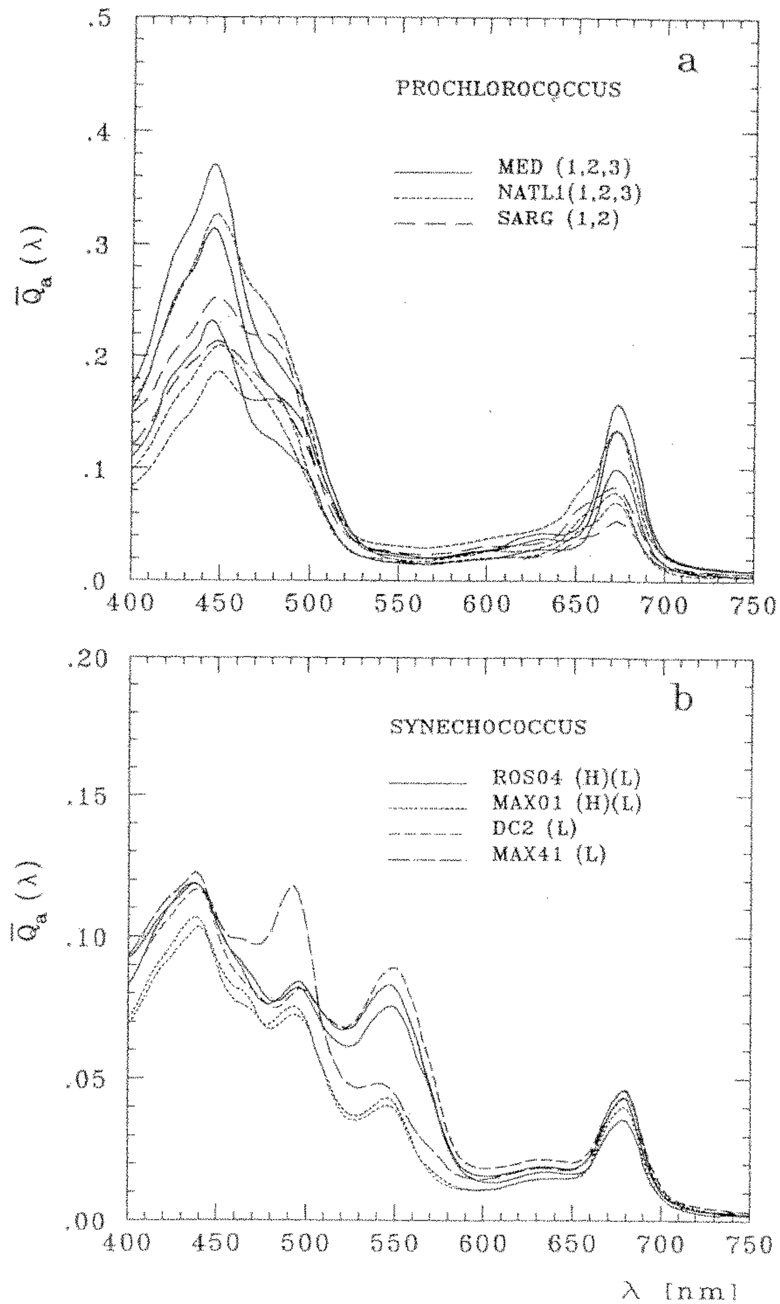

Figure 5. Spectral values of the efficiency factor for absorption for the various strains.

(Morel et al. 1993)

Geometry for defining Inherent Optical Properties

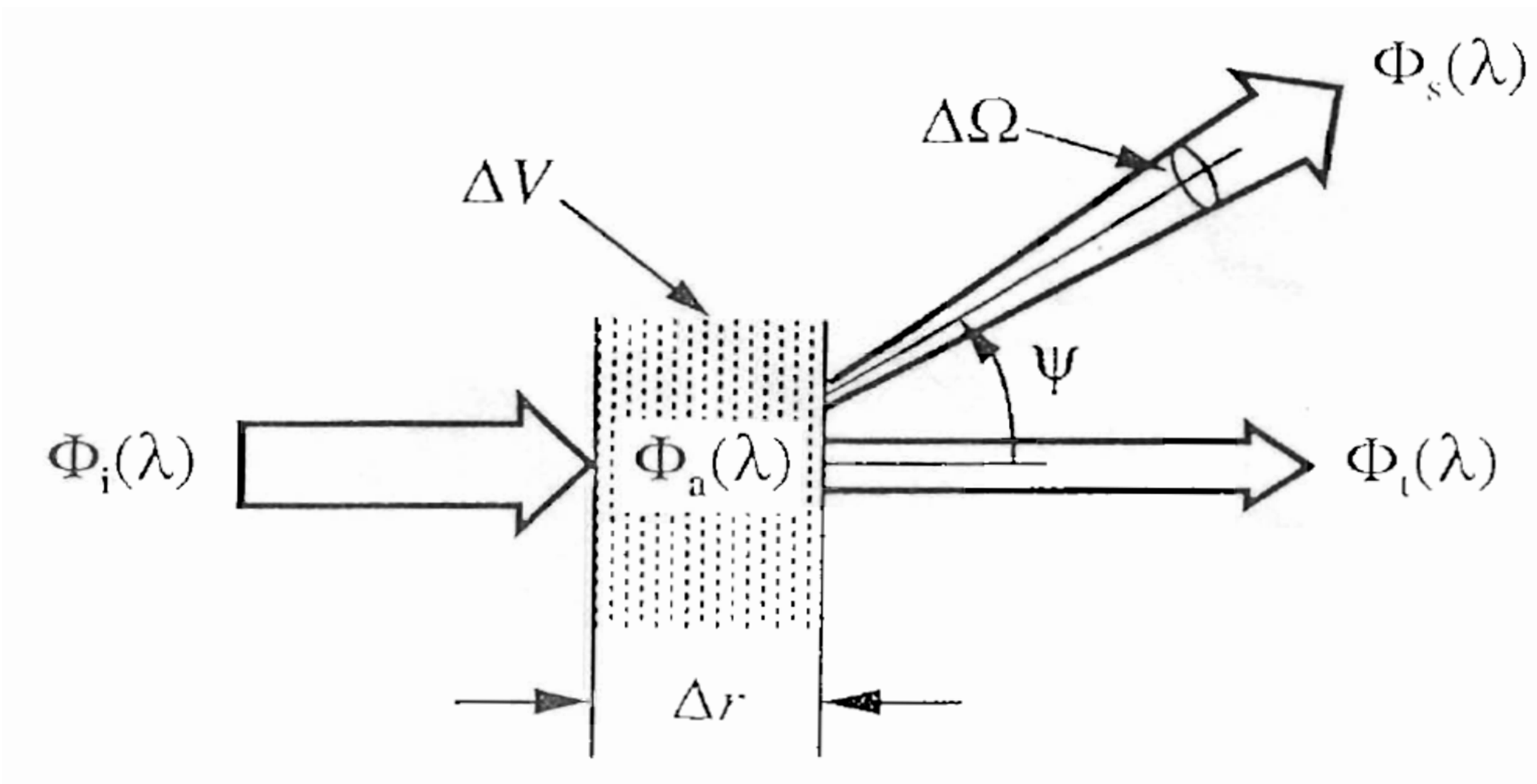

(Mobley,1994)

Measurement of particulate absorption coefficient with a spectrophotometer equipped with a center-mount integrating sphere

Very small or negligible scattering error

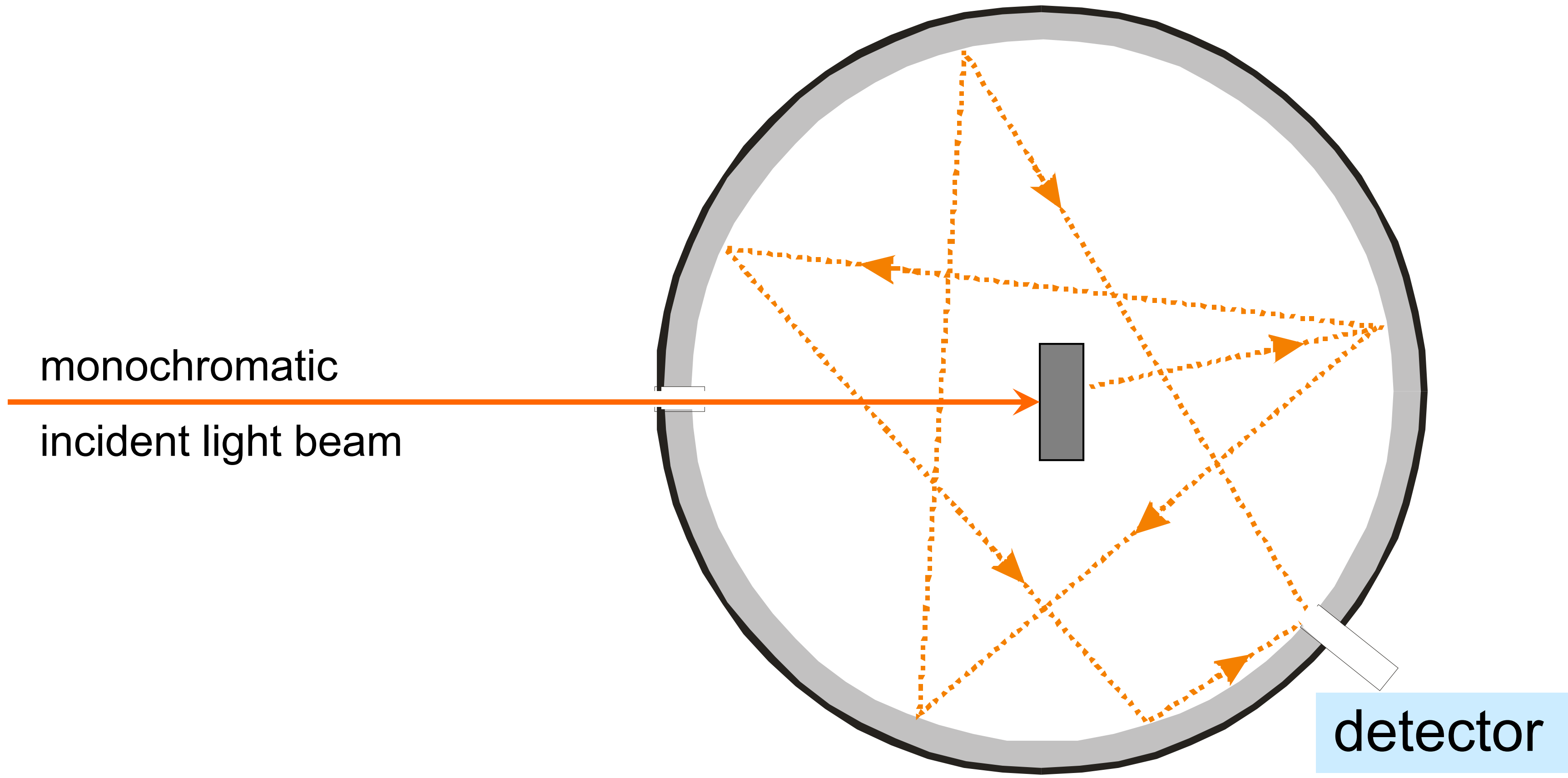

Babin and Stramski (2002)

Absorption and Scattering Spectra of $MgCO_3$ particles
Measurements inside the integrating sphere

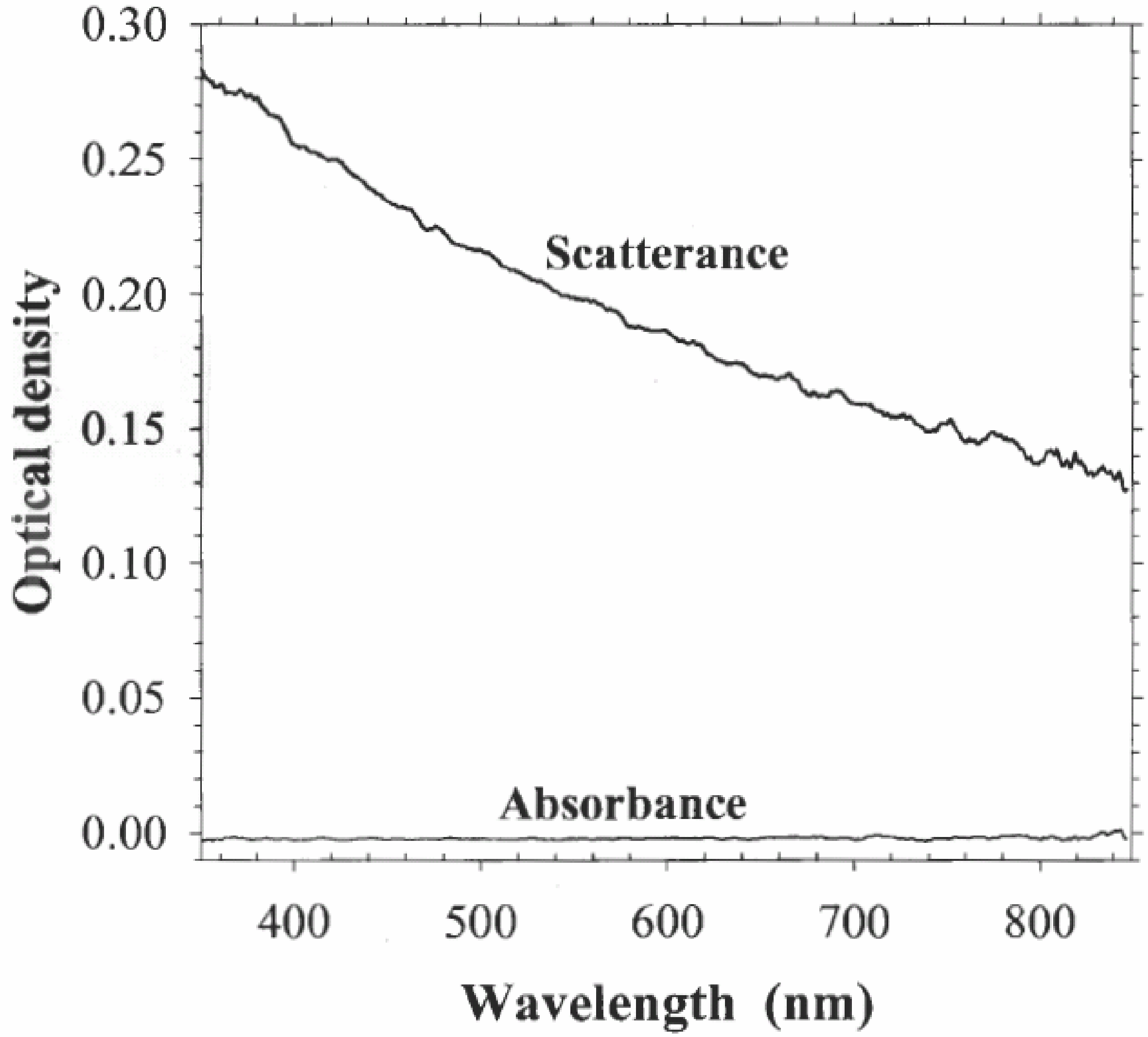

Babin and Stramski (2002)

Scattering Error for Saharan Dust Sample

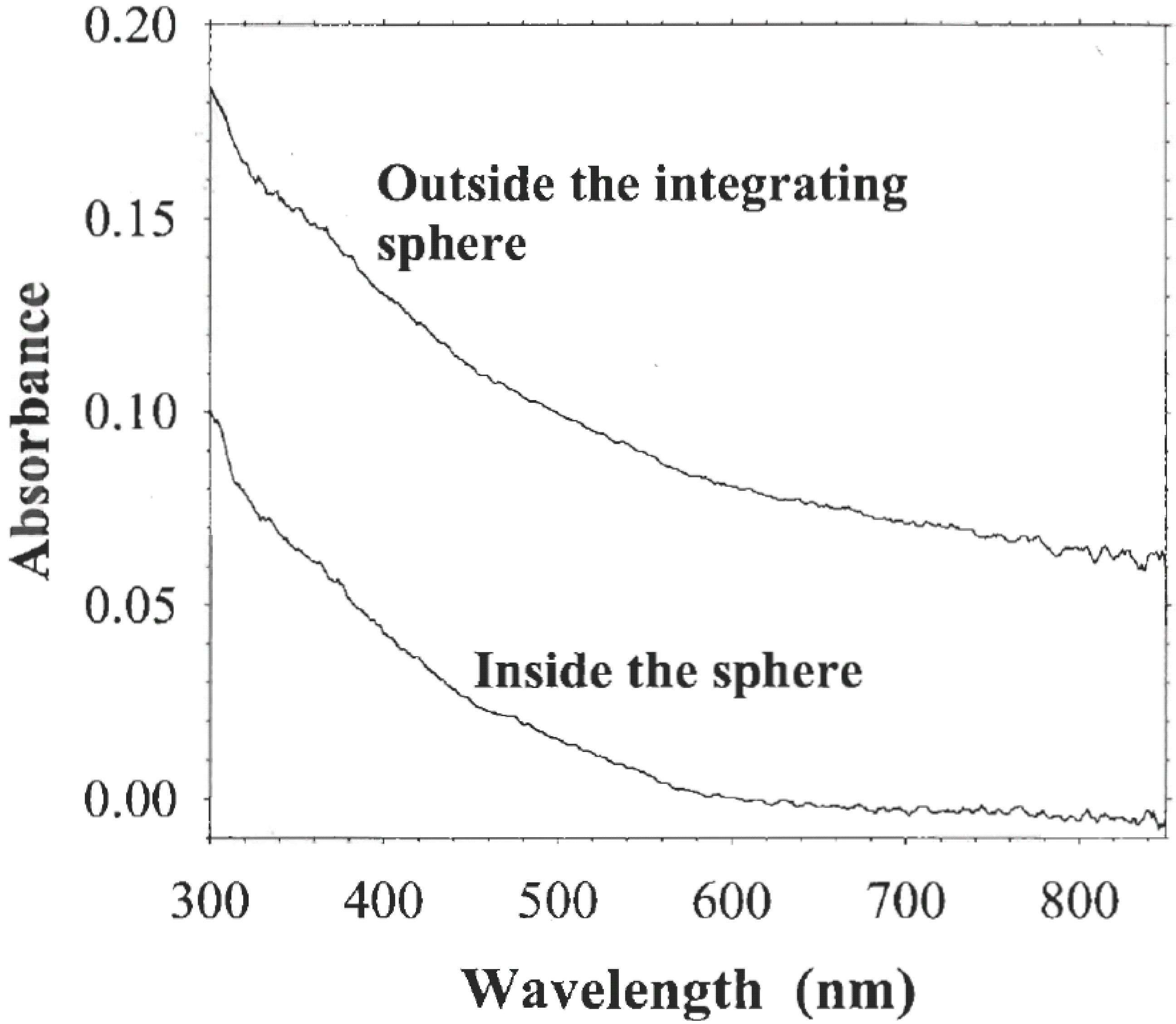

Babin and Stramski (2002)

Particle size distributions of *Prochlorococcus* and *Synechococcus*

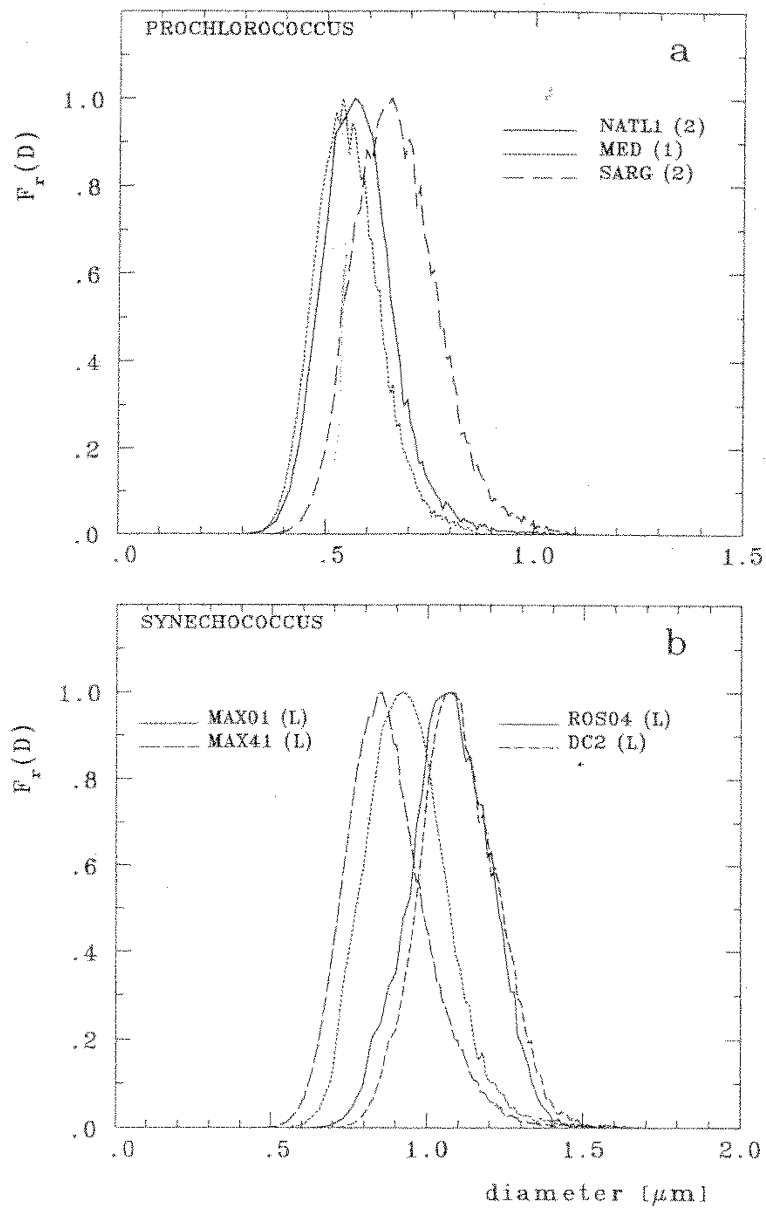

Figure 1. Relative size distribution functions (normalized to their maximum) for the various strains of *Prochlorococcus* (panel a) and *Synechococcus* (panel b), labelled as in Table 1. For clarity only one size distribution per strain is represented; the other curves, not shown, are almost identical apart from slight shifts of the maximum.

(Morel et al. 1993)

Particle size distribution

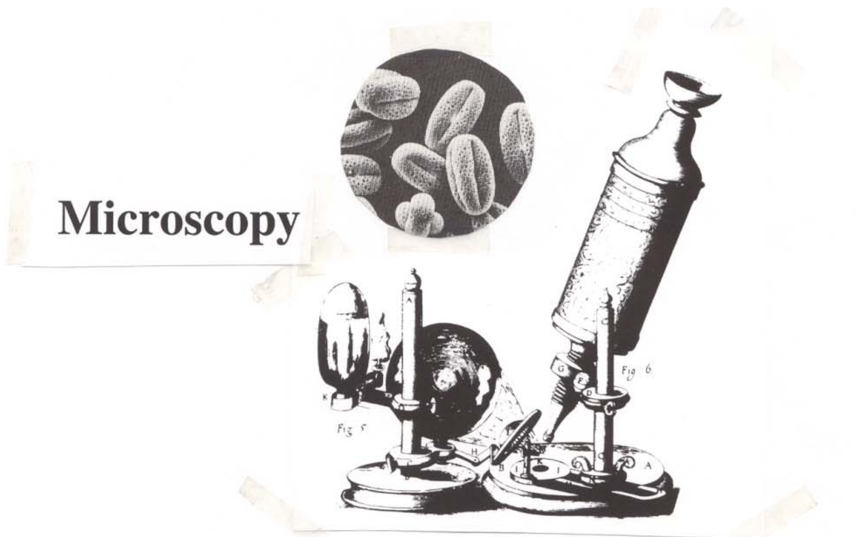

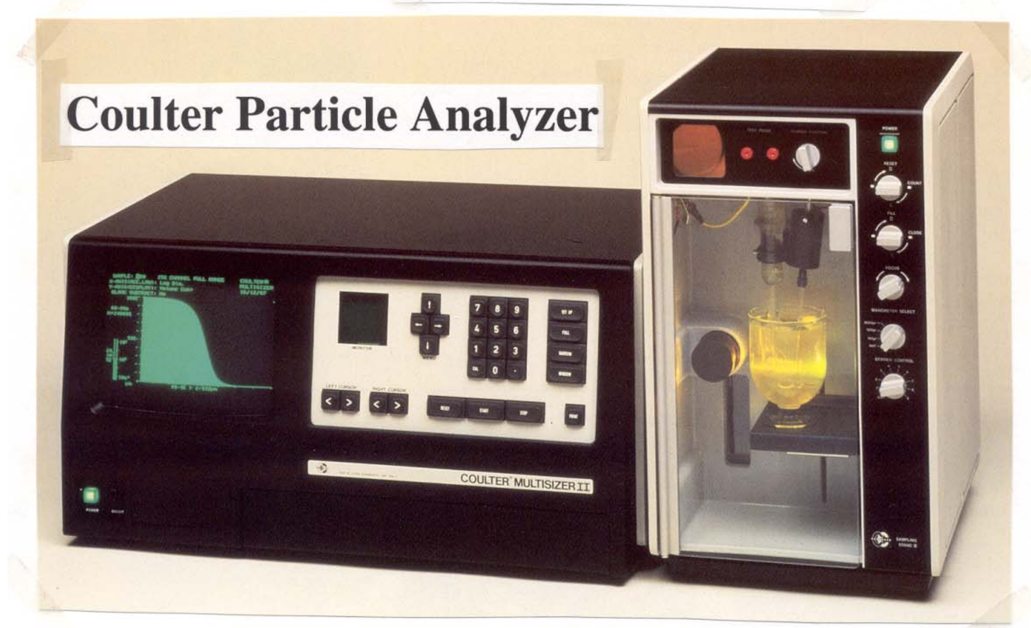

Optical method: LISST-100 Instrument

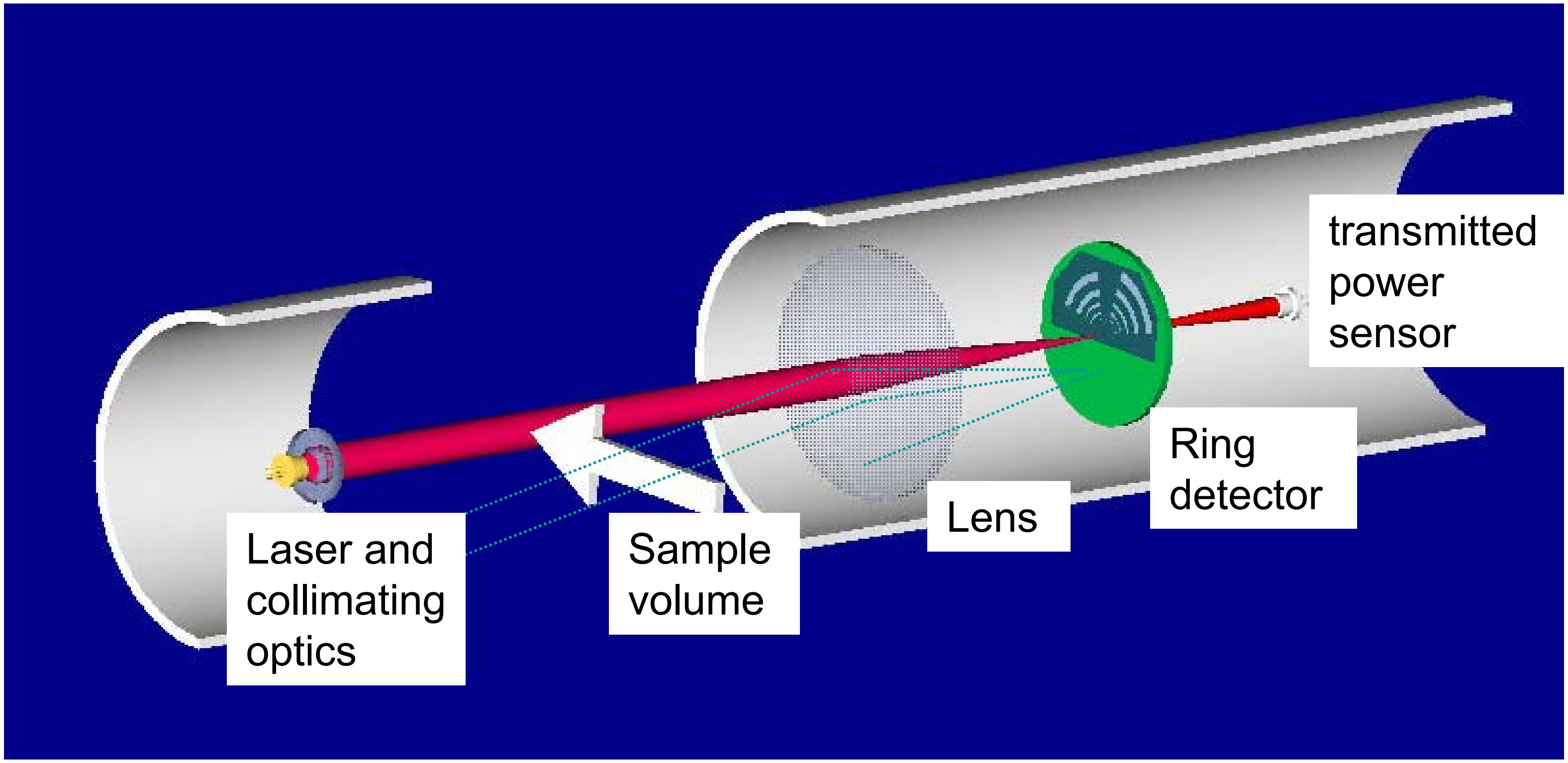

- $0.016 < \psi < 3.2^0$
- $0.1 < \psi < 20^0$

transmissometer acceptance angle: 0.007^0 or 0.036^0

(Agrawal 2005)

Optical efficiency factors versus phase shift parameter

phase shift parameter $\rho = 2\,\alpha\,(n-1)$

$Q_a = F_a/F_o$ $\qquad$ $Q_b = F_b/F_o$ $\qquad$ $Q_c = F_c/F_o$ $\qquad$ $Q_c = Q_a + Q_b$

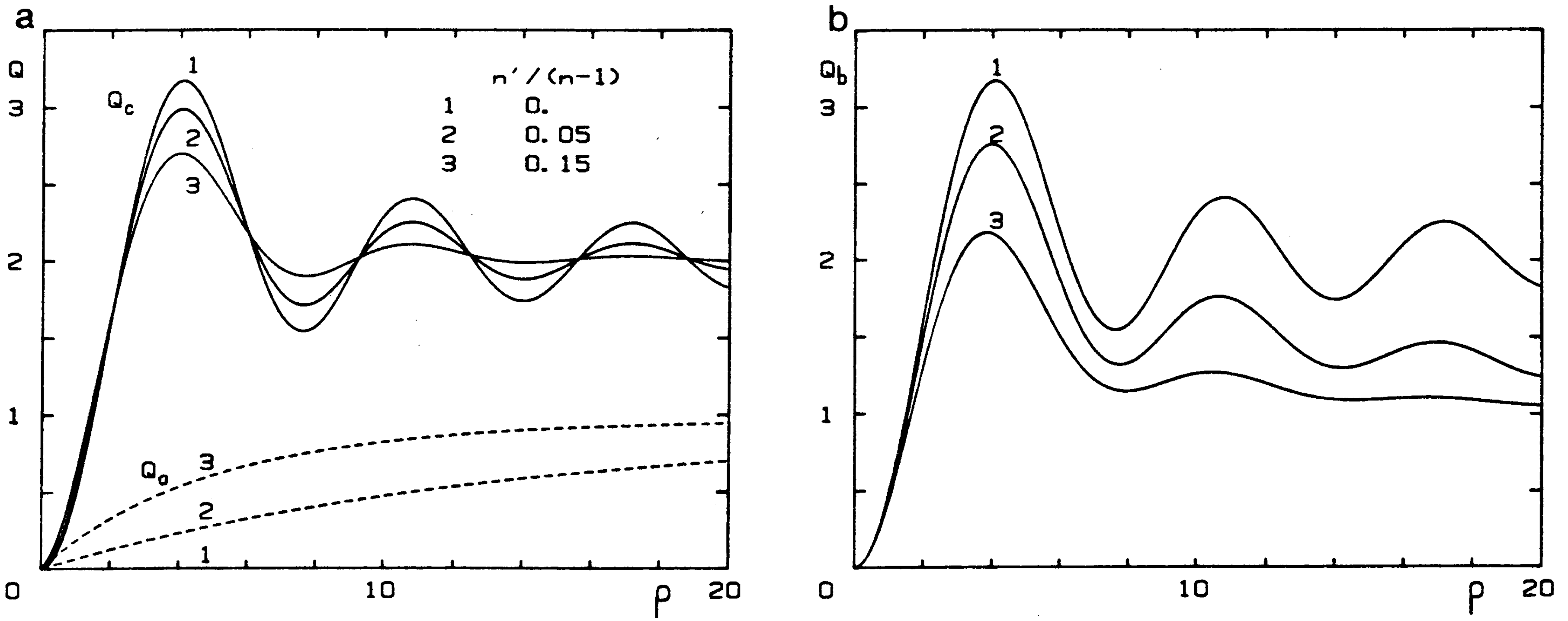

FIG. 3. Variations of the efficiency factors for attenuation, Q_c, *for absorption*, Q_a (a), and for scattering, Q_b (b) vs. the parameter $\rho = 2\,\alpha(n-1)$, for increasing values of the ratio $n'/(n-1)$ where n and n' are the real and imaginary parts of the relative refractive index of the particles.

(Morel and Bricaud 1986)

Scattering by a single particle: Phase shift parameter

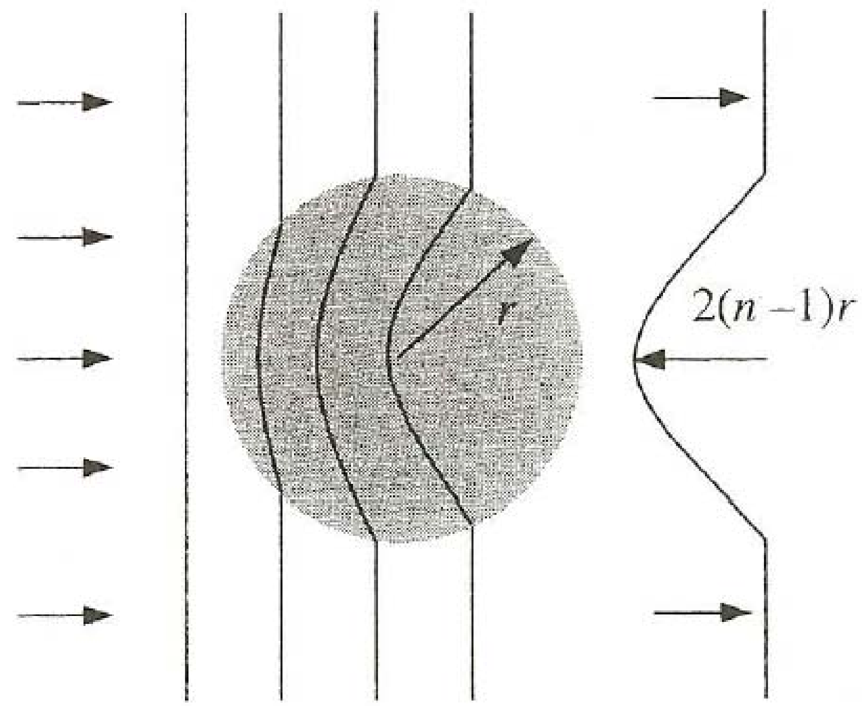

Figure 3.5. Phase fronts of a light wave traveling through a sphere of radius r. The wave slows down while traveling through the particle. The accumulated phase difference is proportional to the total distance traveled through the particle and is a function of the point of entry. The phase difference between the light passing through the center of the sphere and the light passing outside the sphere is $2(n-1)r$.

(Jonasz and Fournier 2007)

The effect of polydispersion on attenuation efficiency

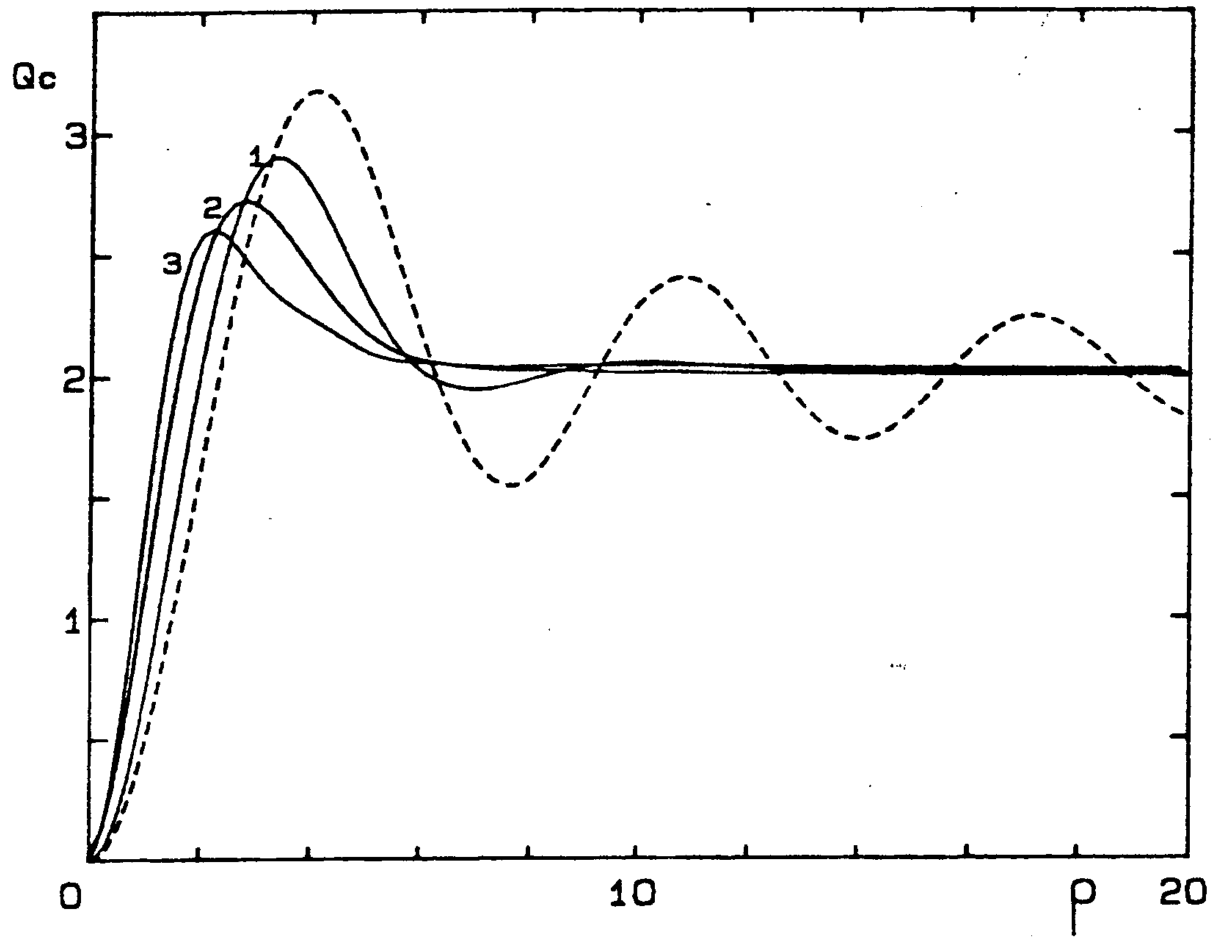

FIG. 4. Mean efficiency factor for attenuation Q_c of a "mean" particle representative of a polydispersed population, plotted as a function of ϱ_m, *the* ϱ value which corresponds to the maximum of the size distribution function $F(\varrho)$ (see Equation 17). The index of refraction is real (no absorption) and the curves 1 and 3 correspond to log-normal distributions such as $F(\varrho_M/2) = F(2\varrho_M)$ = respectively 0.01, 0.1, 0.3 $F(\varrho_M)$. The dashed curve, redrawn from Fig. 3 for $n' = 0$, represents the limiting case of a population of monosized particles.

(Morel and Bricaud 1986)

Scattering and backscattering efficiencies versus particle size

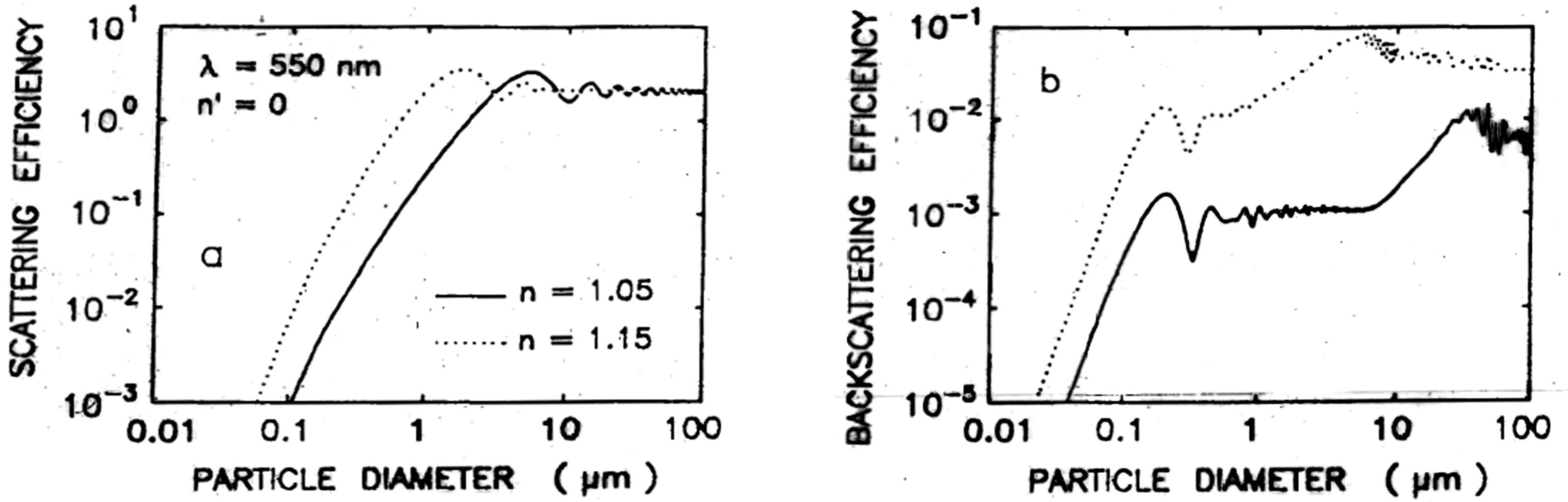

(Stramski and Kiefer 1991)

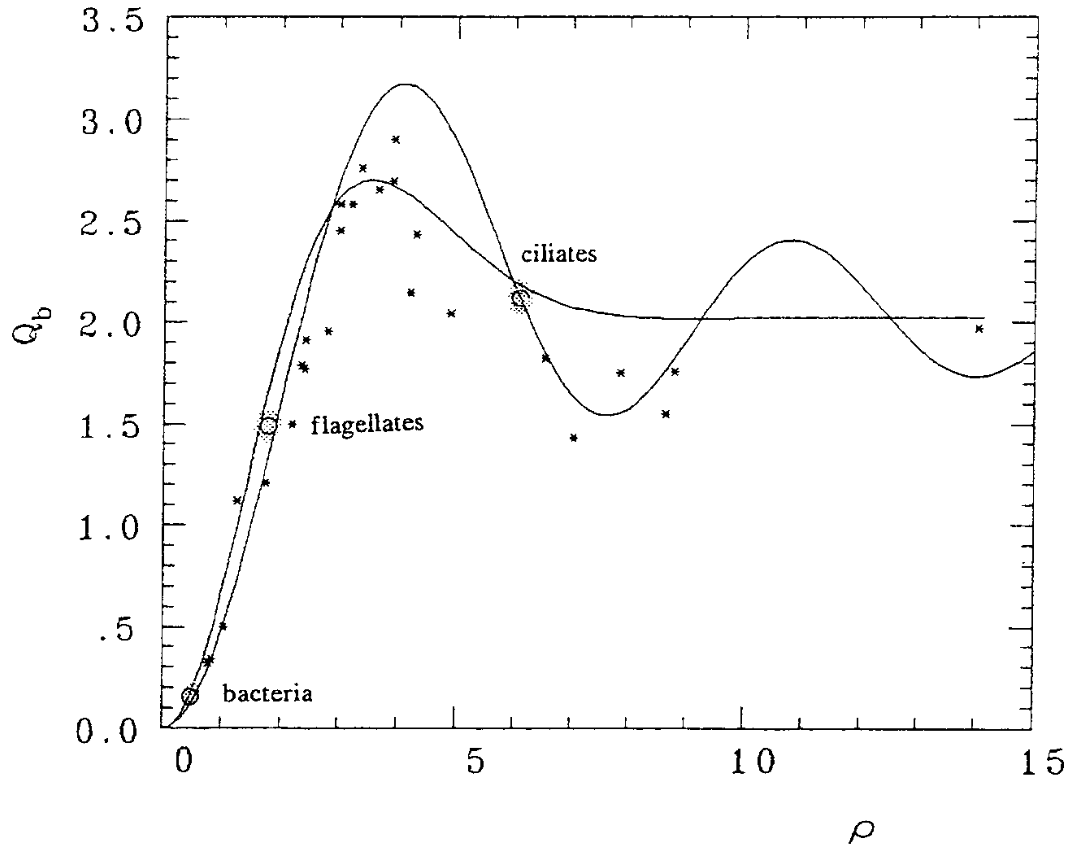

Figure 2. The theoretical variations of Q_b, the efficiency factor for scattering by non absorbing spheres (solid curve with marked oscillations) as a function of the dimensionless parameter ρ. The smoothed curve is for an averaged $\bar{Q}_b$ to be applied for population with a log - normal size distribution. The crosses are the $\bar{Q}_b$ values (at $\lambda \sim 580$ nm) determined for various phytoplankters grown in culture (see Table 1 in Morel and Bricaud, 1986); additional data for algal cells come from Ahn (1990). The circles indicate the $\bar{Q}_b$ values (at $\lambda \sim 550$ nm) determined for free living marine bacteria, heterotrophic flagellates, and naked ciliates, (Morel and Ahn, 1990; 1991).

(Morel 1991)

Spectra of scattering efficiency for various phototrophic and heterotrophic microorganisms

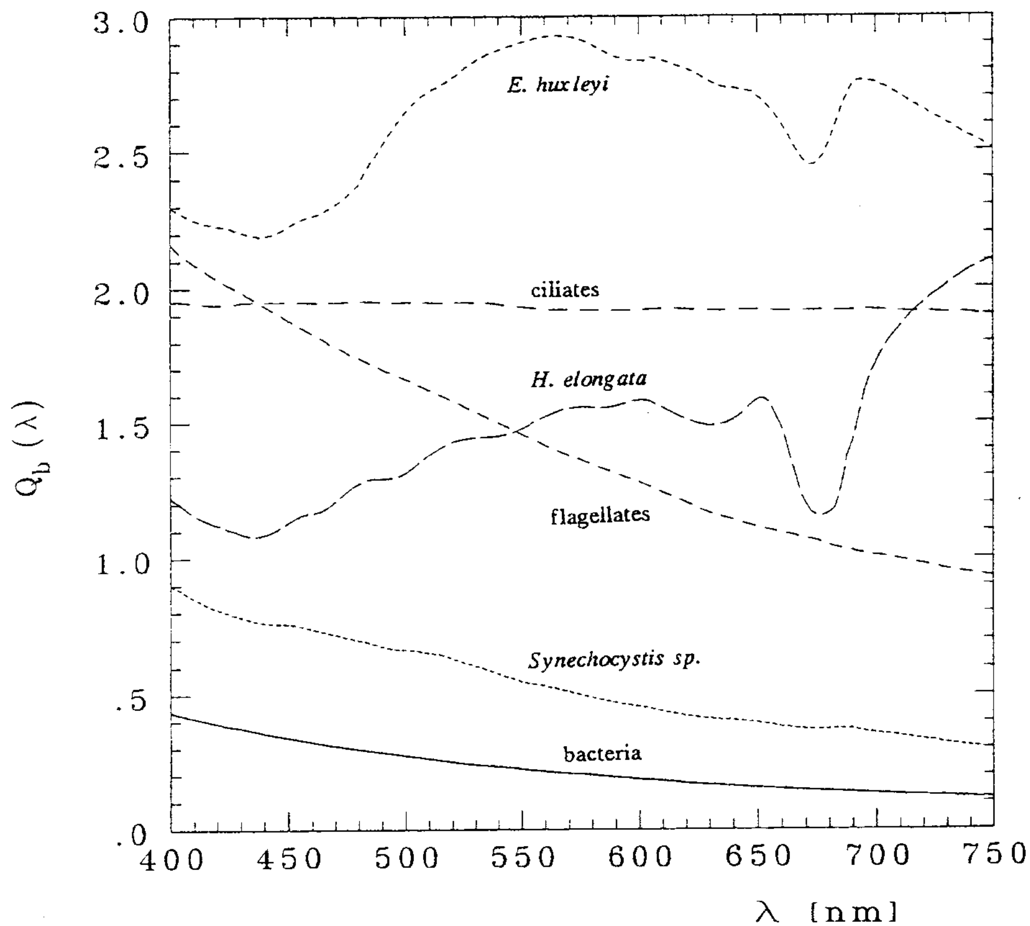

Figure 3. Spectral variations of Q_b within the 400-750 nm range of various phototrophic and heterotrophic organisms as experimentally determined (Morel and Ahn, 1990, 1991).

(Morel 1991)

Anomalous dispersion of the refractive index within the absorption band

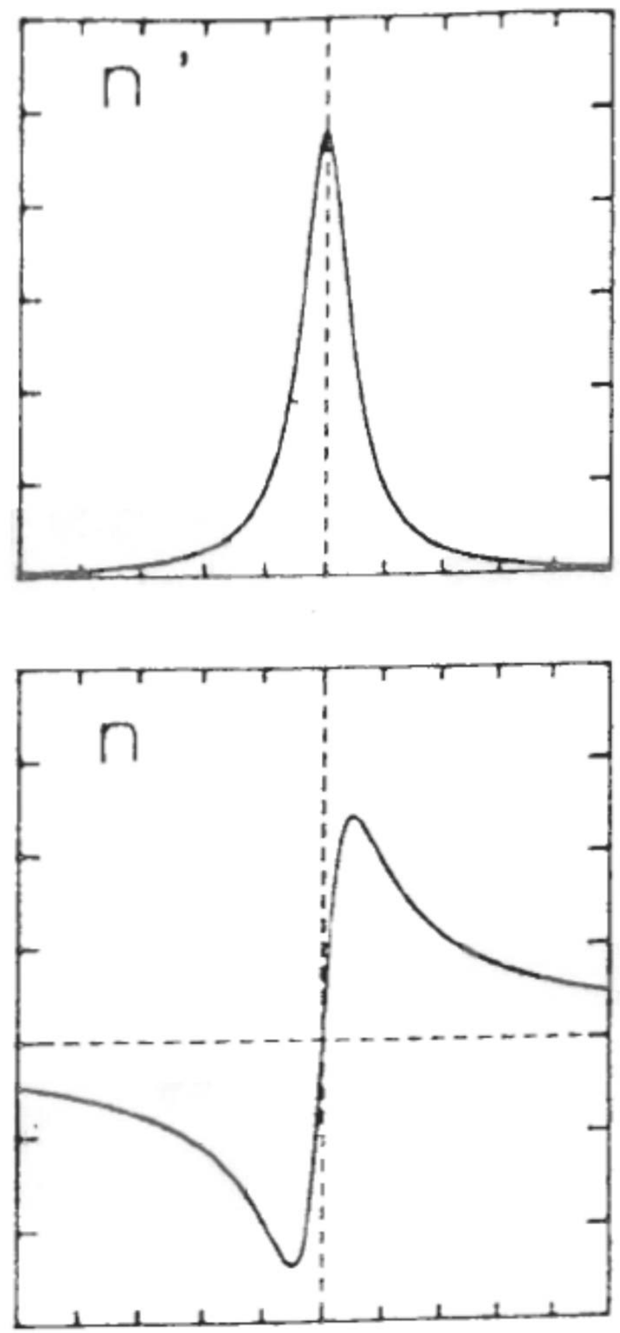

(Morel and Bricaud 1986)

Optical efficiency factors:

Examples for monospecific cultures of algal cells

(deduced from the absorption and attenuation coefficients, and size distribution measurements)

$\bar{d} = 3.4\ \mu m$
$n \simeq 1.07$
$\alpha \simeq 20 \ldots 35$
$\rho \simeq 3 \ldots 5$
for the visible light

$\bar{d} \simeq 1.2\ \mu m$
$n \simeq 1.05\ \mu m$
$\alpha \simeq 7 \ldots 13$
$\rho \simeq 0.5 \ldots 1.5$
for the visible light

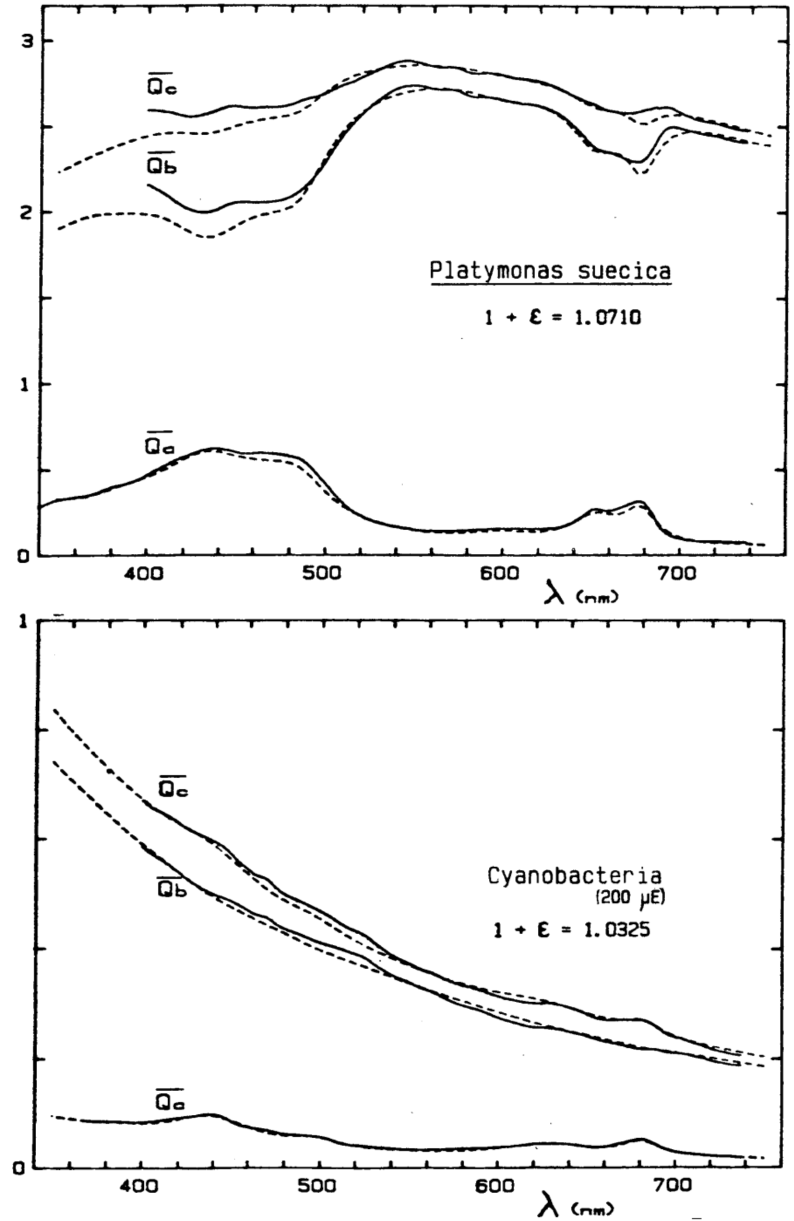

FIG. 14. Spectral variations of the mean efficiency factors for attenuation ($\bar{Q}_c$), scattering ($\bar{Q}_b$) and absorption ($\bar{Q}_a$), deduced from the attenuation and absorption coefficients experimentally determined (continuous lines), for two phytoplanktonic species. The variations of $\bar{Q}_c$, $\bar{Q}_b$ and $\bar{Q}_a$ obtained from a theoretical model (see text) are shown as dashed lines. The central value of the real part of the refractive index, $1 + \epsilon$, leading to the best theory/experiment agreement is indicated on the Figures.

(Morel and Bricaud 1986)

Beam Transmissometer Systems

in situ instrument

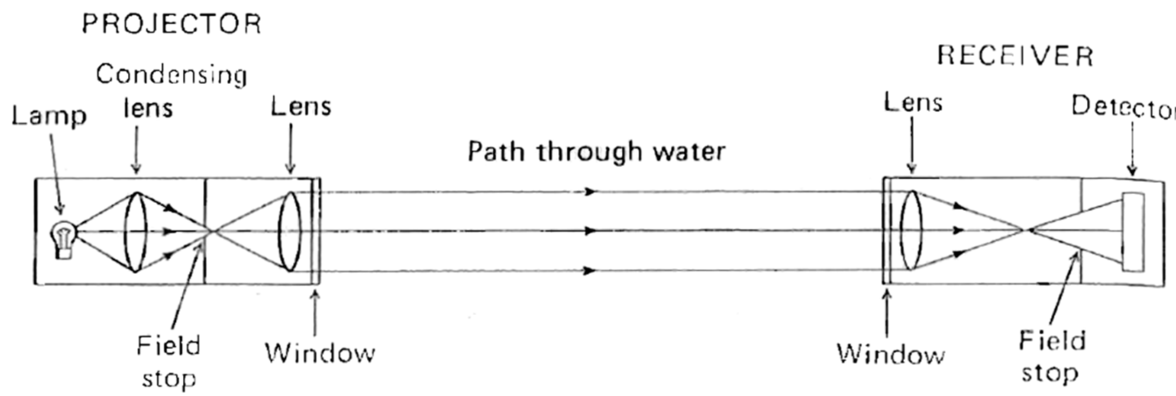

bench-top spectrophotometer

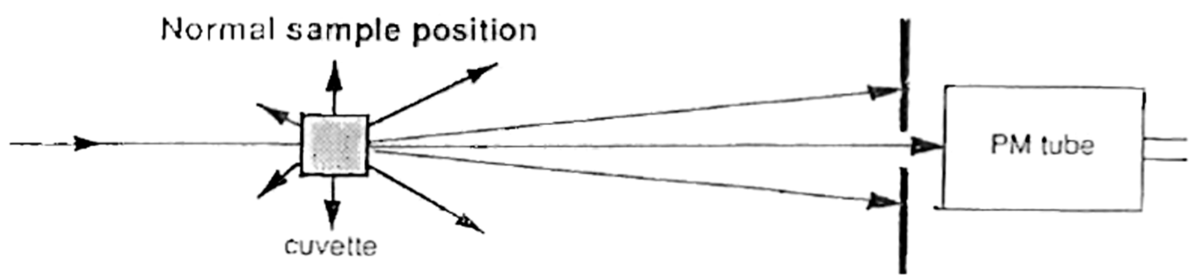

(Kirk, 1994)

Scattering phase function: Effect of polydispersion

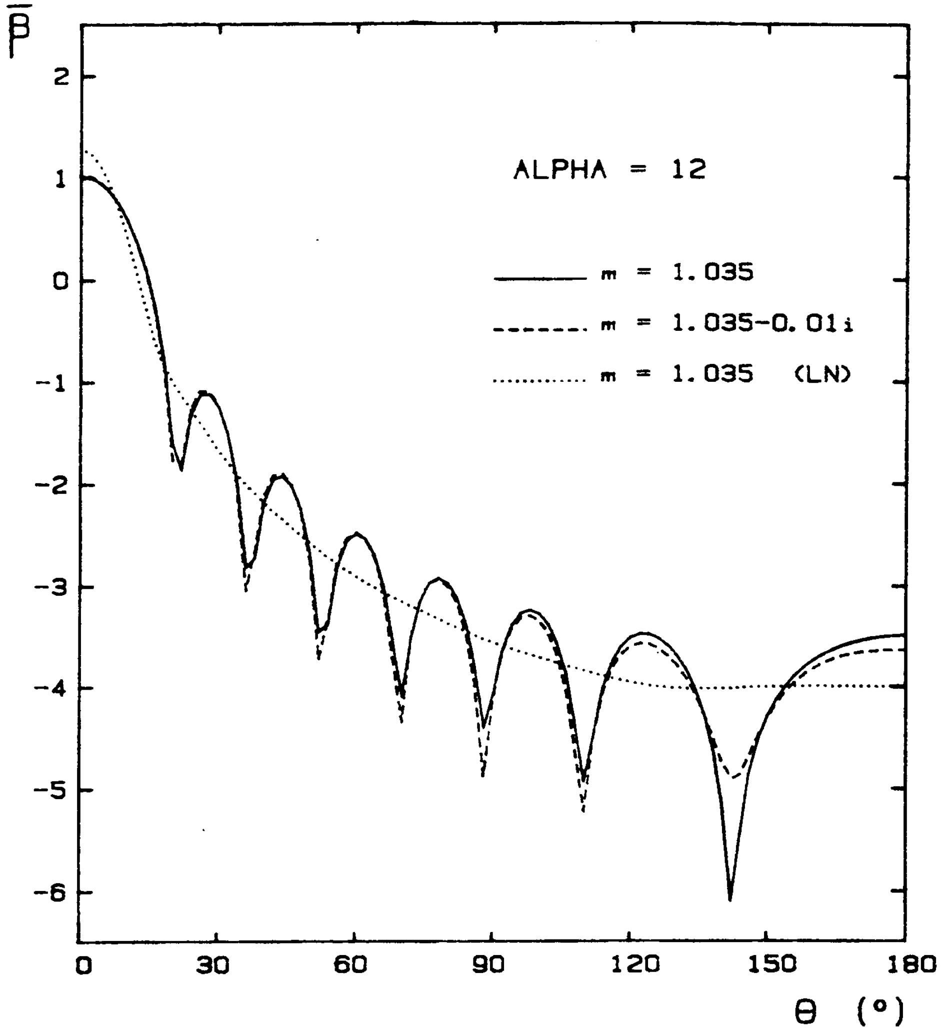

FIG. 5. Normalized volume scattering functions, $\bar{\beta}(\theta)$ (Equations 5′ and 18), for a particle of relative size α = 12, when the refractive index is 1.035 and 1.035–0.01 i. The dotted curve represents the same $\bar{\beta}(\theta)$ function for a polydispersed population of particles with n = 1.035, computed according to Equation 20. The size distribution function $F(\alpha)$ is a log-normal law such that the modal relative size $\bar{\alpha}_M$ is also 12, and $F(\alpha_M/2) = F(2\alpha_M) = 0.01\ F(\alpha_M)$.

(Morel and Bricaud 1986)

Scattering phase function: Effects of particle size and refractive index

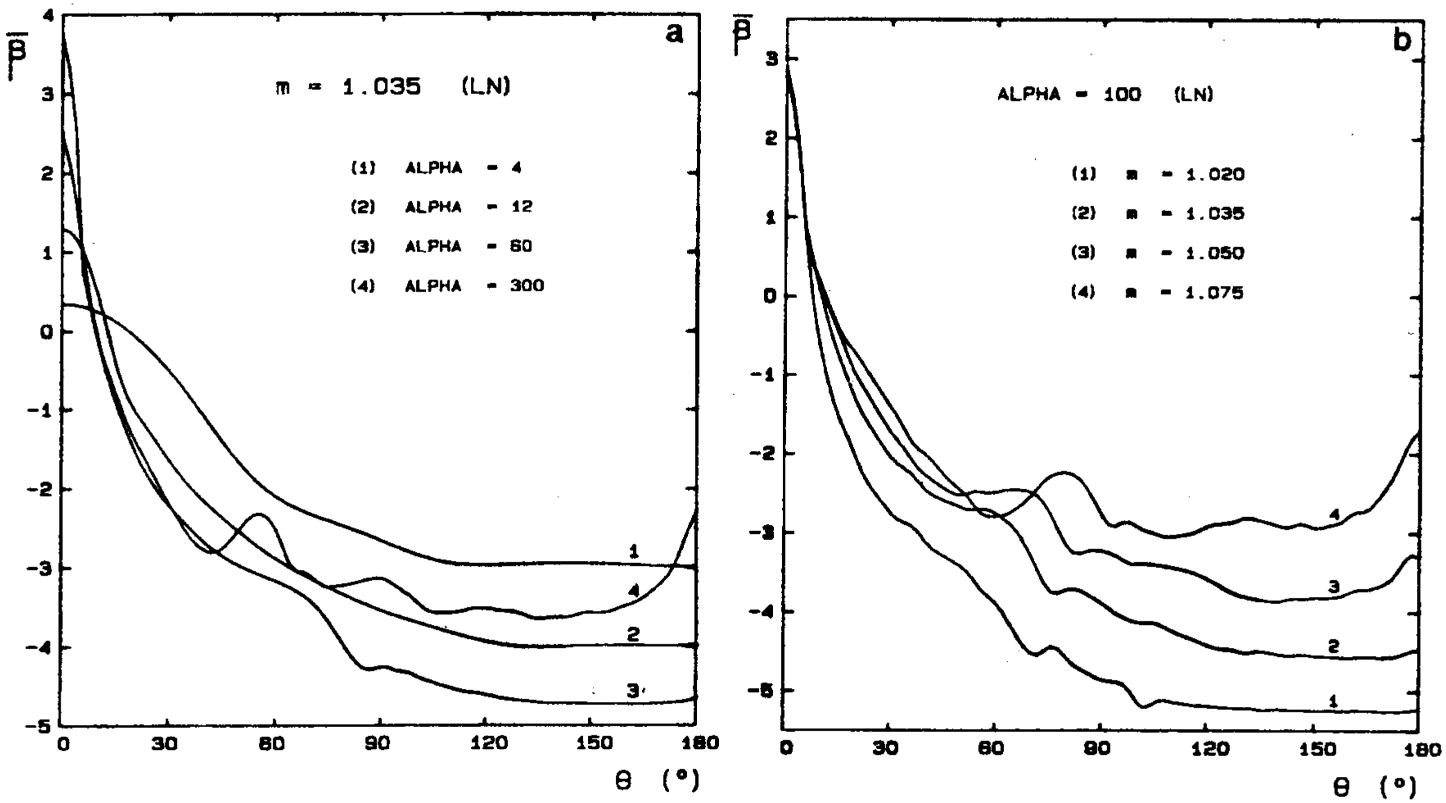

FIG. 6. (a) Normalized volume scattering function $\bar{\beta}(\theta)$ for increasing α_M values (increasing size) and for $m = 1.035$. (b) Normalized volume scattering function $\bar{\beta}(\theta)$ for increasing (real) index of refraction and for $\alpha_M = 100$. For Fig. 6a and b the log normal size distribution used is as in Fig. 5. The "bump" which occurs at about 75° for $m = 1.075$ and at smaller angles when the refractive index decreases (see also Fig. 6a) is the first "rainbow", at 138° for water droplets ($n = 1.33$). It appears for sufficiently large and perfect spheres. Thus it is unlikely that it can be observed for algal cells.

(Morel and Bricaud 1986)

Normalized scattering function for various microorganisms (from Mie calculations)

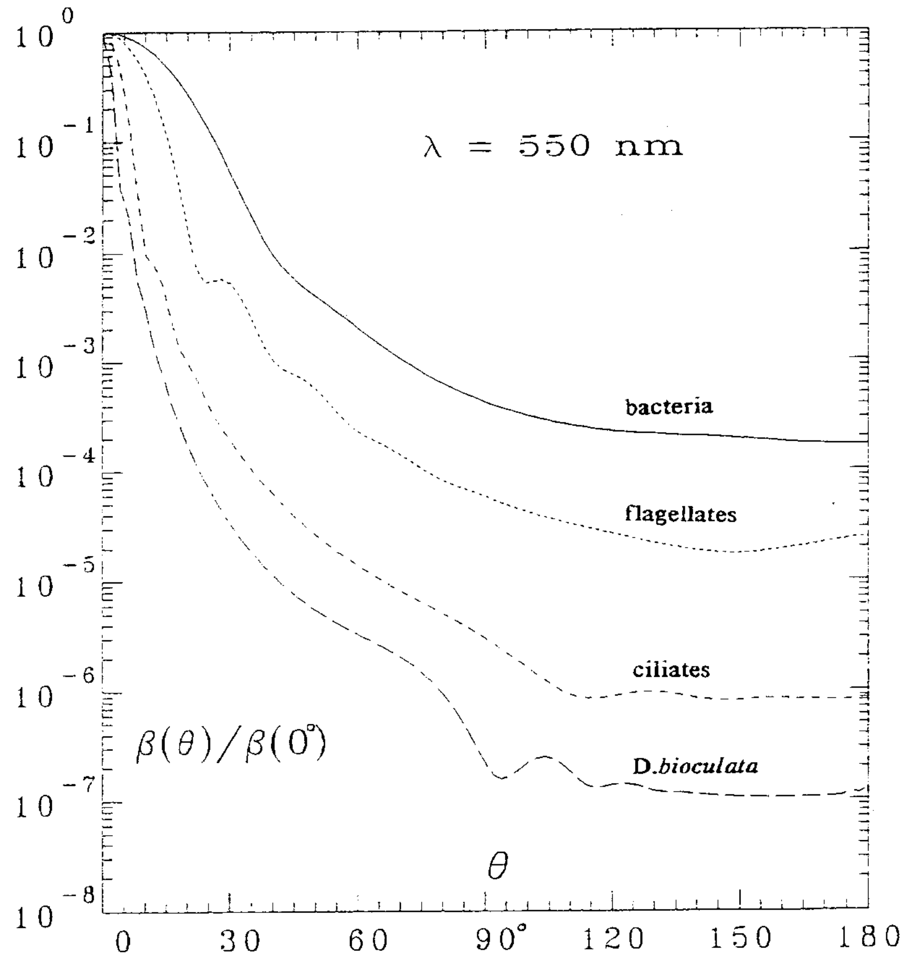

Figure 6. Volume scattering function (normalized at $\theta = 0°$ and for $\lambda = 550$ nm) computed for various organisms by using their refractive index and size distribution as experimentally determined (see text).

(Morel 1991)

Backscattering ratio versus relative size parameter

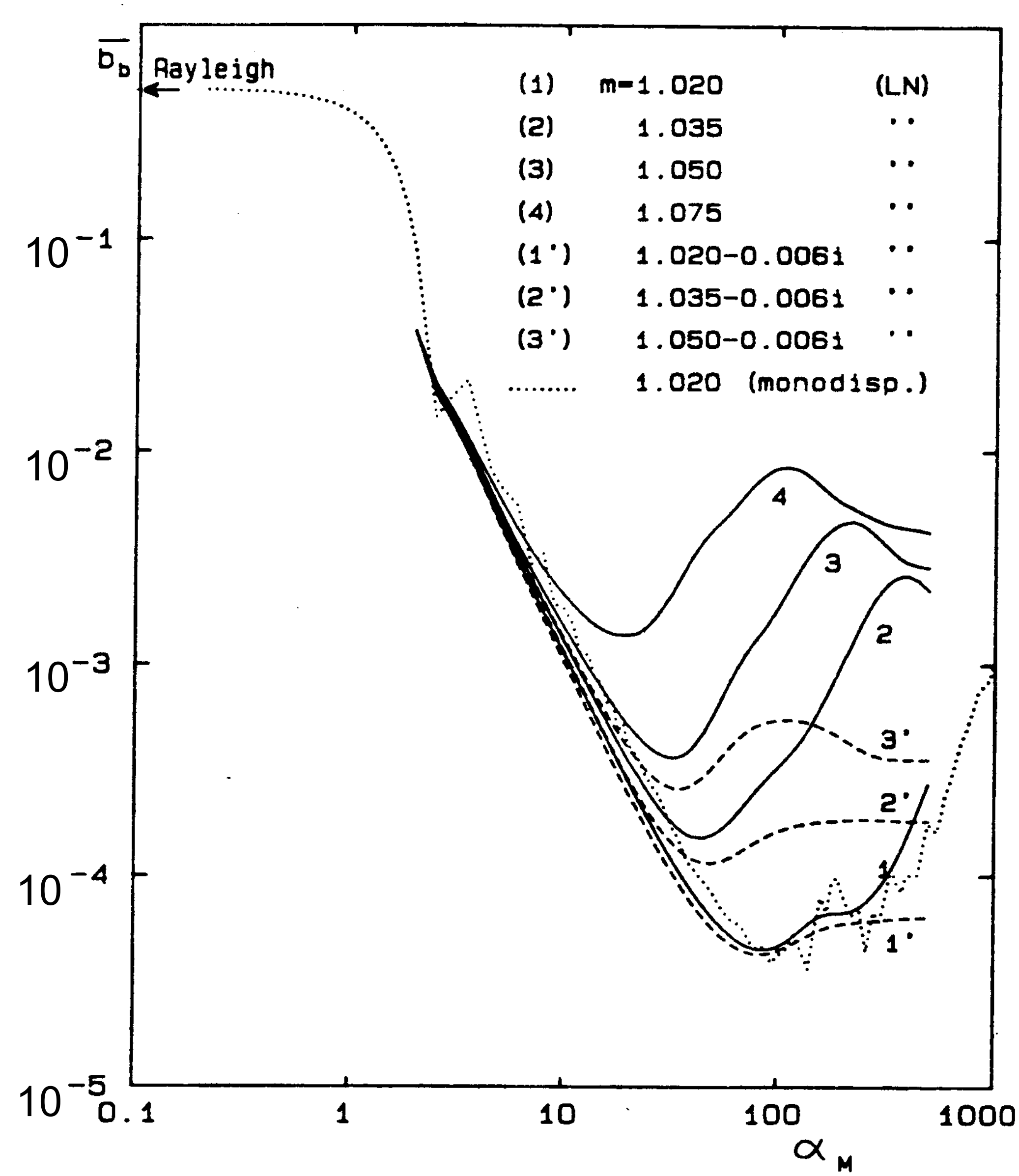

FIG. 8. Variations of the backscattering ratio $\tilde{b}_b$ (= b_b/b) vs. the modal relative size α_M (same log-normal law as before in Fig. 5). The different curves correspond to various values of the refractive index given in inset. The curve for a monodispersed population (with m = 1.02) is also shown (dotted line). The arrow indicates the limiting value of b_b/b (=0.5) when α tends toward 0 (Rayleigh domain).

(Morel and Bricaud 1986)

Schematic diagram of general-angle scattering meter

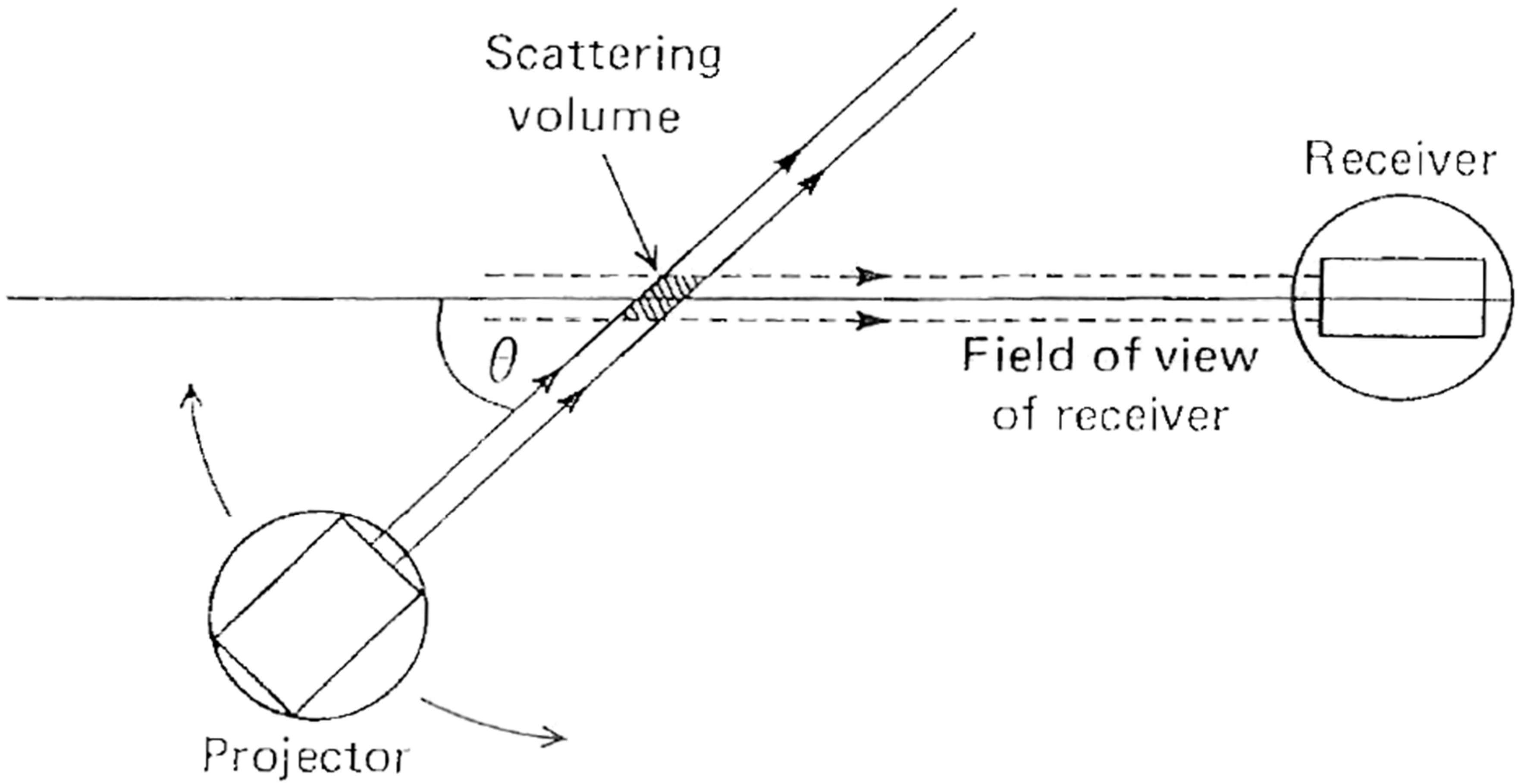

(Kirk 1994)

Plankton microorganisms

Table 1. Microbial components in the database and source of raw data. Values for the average equivalent spherical diameter (D), the real part of refractive index at 550 nm (n), and imaginary part of refractive index at 440 and 675 nm (n') are also given for each component.

i	Label	Microbial species	D [μm]	n 550 nm	$n' \cdot 10^3$ 440 nm	$n' \cdot 10^3$ 675 nm	Source of raw data
1	VIRU	Viruses	0.07	1.050	0	0	Stramski and Kiefer, 1991
2	HBAC	Heterotrophic bacteria	0.55	1.055	0.509	0.057	Stramski and Kiefer, 1990
3	PROC	generic Prochlorophyte; the average of:	0.66	1.051	18.51	10.30	
		PMED - Prochlorococcus strain MED	0.59	1.055	23.25	13.77	Morel et al., 1993
		PNAS - average of Prochlorococcus strains NATL and SARG	0.70	1.046	13.78	6.687	Morel et al., 1993
4	SYNE	generic Synechococcus; the average of:	1.05	1.051	5.587	2.930	
		SM41 - Synechococcus strain MAX41 (Cyanophyceae)	0.92	1.047	5.415	2.905	Morel et al., 1993
		SM01 - Synechococcus strain MAX01 (Cyanophyceae)	0.94	1.049	4.505	2.547	Morel et al., 1993
		SROS - Synechococcus strain ROS04 (Cyanophyceae)	1.08	1.049	4.516	2.154	Morel et al., 1993
		SDC2 - Synechococcus strain DC2 (Cyanophyceae)	1.14	1.050	4.249	2.375	Morel et al., 1993
		S103 - Synechococcus strain WH8103 (Cyanophyceae)	1.14	1.062	9.251	4.668	Stramski et al., 1995
5	SYMA	generic phycocyanin-rich picophytoplankton; the average of:	1.41	1.055	6.495	2.757	
		SCYS - Synechocystis (Cyanophyceae)	1.39	1.050	4.530	1.910	Ahn et al., 1992
		MARI - Anacystis marina (Cyanophyceae)	1.43	1.060	8.460	3.603	Ahn et al., 1992
6	PING	Pavlova pinguis (Haptophyceae)	3.97	1.046	4.177	2.709	Bricaud et al., 1988
7	PSEU	Thalassiosira pseudonana (Bacillariophyceae)	3.99	1.045	9.231	7.397	Stramski and Reynolds, 1993
8	LUTH	Pavlova lutheri (Haptophyceae)	4.26	1.045	5.767	2.403	Bricaud et al., 1988
9	GALB	Isochrysis galbana (Haptophyceae)	4.45	1.056	7.673	5.101	Ahn et al., 1992
10	HUXL	Emiliania huxleyi (Haptophyceae)	4.93	1.050	5.012	2.950	Ahn et al., 1992
11	CRUE	Porphyridium cruentum (Rhodophyceae)	5.22	1.051	3.351	2.443	Bricaud et al., 1988
12	FRAG	Chroomonas fragarioides (Cryptophyceae)	5.57	1.039	4.275	2.904	Ahn et al., 1993
13	PARV	Prymnesium parvum (Haptophyceae)	6.41	1.045	2.158	1.329	Bricaud et al., 1988
14	BIOC	Dunaliella bioculata (Chlorophyceae)	6.71	1.038	10.49	7.839	Ahn et al., 1993
15	TERT	Dunaliella tertiolecta (Chlorophyceae)	7.59	1.063	6.260	5.076	Stramski et al., 1993
16	CURV	Chaetoceros curvisetum (Bacillariophyceae)	7.73	1.024	2.877	1.480	Bricaud et al., 1988
17	ELON	Hymenomonas elongata (Haptophyceae)	11.77	1.046	13.87	7.591	Ahn et al., 1992
18	MICA	Prorocentrum micans (Dinophyceae)	27.64	1.045	2.466	1.710	Ahn et al., 1992

(Stramski et al., 2001)

Interspecies variability in absorption

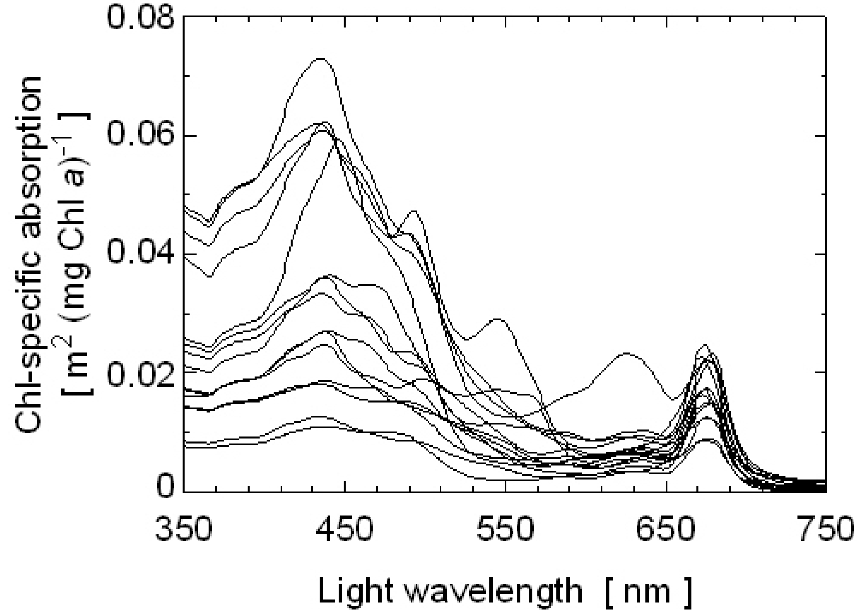

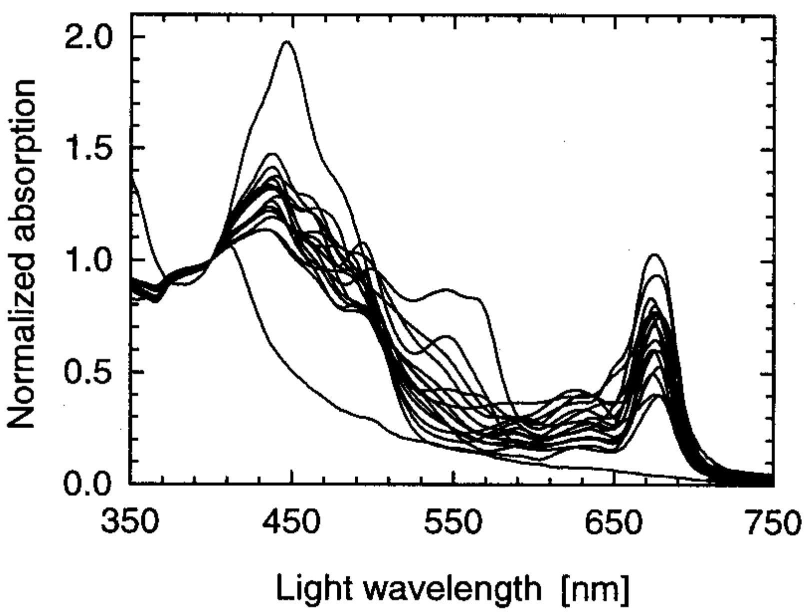

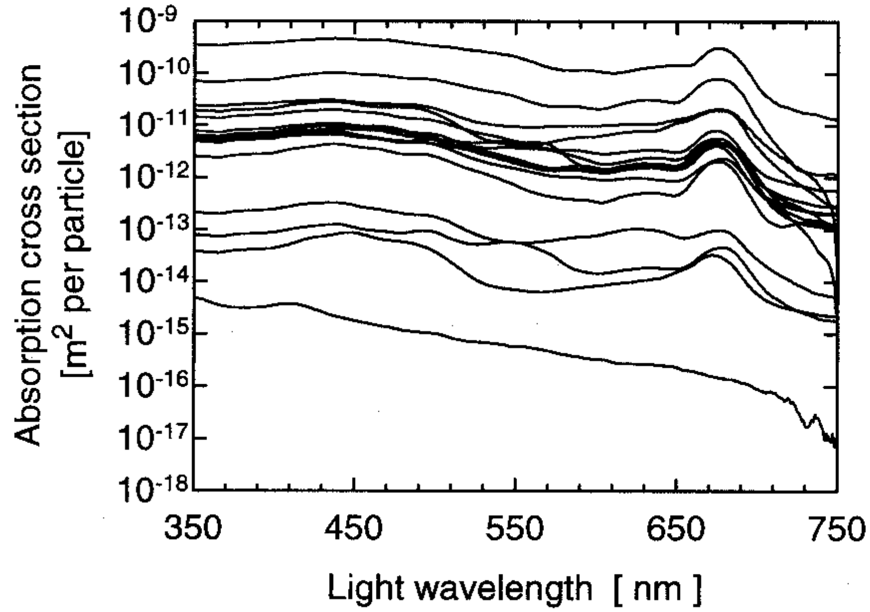

(Stramski et al. 2001)

Interspecies variability in scattering

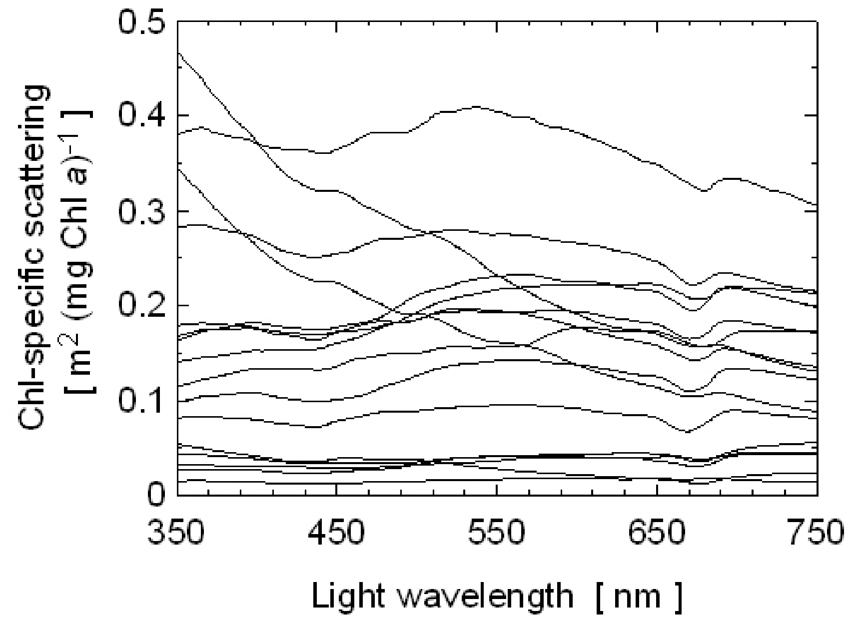

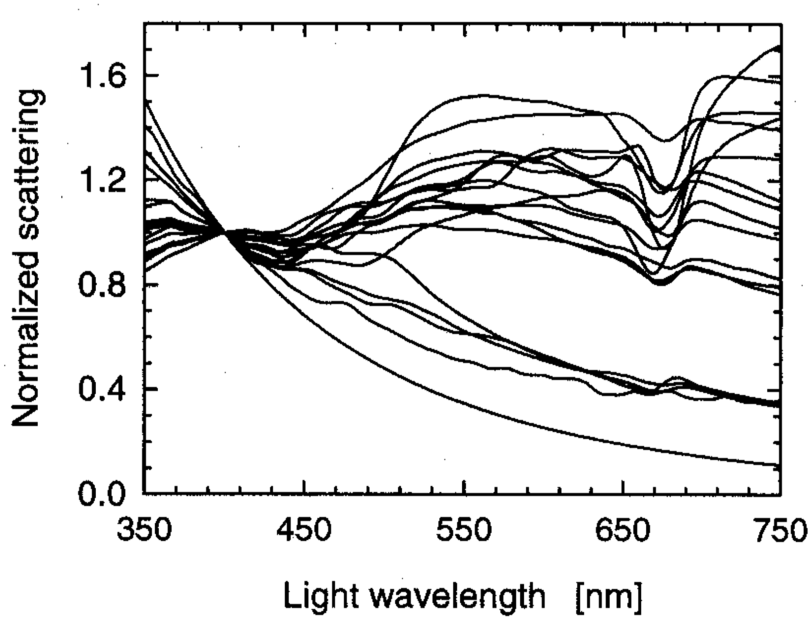

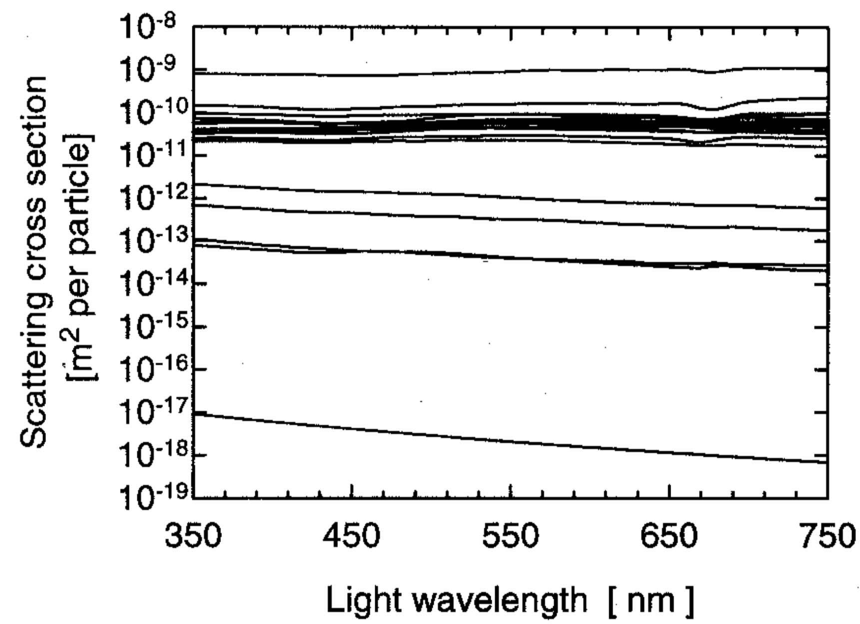

(Stramski et al. 2001)

Interspecies variability in single scattering albedo

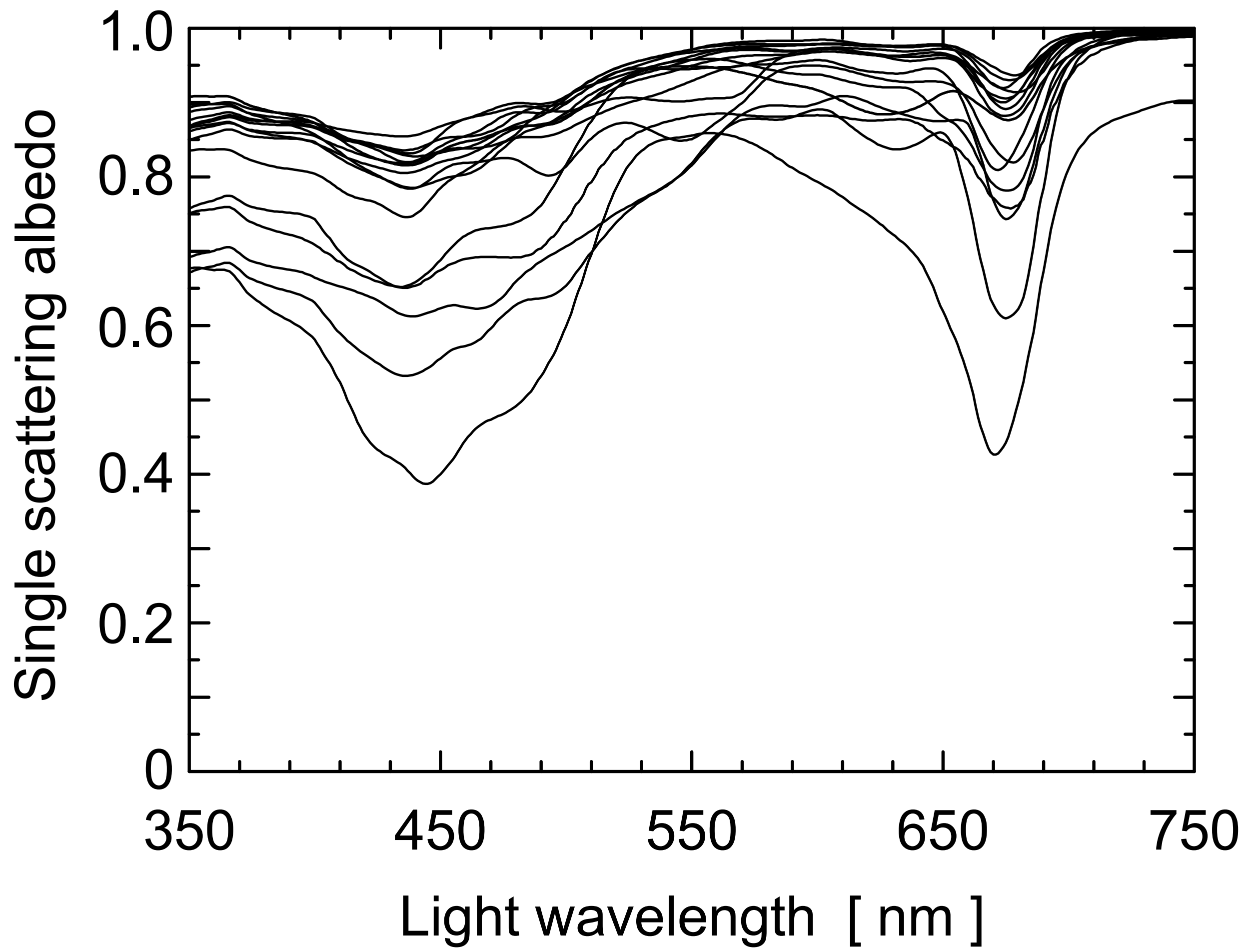

(based on data from Stramski et al. 2001)

Mie calculations of scattering phase function for plankton microorganisms

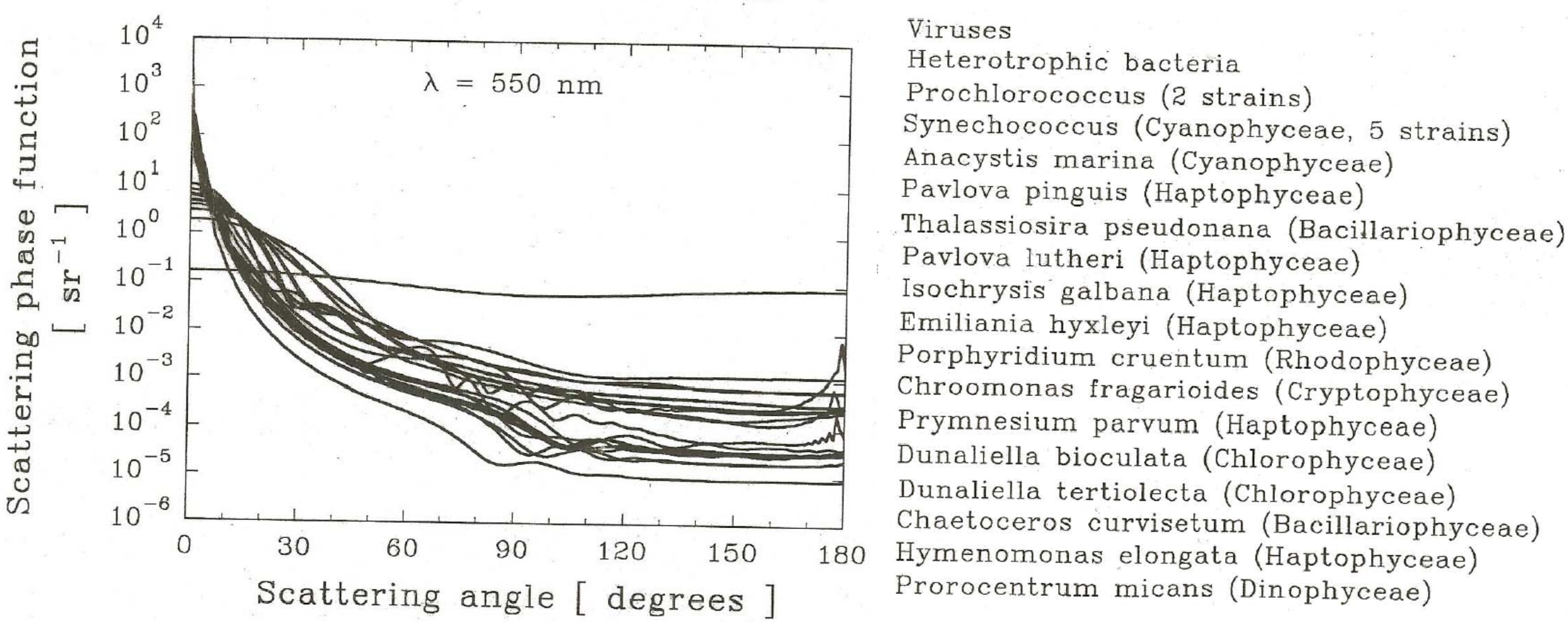

(Stramski et al. 2001)

Backscattering properties of plankton microorganisms

(subject to uncertainties associated with Mie scattering calculations for homogeneous spheres)

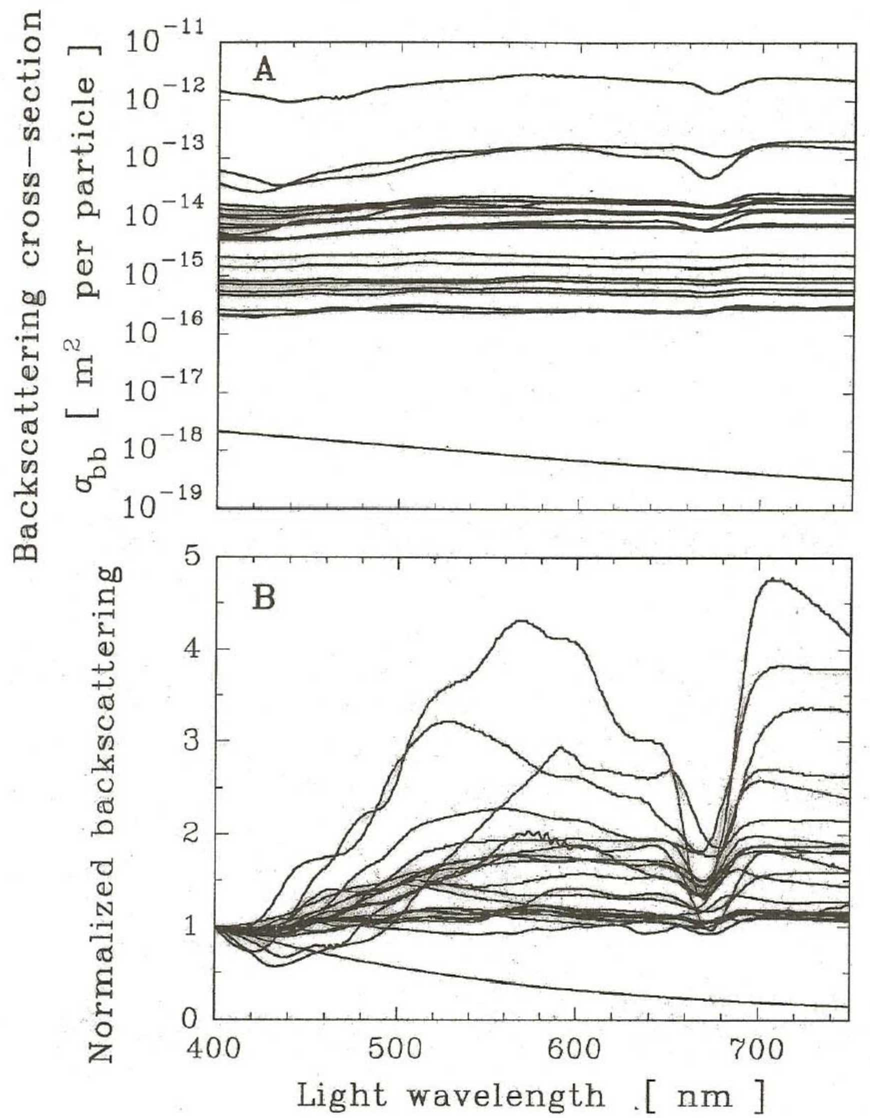

(Stramski et al. 2001)

Intraspecies variability due to irradiance - *Synechocystis*

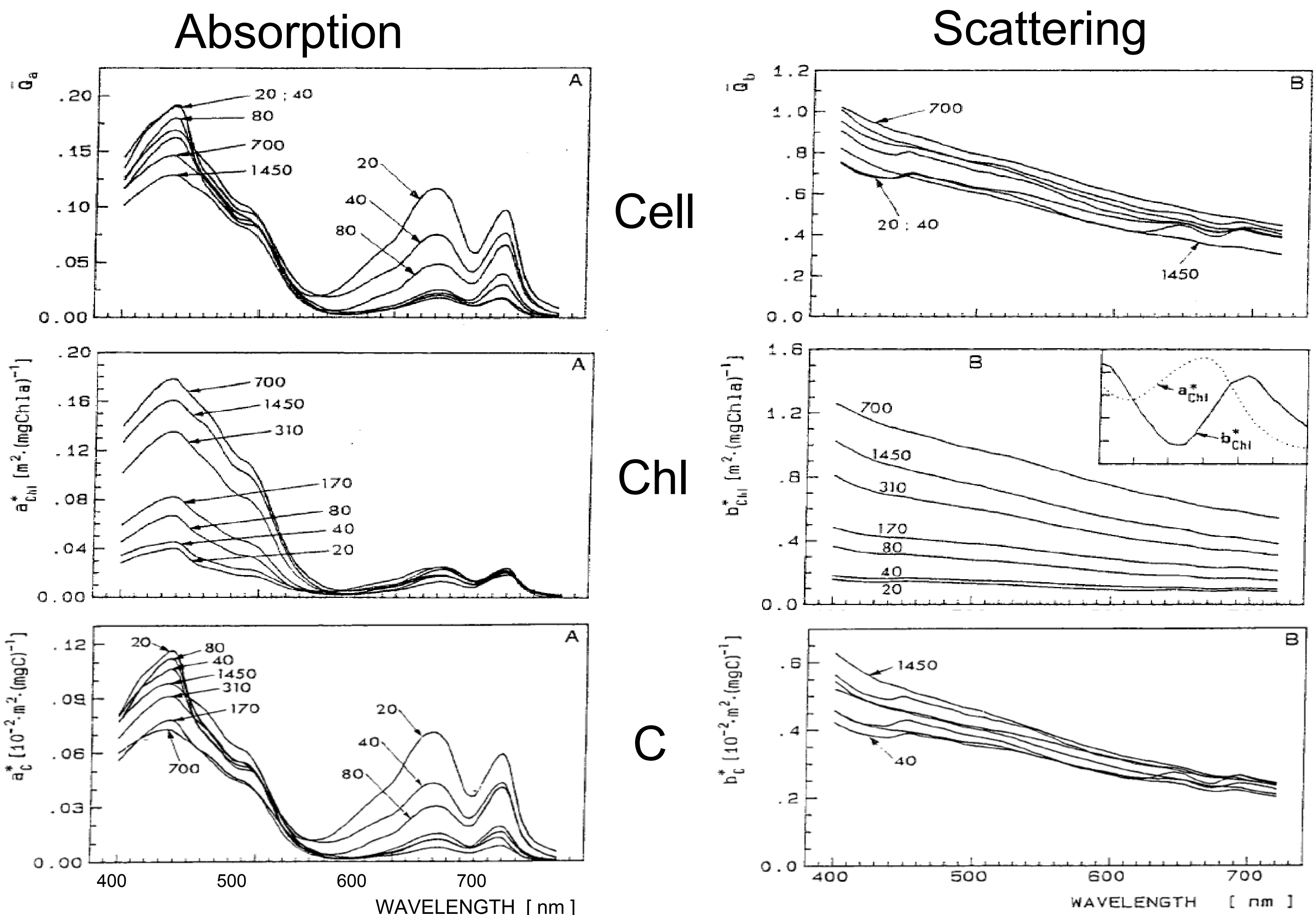

(Stramski and Morel 1990)

Intraspecies variability due to temperature, nitrogen, and light limitation – *Thalassiosira pseudonana*

Absorption vs. growth rate

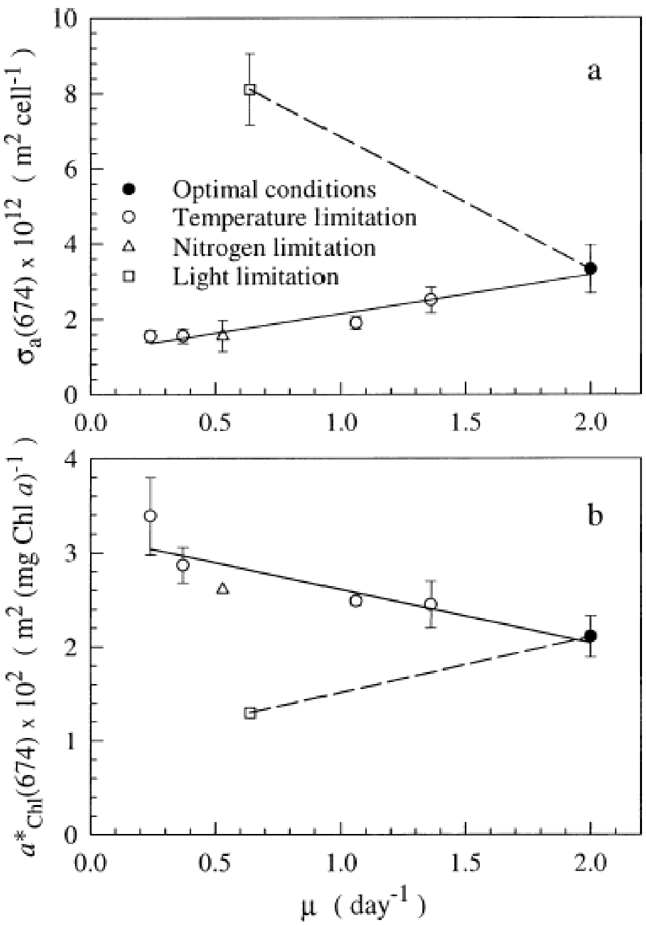

Scattering vs. growth rate

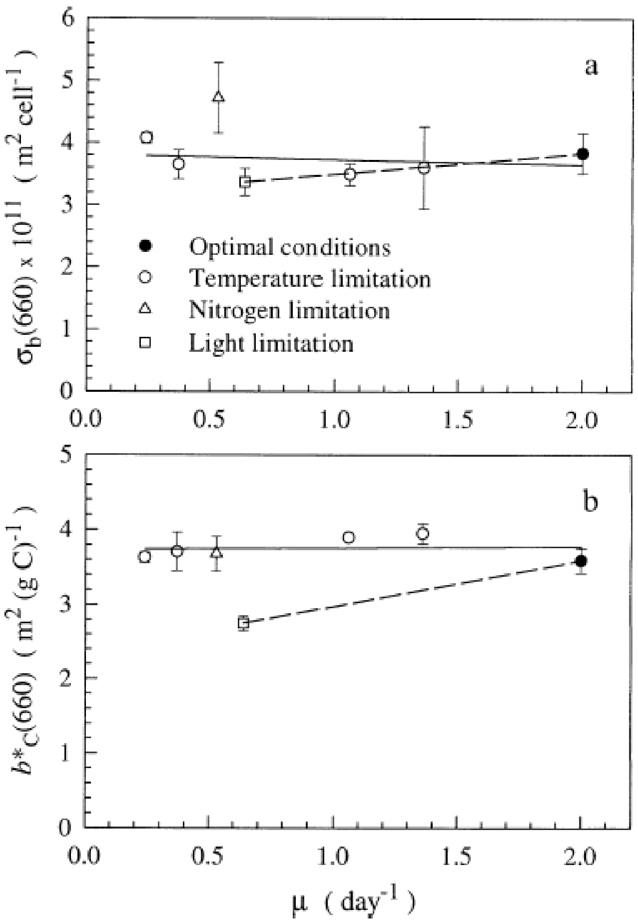

(Stramski et al. 2002)

Intraspecies variability over a diel cycle

Thalassiosira pseudonana

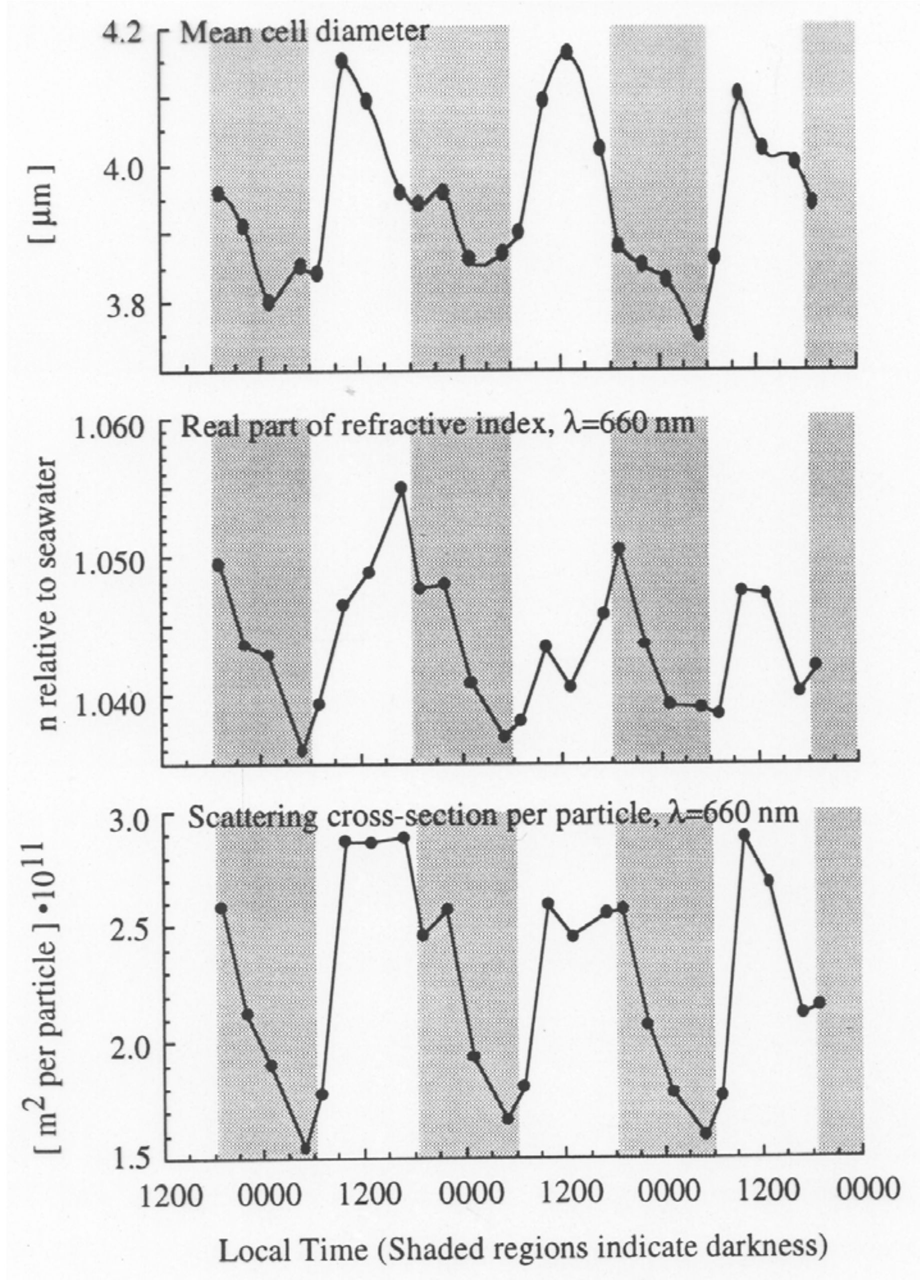

(Stramski and Reynolds 1993)

Cellular carbon and chlorophyll-a from refractive index

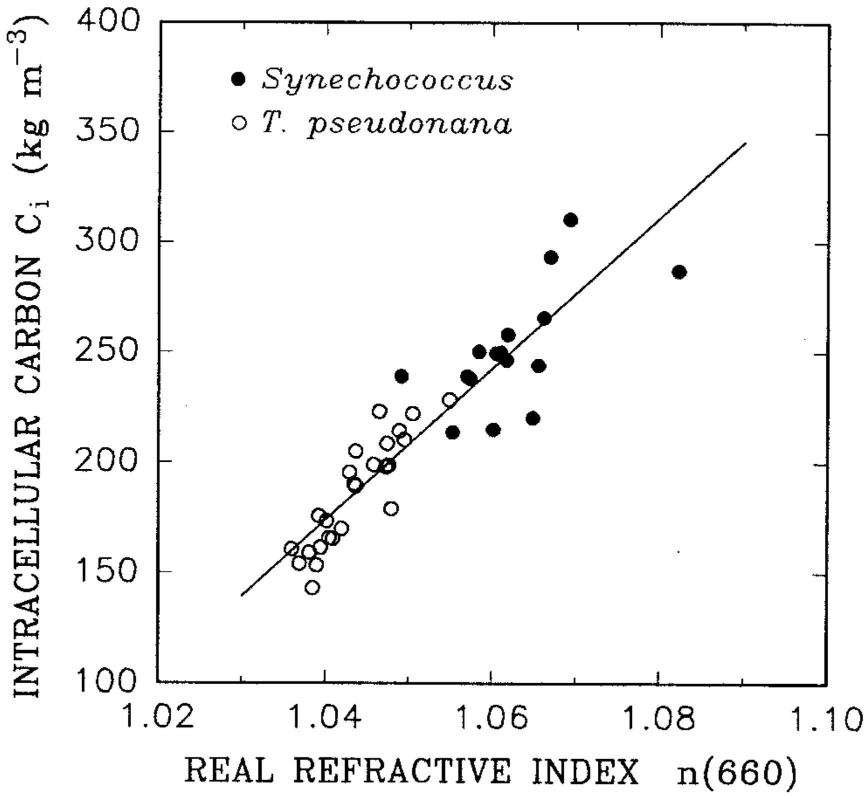

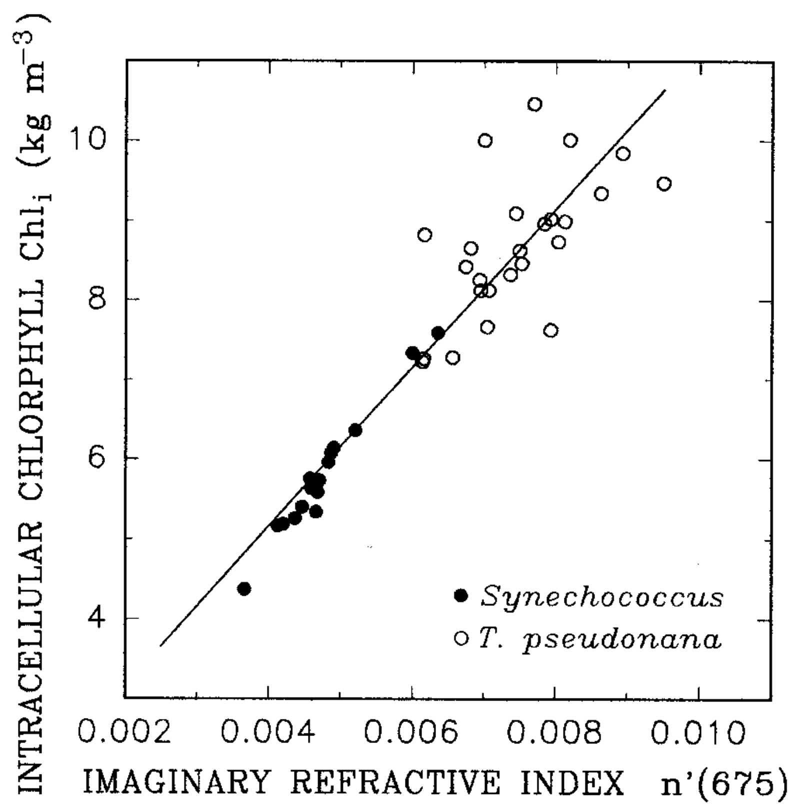

(Stramski 1999)

Cellular carbon and chlorophyll from refractive index

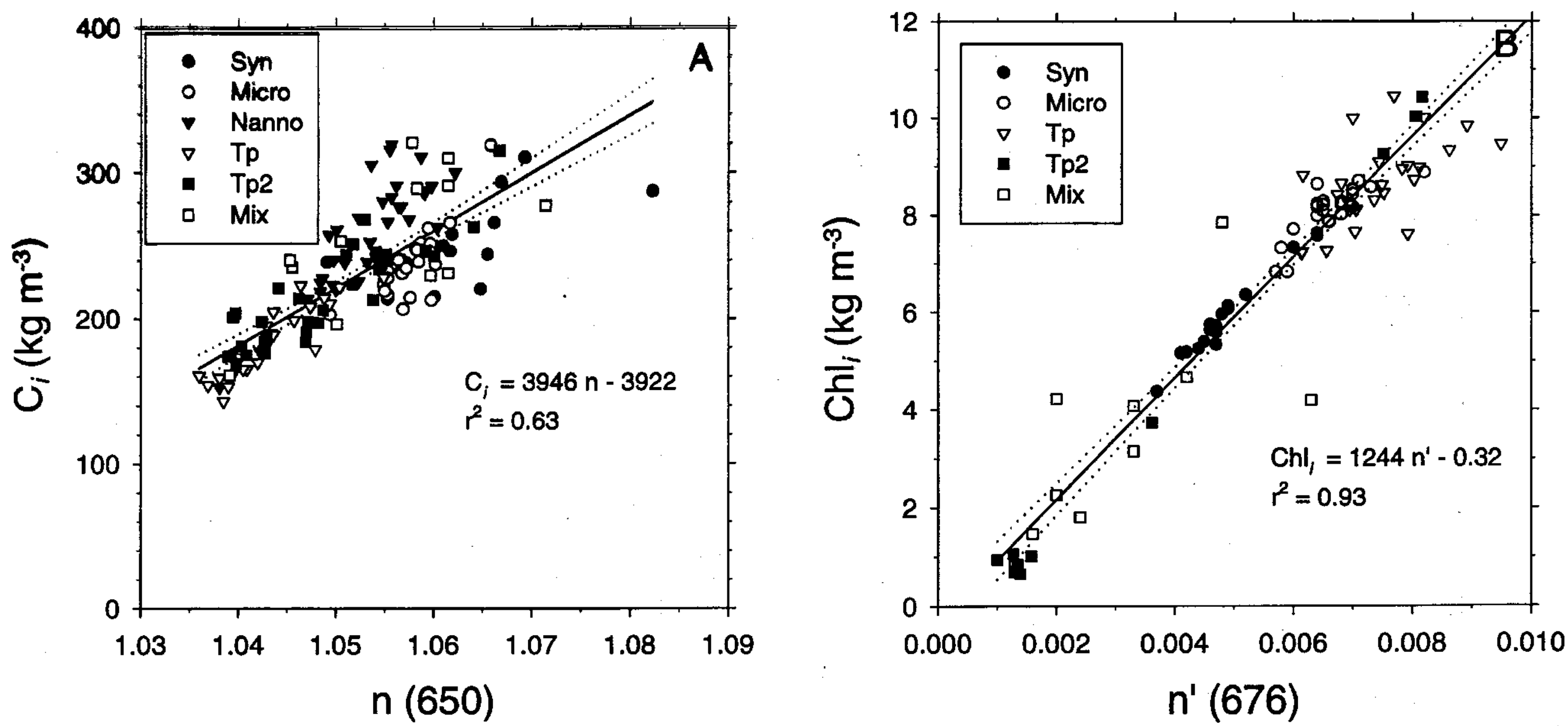

DuRand et al. (2002)

Optical variability for heterotrophic bacteria

Absorption

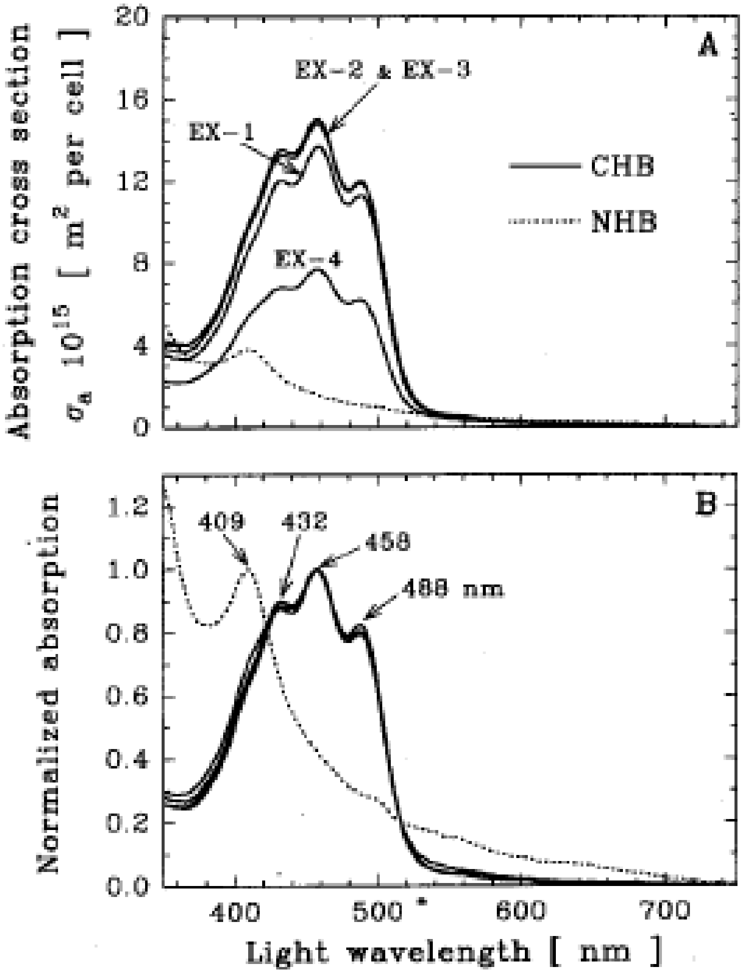

Beam attenuation

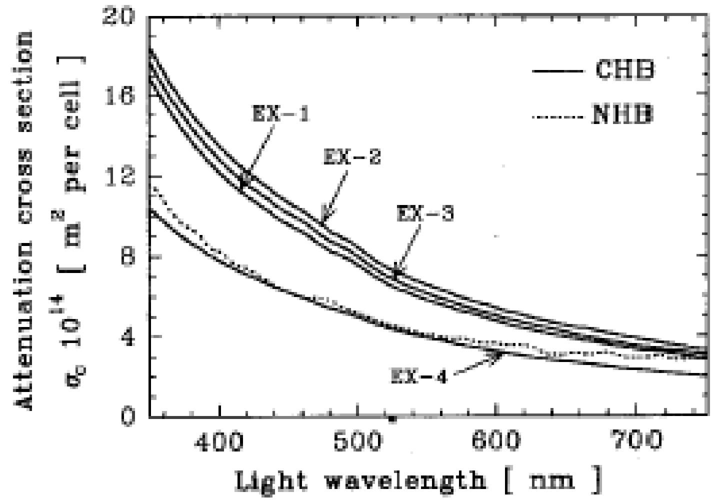

CHB Carotenoid-rich bacteria:
grown in nutrient-enriched seawater [EX-1 (light-dark cycle), EX-2 and EX-3 (dark)], and in nutrient-poor seawater (EX-4)

NHB Non-pigmented bacteria:
fast-growing in the absorption experiment and starved in the attenuation experiment

(Stramski and Kiefer 1998)

Prey-predator interactions (cyanobacteria and ciliates)

Particle size distributions

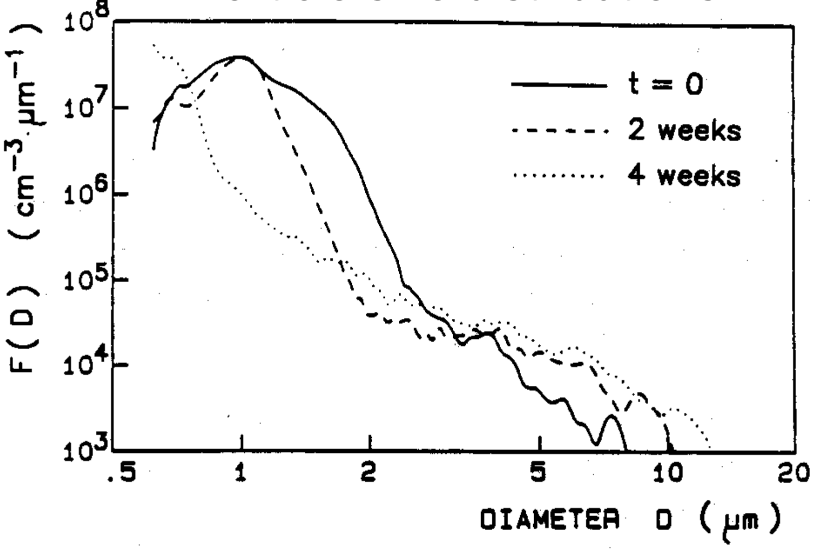

Absorption spectra

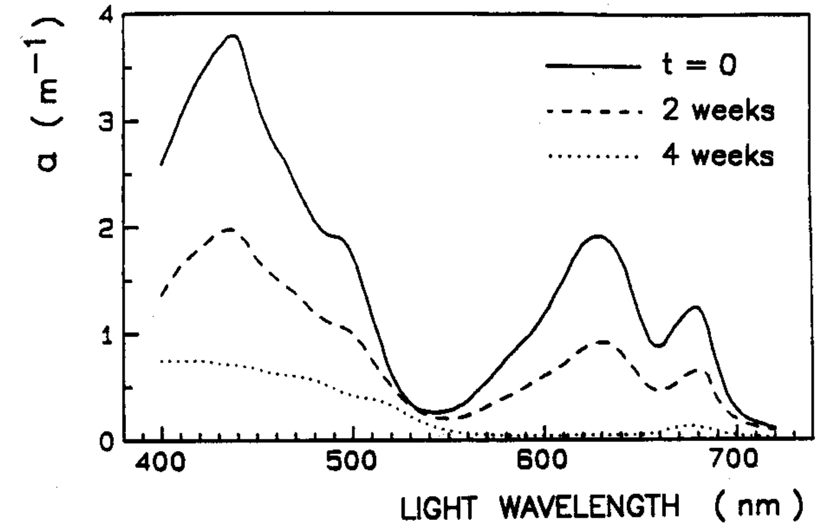

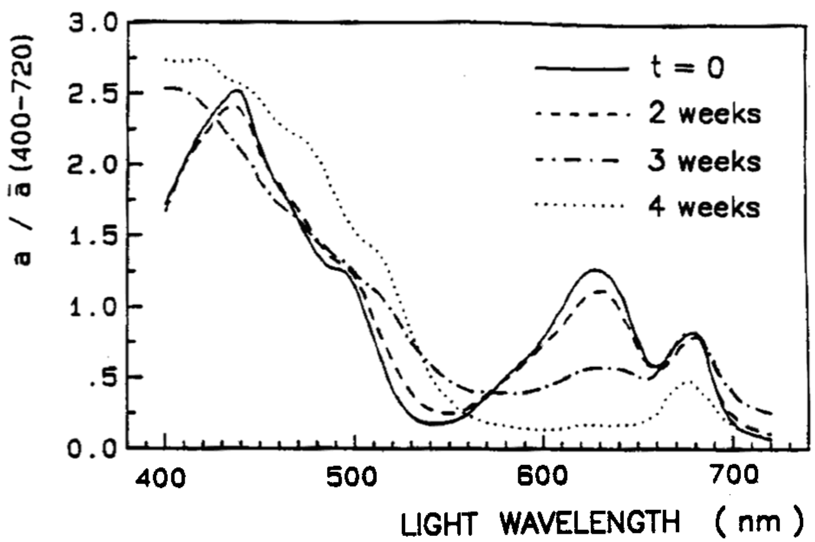

Scattering spectra

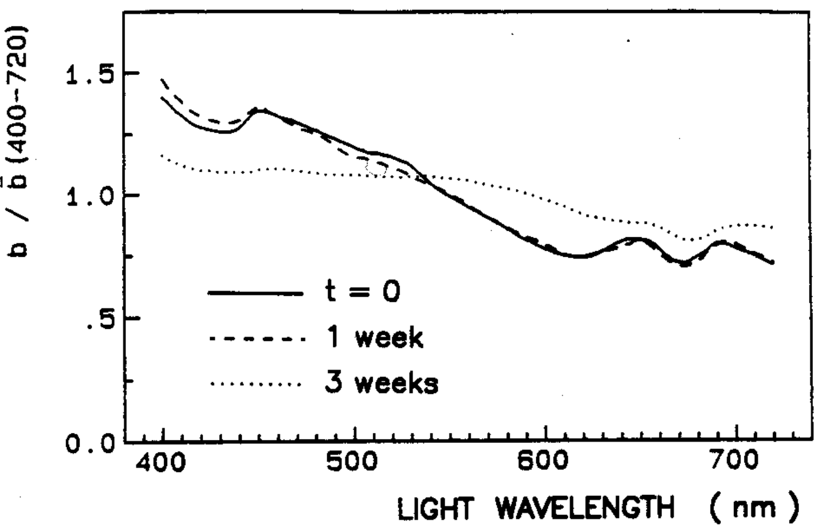

(Stramski et al. 1992)

Viral infection of marine bacteria

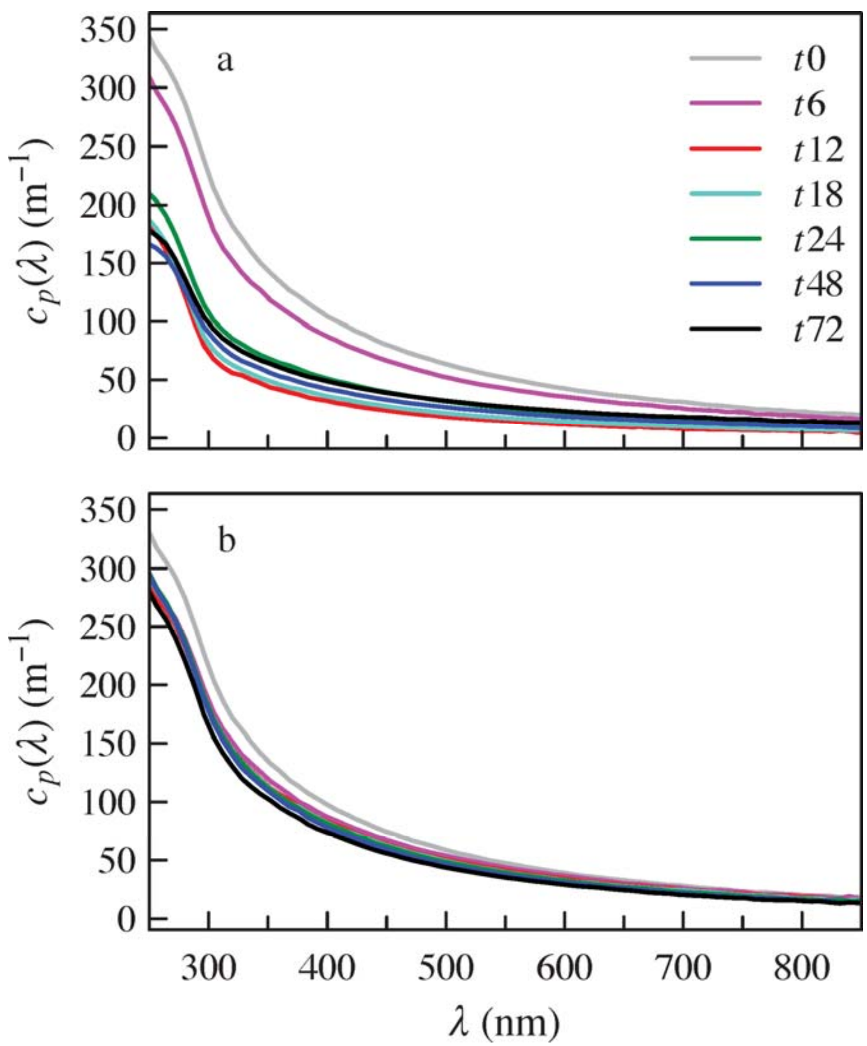

Spectral particulate beam attenuation coefficient, $c_p(\lambda)$, for (a) infected and (b) control samples at different sampling times, as indicated.

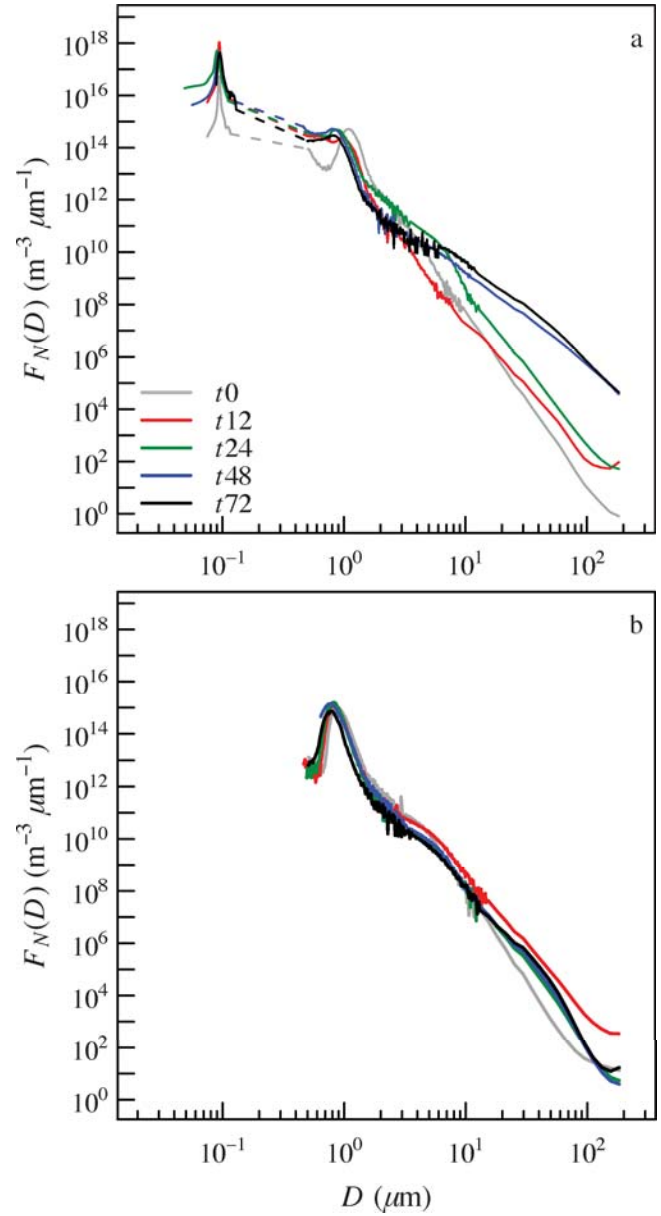

Density function of particle size distribution, *FN*(*D*), for (a) infected and (b) control samples at different sampling times, as indicated.

(Uitz et al. 2010)

Mineral particles

Saharan dust

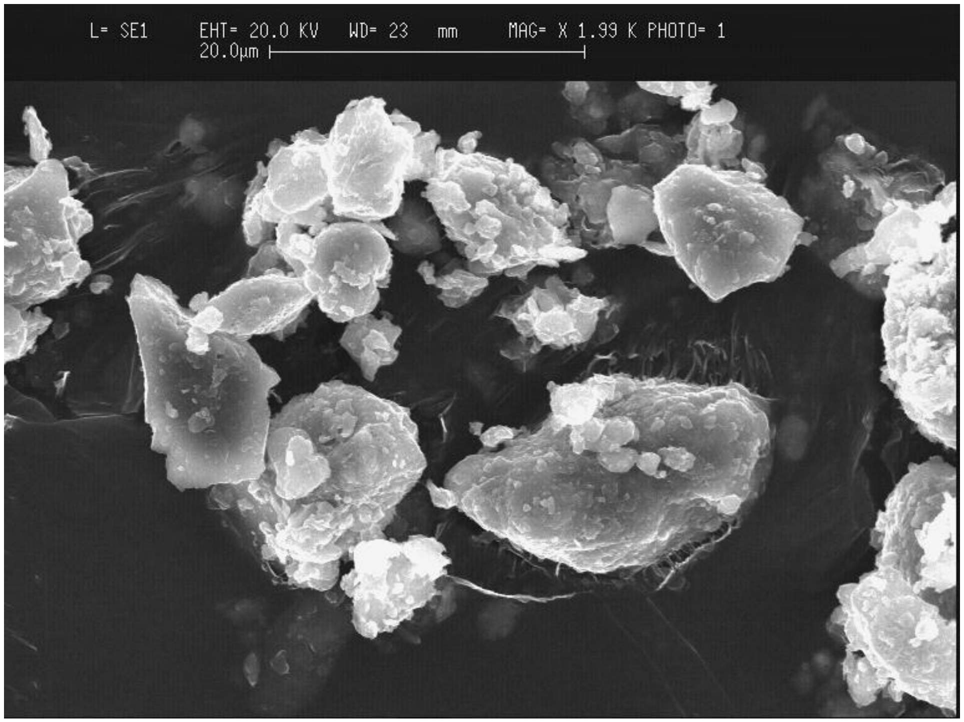

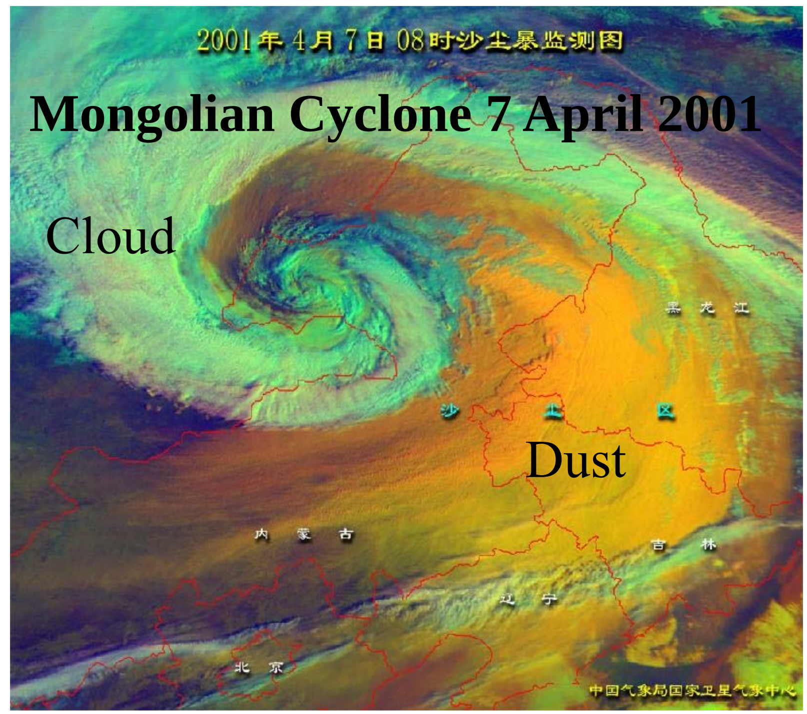

Terrigenous mineral-rich particulate matter

Sample ID	Description	Origin
ILL_1	illite	Source Clay Minerals Repository, University of Missouri (ref. IMt-1)
ILL_2	as above but different PSD	as above
KAO_1	kaolinite (poorly crystallized)	as above (ref. KGa-2)
KAO_2	as above but different PSD	as above
MON_1	Ca-montmorillonite	as above (ref. SAz-1)
MON_2	as above but different PSD	as above
CAL_1	calcite	natural crystal
CAL_2	as above but different PSD	as above
QUA_1	quartz	natural crystal
SAH_1	atmospheric dust from Sahara	red rain event, Villefranche-sur-Mer, France
SAH_2	as above but different PSD	as above
AUS_1	surface soil dust	cliff shore, Palm Beach near Sydney, Australia
AUS_2	as above but different PSD	as above
ICE_1	ice-rafted particles	glacier runoff, Kongsfjord, Spitsbergen
ICE_2	as above but different PSD	as above
OAH_1	surface soil dust	Oahu, Hawaii Islands
OAH_2	as above but different PSD	as above
KUW_1	surface soil dust	Kuwait (eastern part, close to ocean)
KUW_2	as above but different PSD	as above
NIG_1	surface soil dust	southwest Nigeria
SAN_1	atmospheric dust	San Diego, California

(Stramski et al. 2007)

Mass-specific absorption

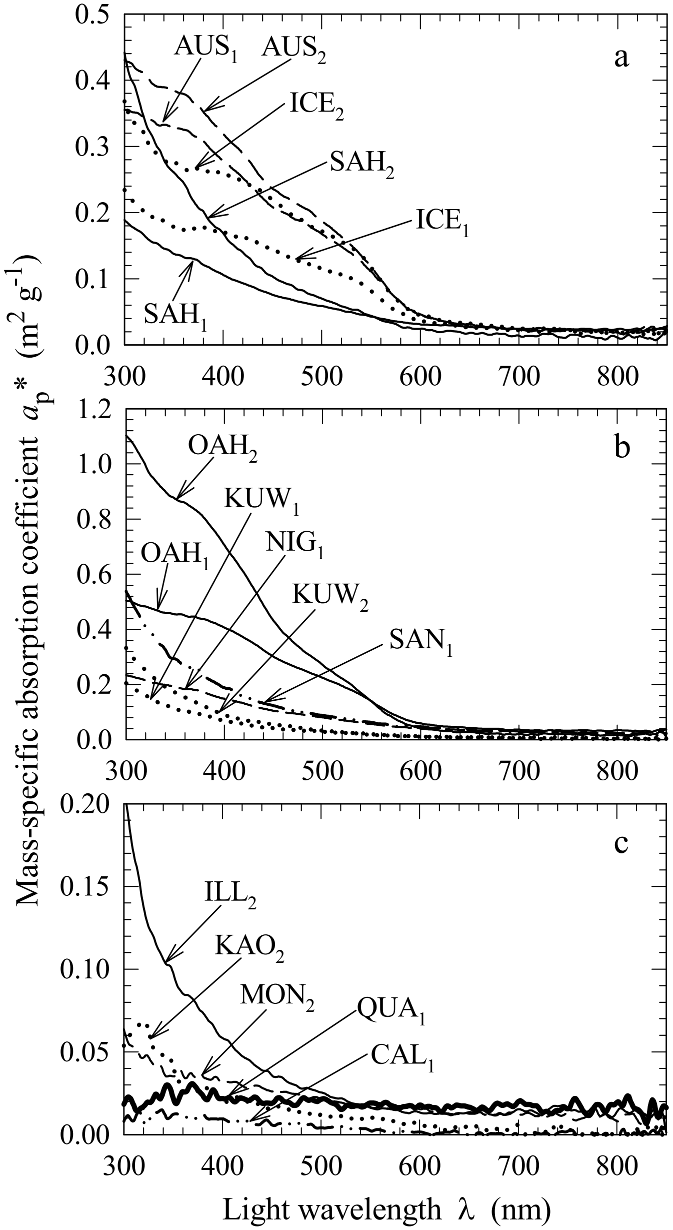

Mass-specific scattering

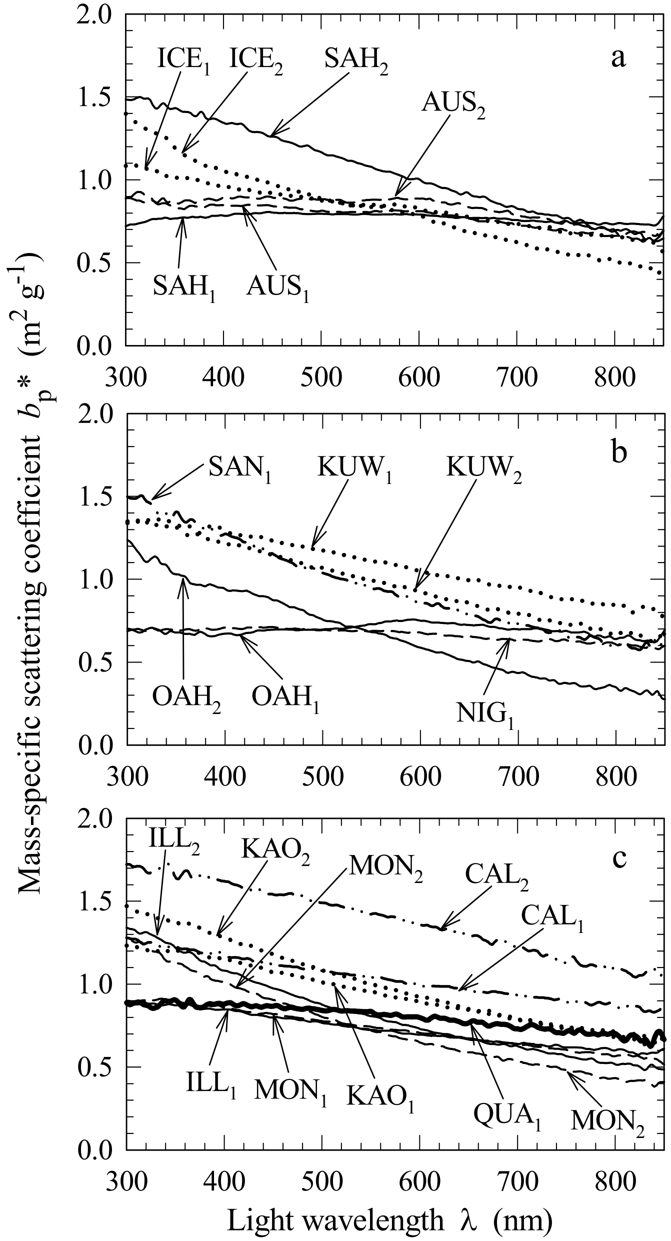

(Stramski et al. 2007)

Particle Size Distributions

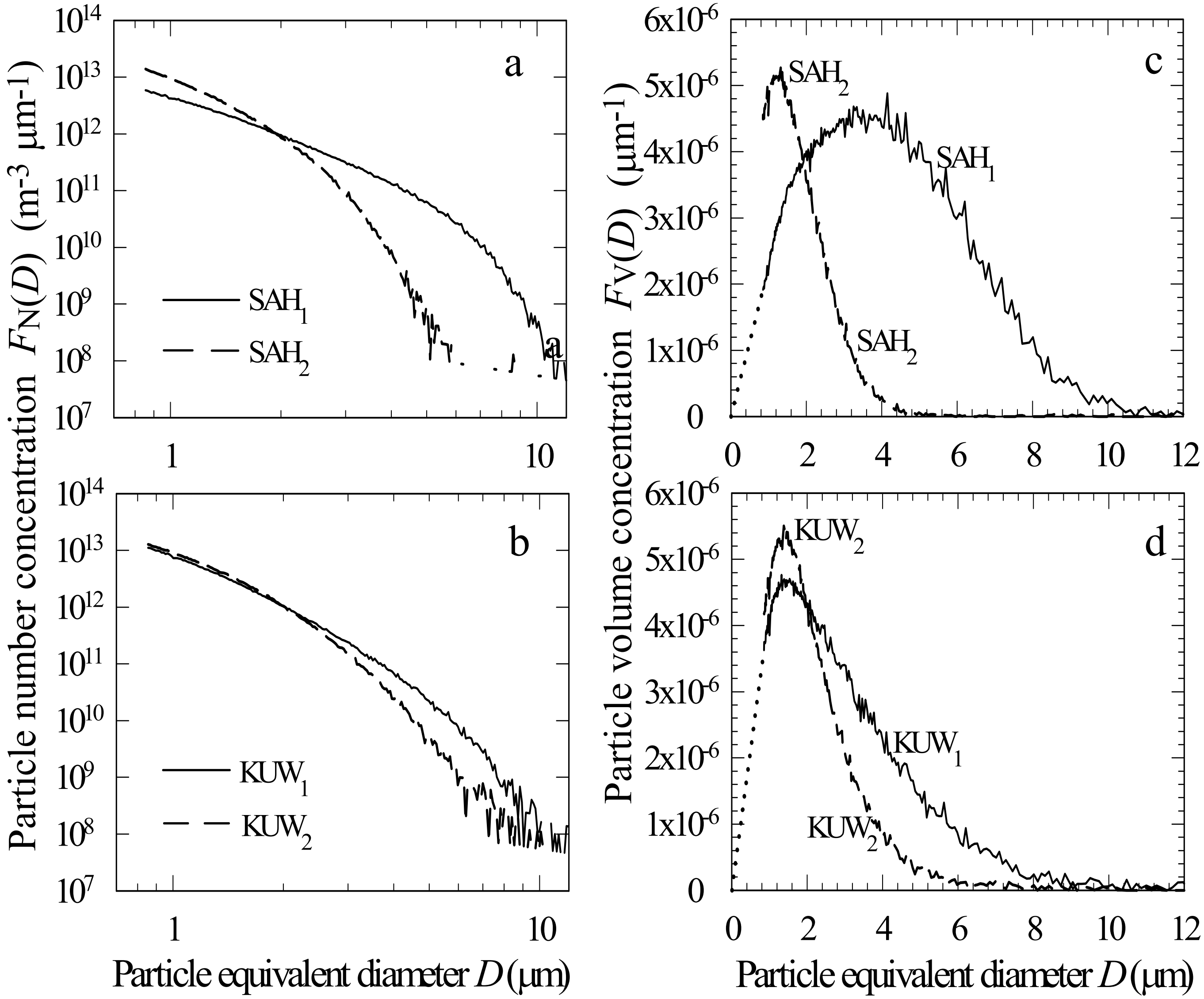

(Stramski et al. 2007)

(Babin and Stramski 2004)

Absorption of mineral-rich particulate assemblages

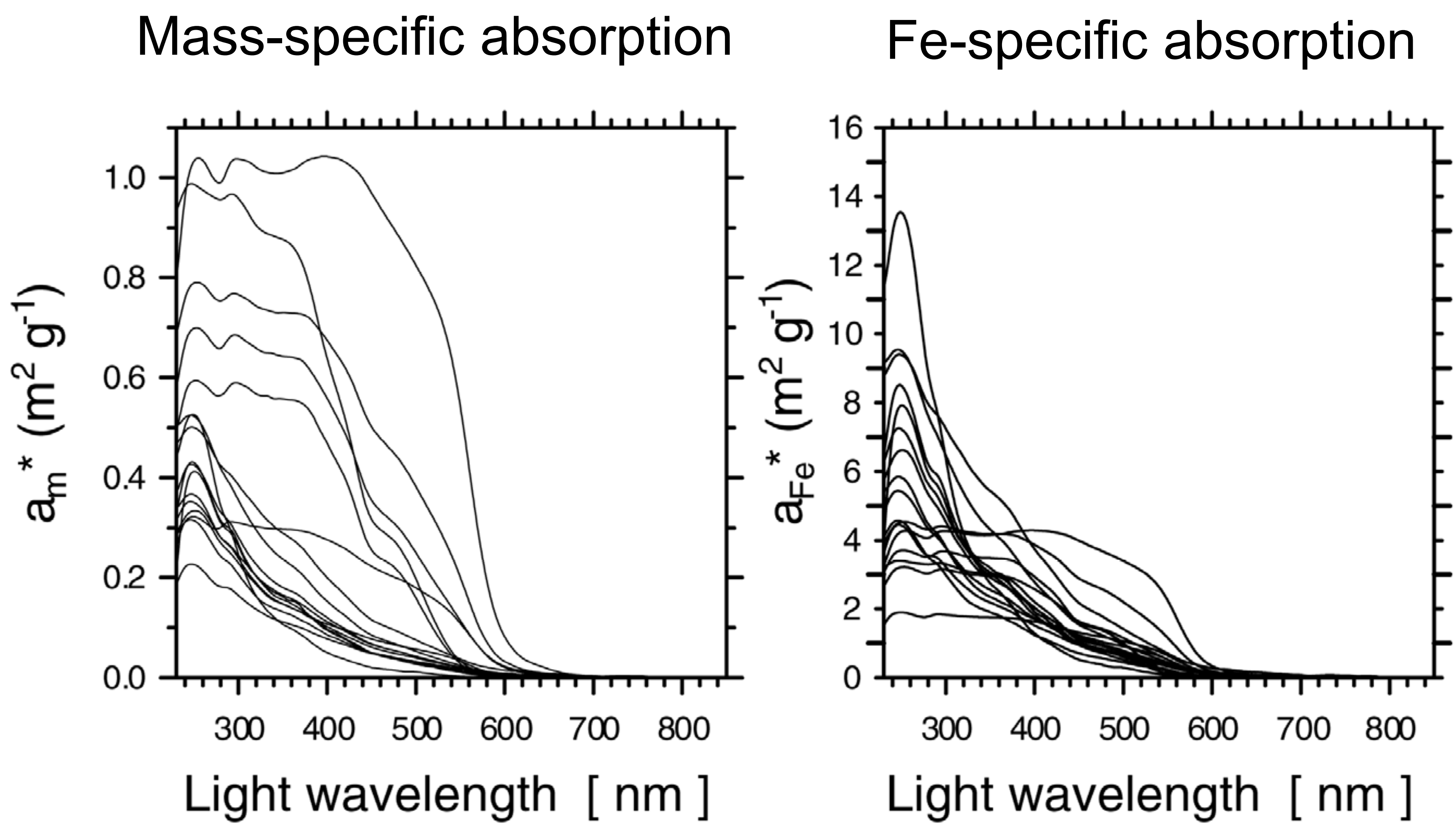

(Babin and Stramski 2004)

Size distributions of colloids

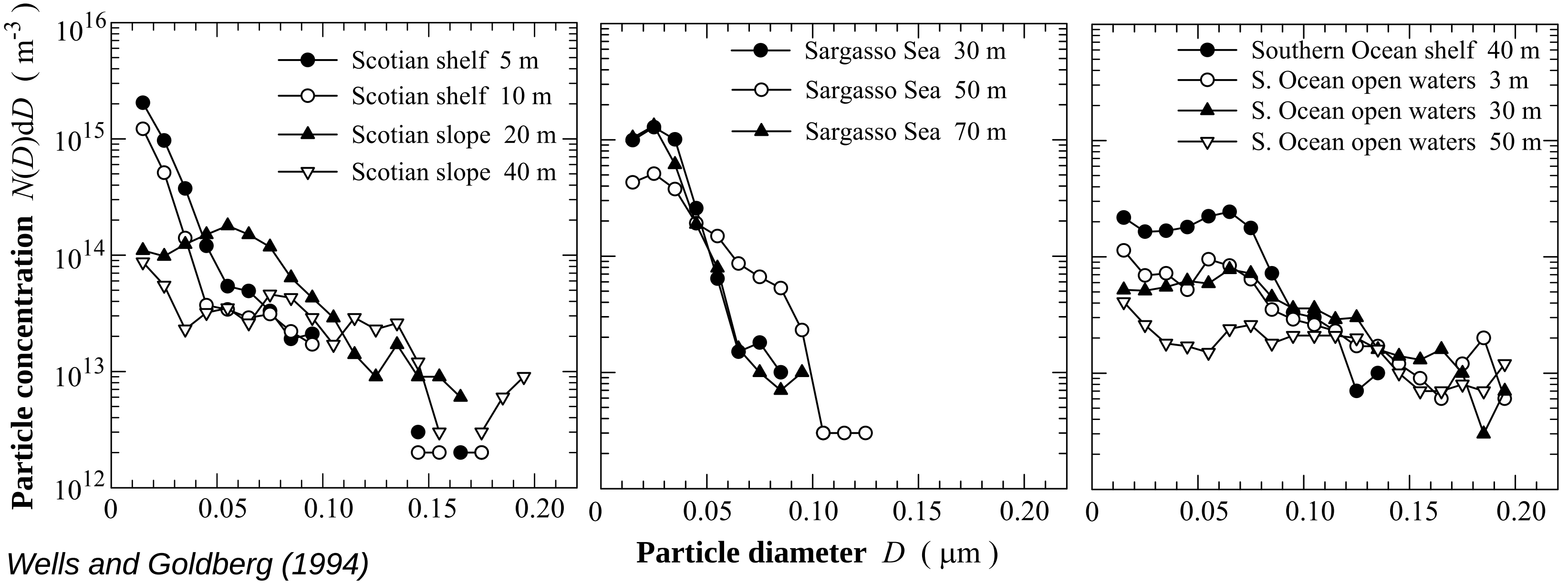

Wells and Goldberg (1994)

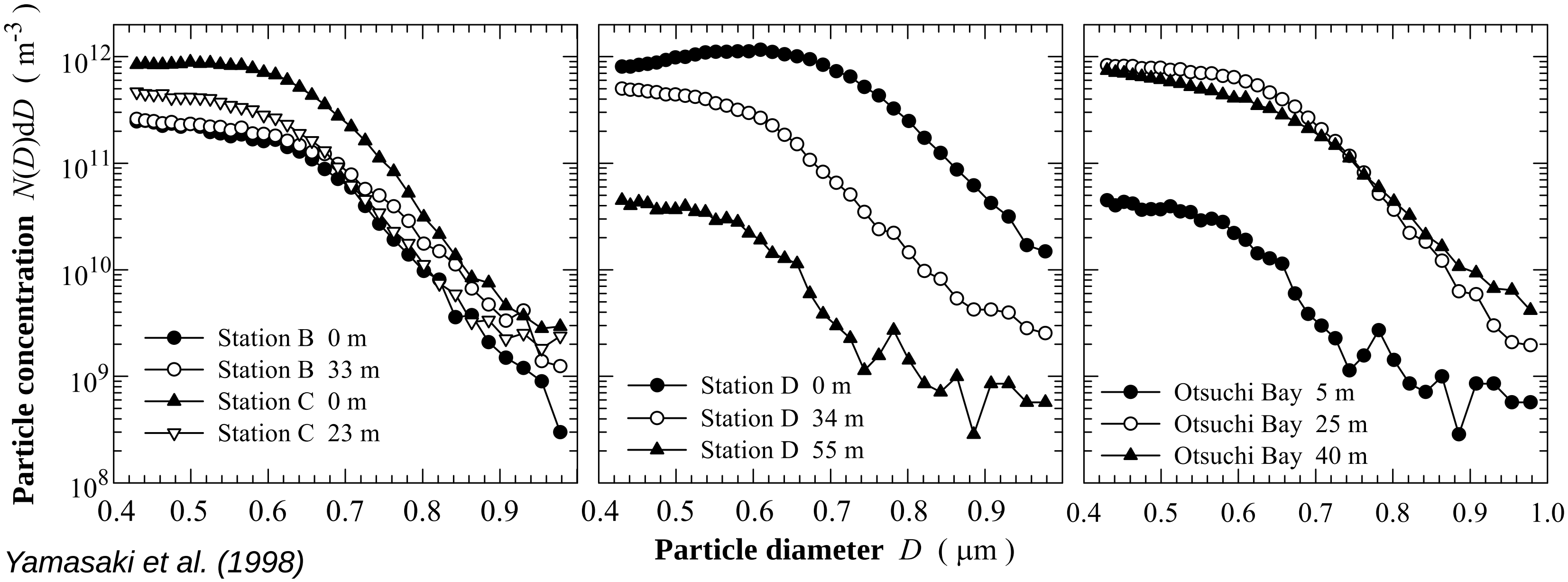

Yamasaki et al. (1998)

Results for colloidal particles

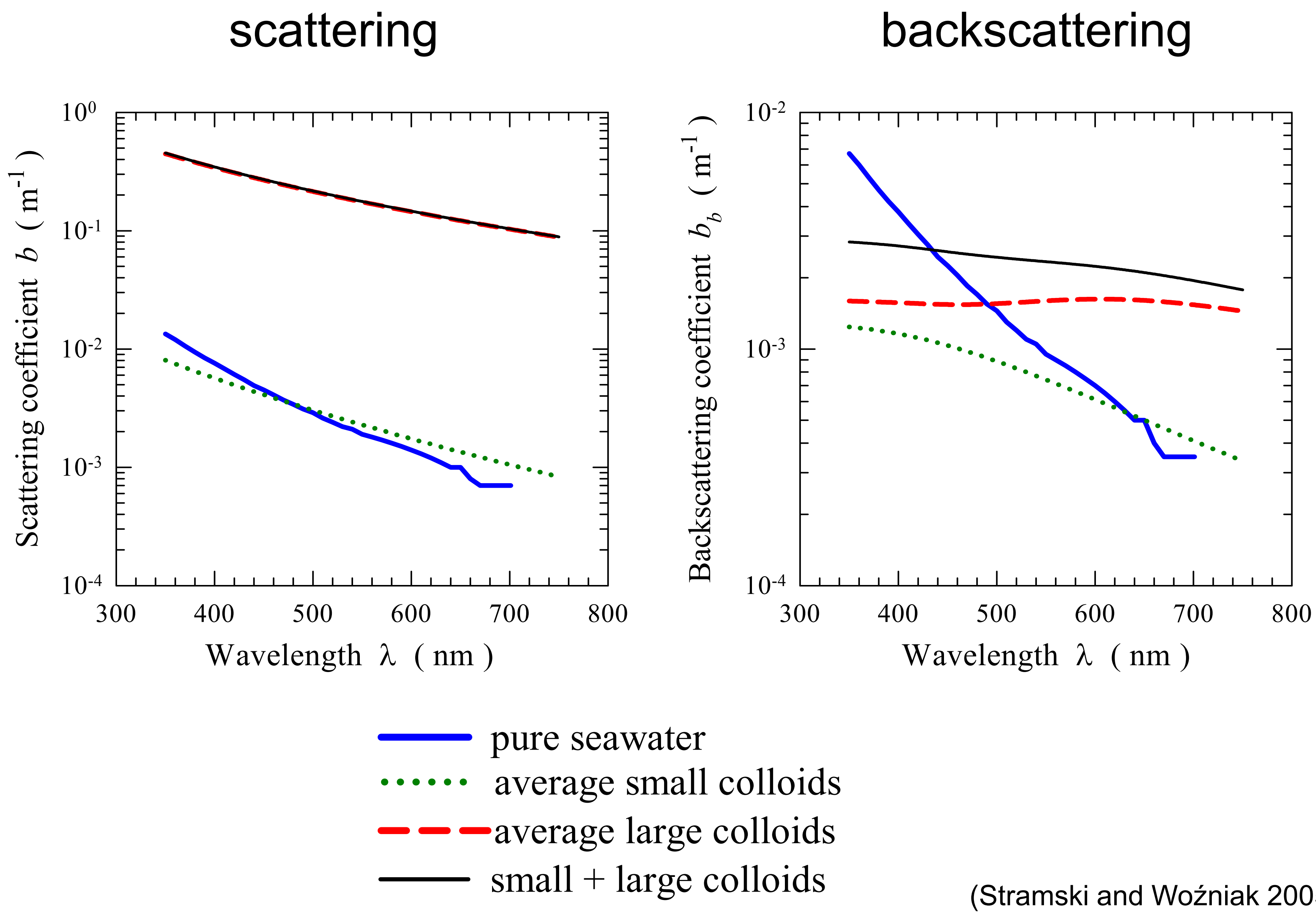

(Stramski and Woźniak 2005)

Scattering budget in terms of particle size fractions

Low-index particles

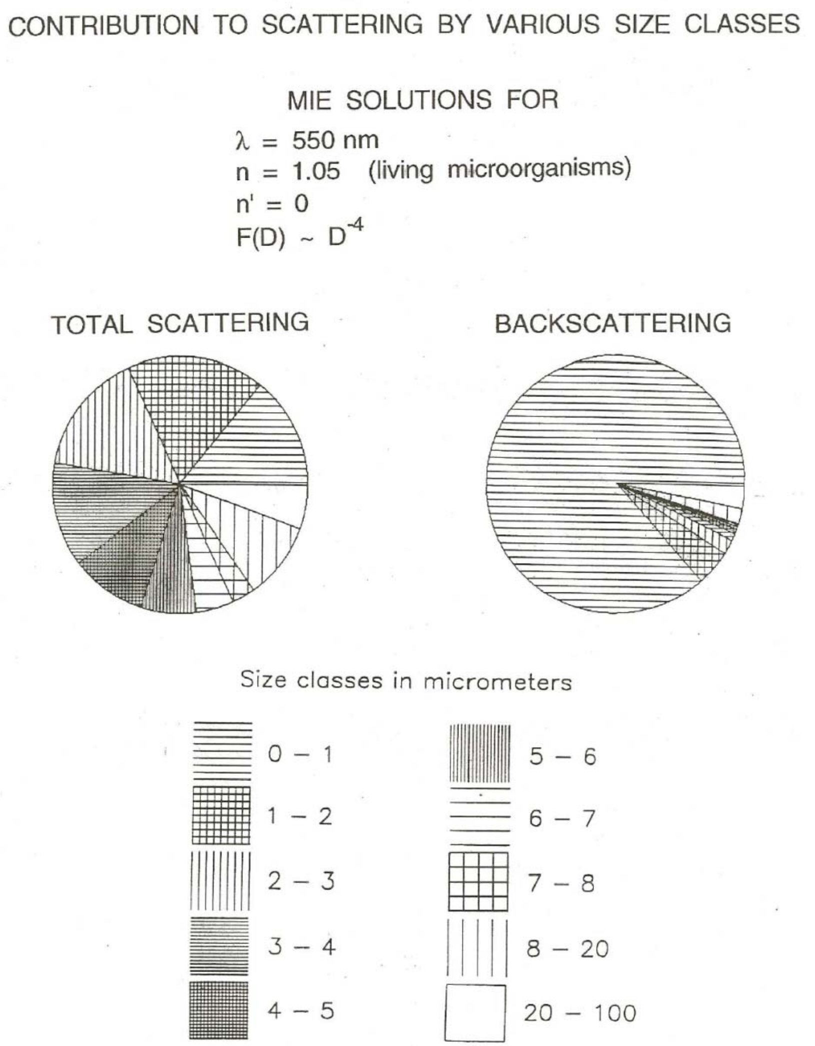

High-index particles

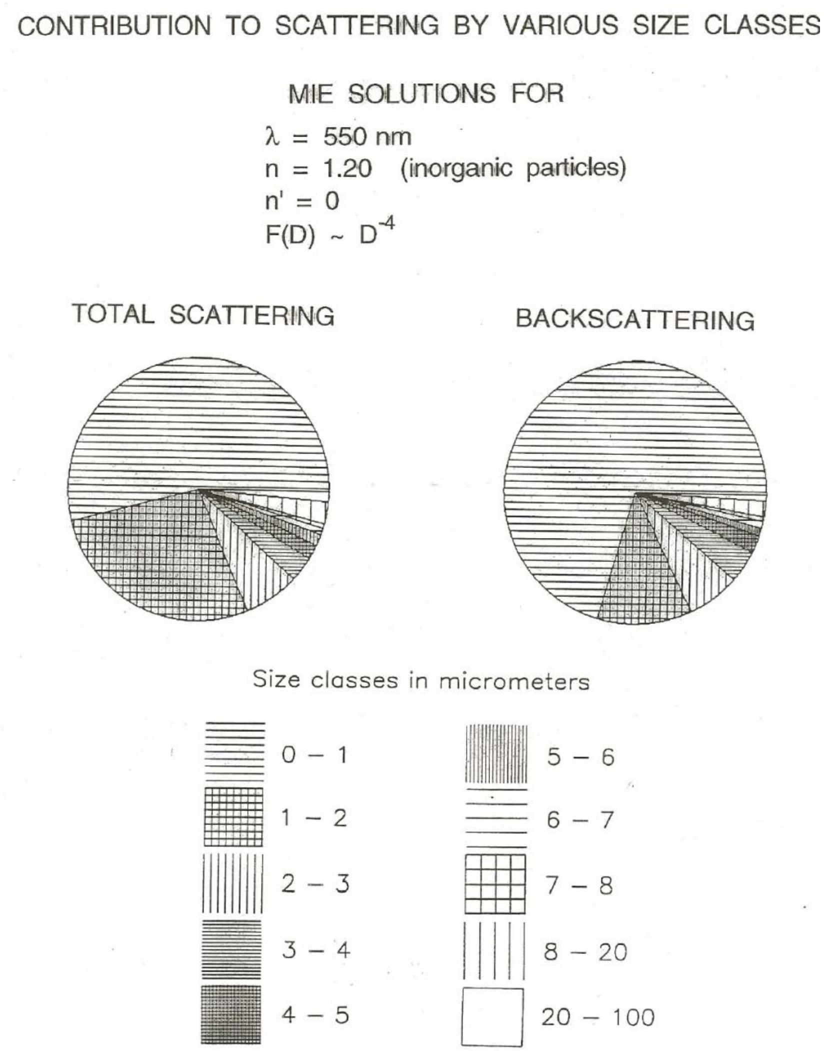

(Stramski and Kiefer 1991)

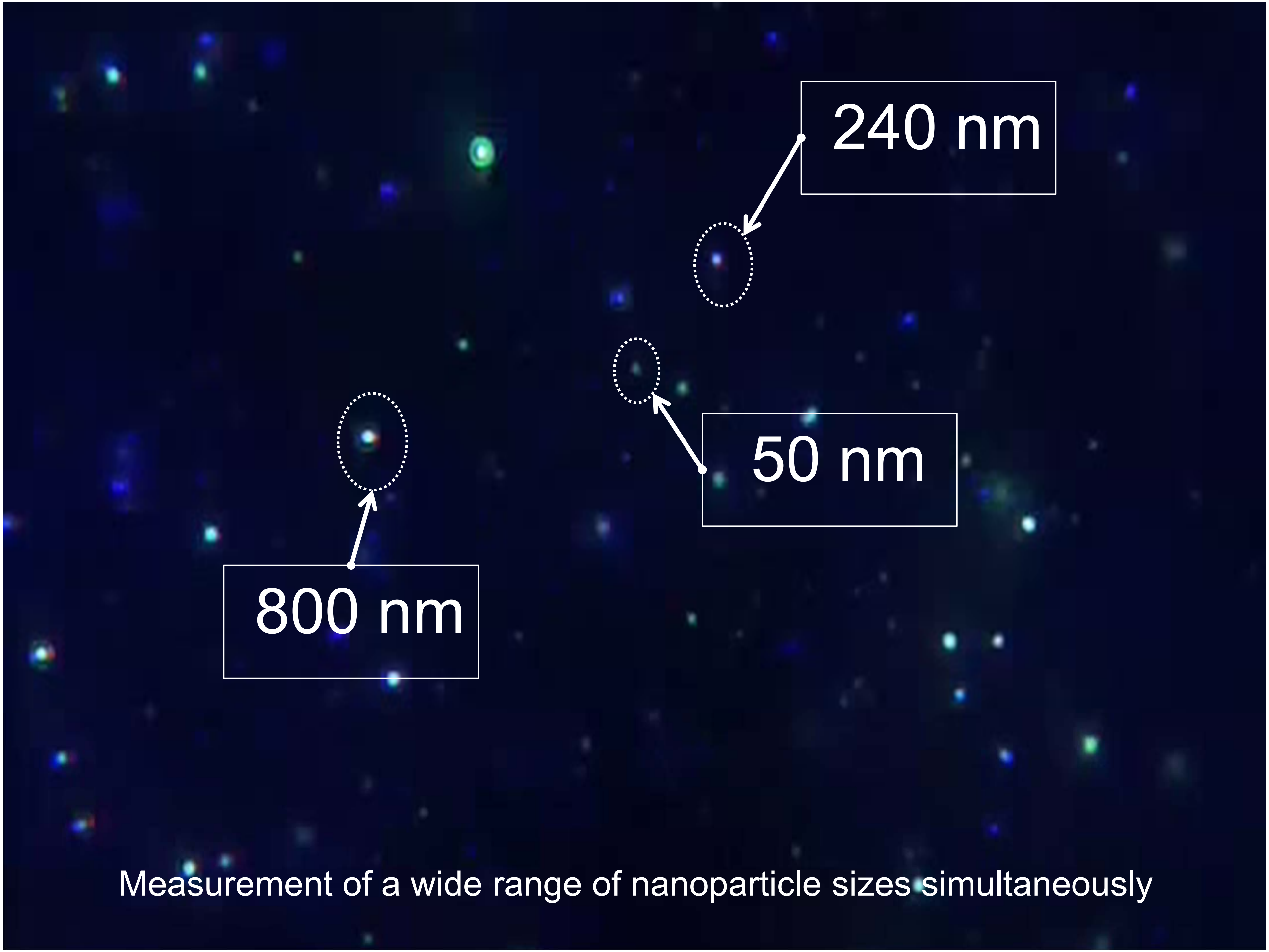

Measurement of a wide range of nanoparticle sizes simultaneously

A superposition of 300 video frames acquired during 10 seconds illustrating trajectories of individual nanoparticles through time

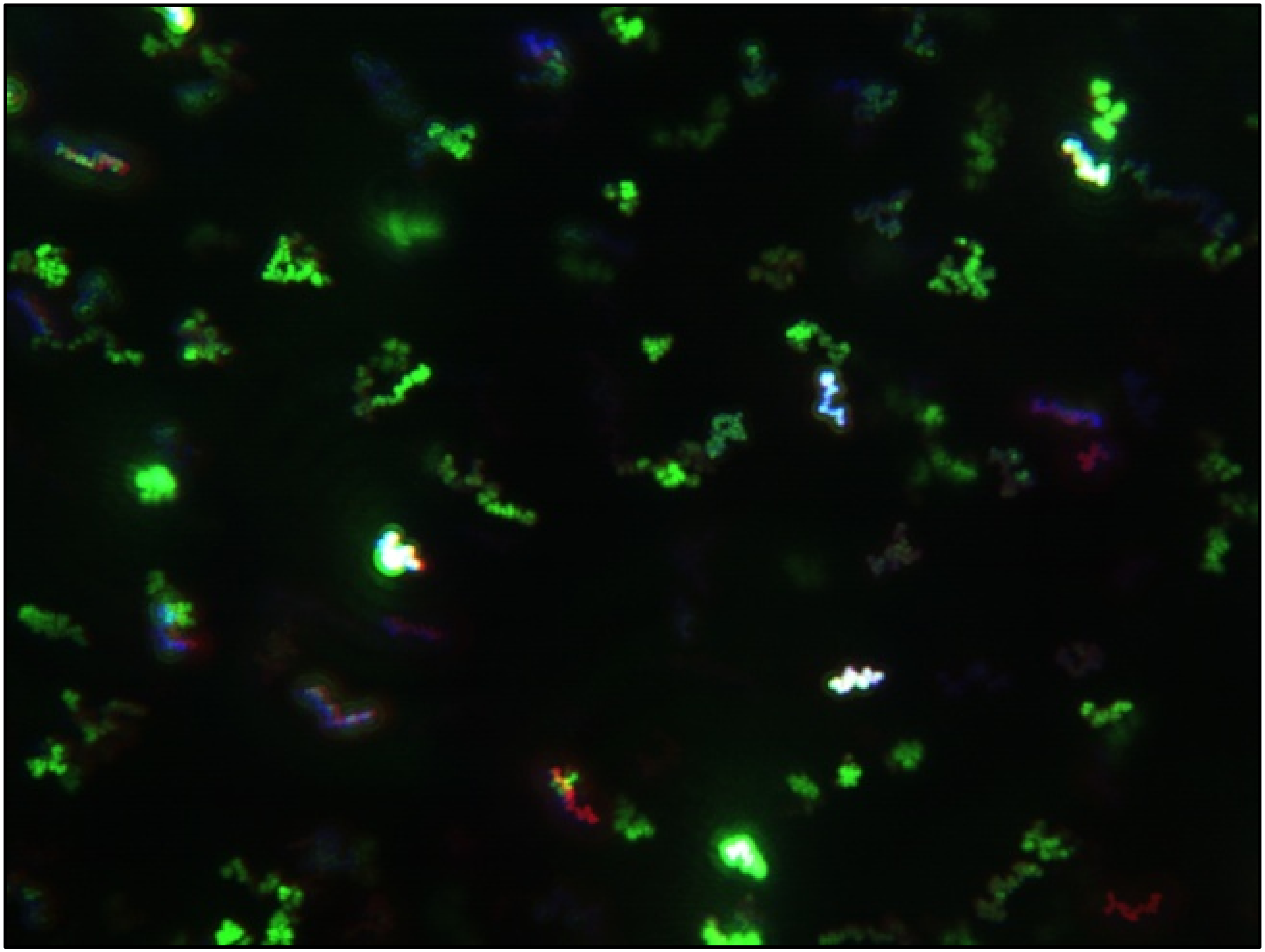

A mix of polystyrene nanosphere size standards of 50, 240, and 800 nm in diameter suspended in water

1905 Albert Einstein's Year of Miracles: One of four "Annus Mirabilis" papers:

5. *Über die von der molekularkinetischen Theorie der Wärme geforderte Bewegung von in ruhenden Flüssigkeiten suspendierten Teilchen;* *von A. Einstein.*

In dieser Arbeit soll gezeigt werden, daß nach der molekularkinetischen Theorie der Wärme in Flüssigkeiten suspendierte Körper von mikroskopisch sichtbarer Größe infolge der Molekularbewegung der Wärme Bewegungen von solcher Größe ausführen müssen, daß diese Bewegungen leicht mit dem Mikroskop nachgewiesen werden können. Es ist möglich, daß die hier zu behandelnden Bewegungen mit der sogenannten „Brownschen Molekularbewegung" identisch sind; die mir erreichbaren Angaben über letztere sind jedoch so ungenau, daß ich mir hierüber kein Urteil bilden konnte.

Wenn sich die hier zu behandelnde Bewegung samt den für sie zu erwartenden Gesetzmäßigkeiten wirklich beobachten läßt, so ist die klassische Thermodynamik schon für mikroskopisch unterscheidbare Räume nicht mehr als genau gültig anzusehen und es ist dann eine exakte Bestimmung der wahren Atomgröße möglich. Erwiese sich umgekehrt die Voraussage dieser Bewegung als unzutreffend, so wäre damit ein schwerwiegendes Argument gegen die molekularkinetische Auffassung der Wärme gegeben.

§ 1. Über den suspendierten Teilchen zuzuschreibenden osmotischen Druck.

Im Teilvolumen V^* einer Flüssigkeit vom Gesamtvolumen V seien z-Gramm-Moleküle eines Nichtelektrolyten gelöst. Ist das Volumen V^* durch eine für das Lösungsmittel, nicht aber für die gelöste Substanz durchlässige Wand vom reinen Lösungs-

ON THE MOVEMENT OF SMALL PARTICLES SUSPENDED IN STATIONARY LIQUIDS REQUIRED BY THE MOLECULAR-KINETIC THEORY OF HEAT

by A. Einstein

[*Annalen der Physik* 17 (1905): 549-560]

It will be shown in this paper that, according to the molecular-kinetic theory of heat, bodies of microscopically visible size suspended in liquids must, as a result of thermal molecular motions, perform motions of such magnitude that these motions can easily be detected by a microscope. It is possible that the motions to be discussed here are identical with the so-called "Brownian molecular motion"; however, the data available to me on the latter are so imprecise that I could not form a definite opinion on this matter.

If it is really possible to observe the motion to be discussed here, along with the laws it is expected to obey, then classical thermodynamics can no longer be viewed as strictly valid even for microscopically distinguishable spaces, and an exact determination of the real size of atoms becomes possible. Conversely, if the prediction of this motion were to be proved wrong, this fact would provide a weighty argument against the molecular-kinetic conception of heat.

$$D = \frac{k_B\, T}{3\, \pi\, \eta\, D_{diff}}$$

D – diameter of particle

D_{diff} – diffusion coefficient of particle

T – temperature of the liquid medium (seawater)

η – dynamic viscosity of the medium (seawater)

k_B - Boltzmann constant

Light scattering by bubbles entrained by wave breaking

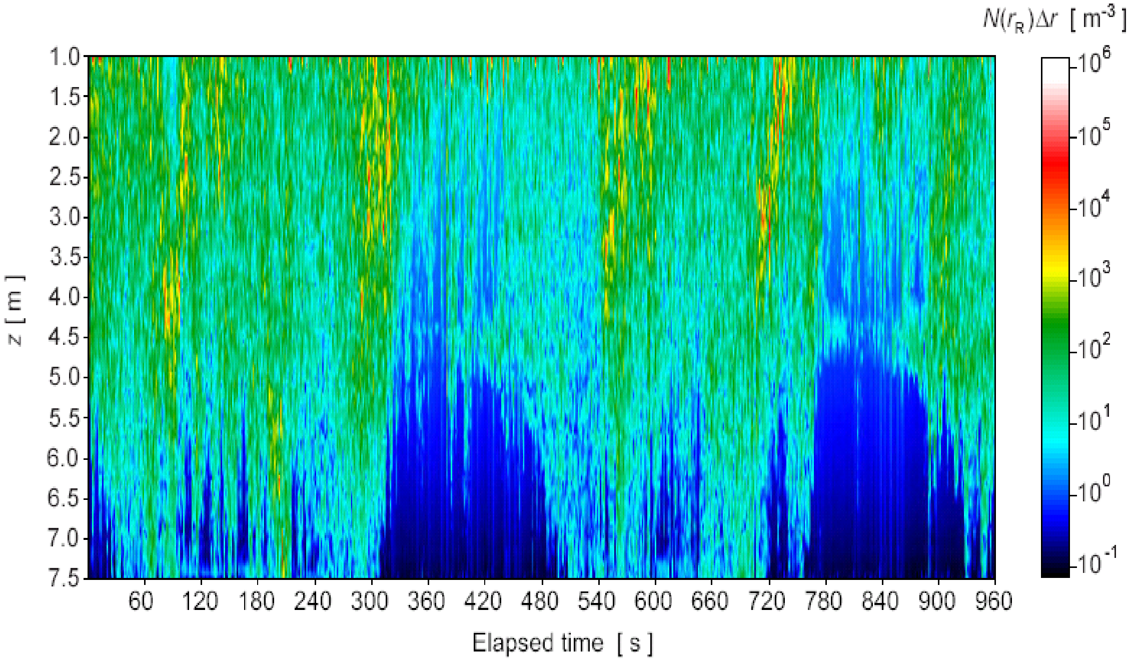

(Stramski and Tęgowski 2001)

Scattering and backscattering by bubbles as a function of void fraction

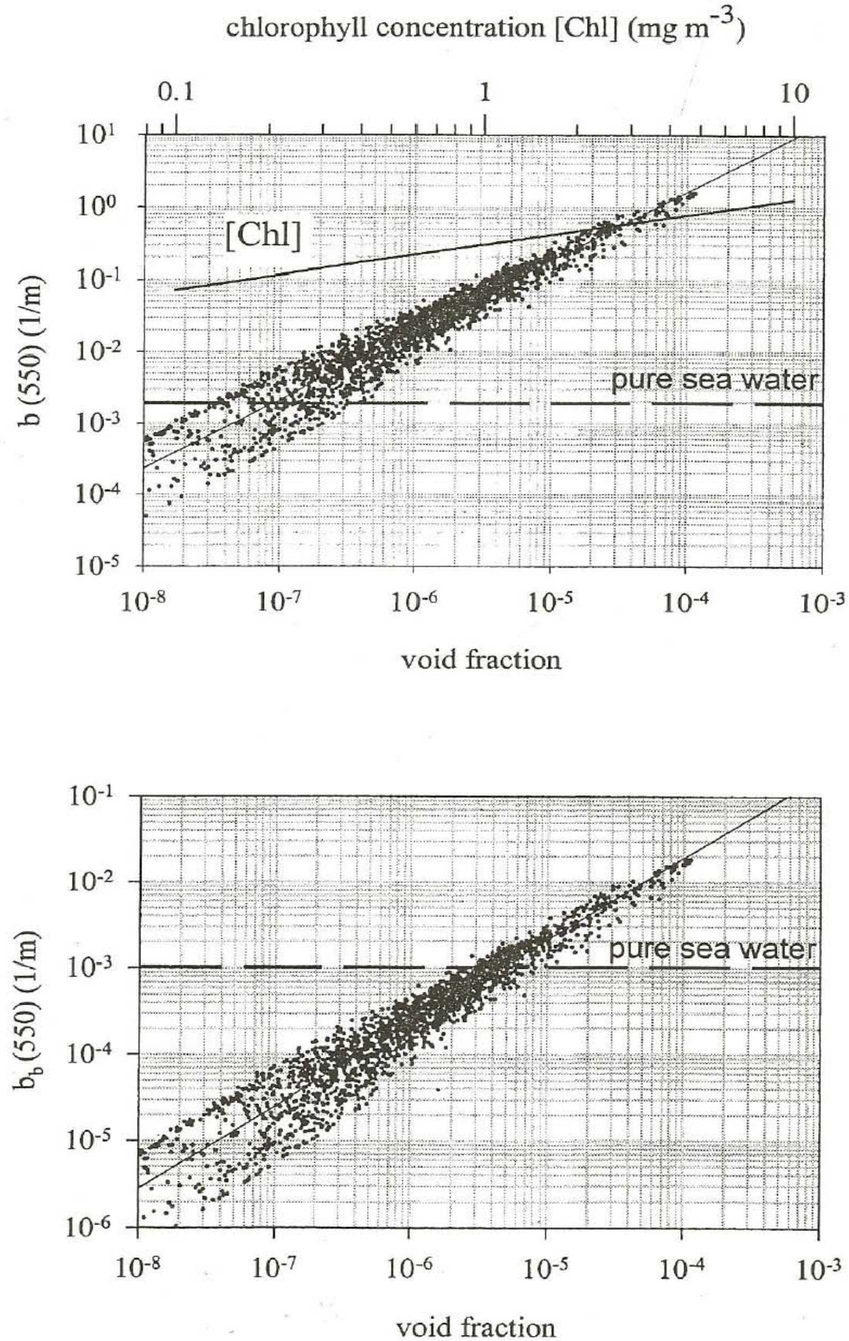

(Terrill et al. 2001)

Traditional approach

Inherent Optical Properties (IOPs) described in terms of a few broadly-defined categories of seawater constituents

$$IOP(\lambda) = IOP_w(\lambda) + IOP_p(\lambda) + IOP_{CDOM}(\lambda)$$

$$IOP_p(\lambda) = IOP_{ph}(\lambda) + IOP_{NAP}(\lambda)$$

Example IOPs:

absorption coefficient, scattering coefficient,

beam attenuation coefficient, volume scattering function

A four-component model of absorption

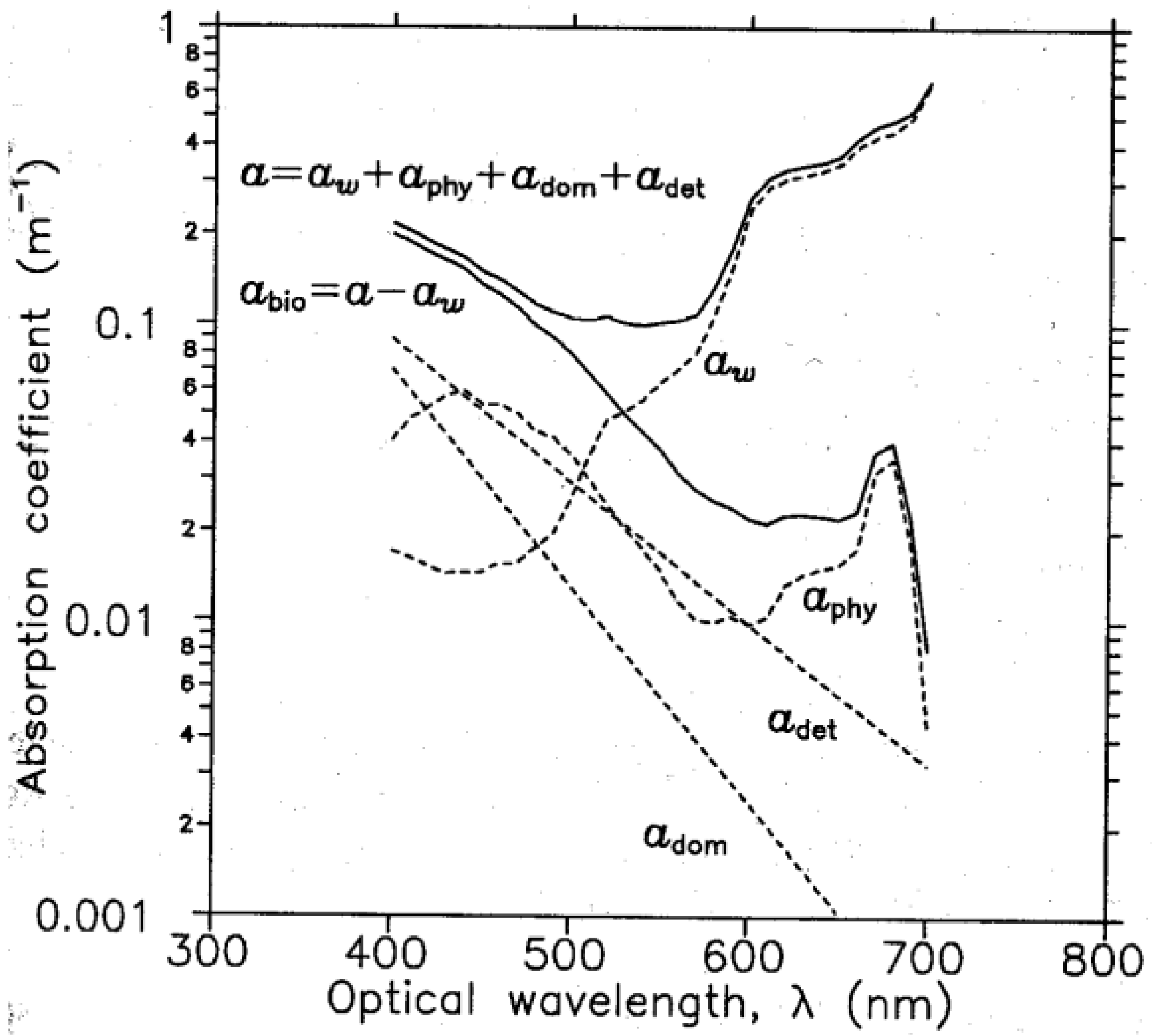

Examples of particulate absorption coefficients a_p, $a_{d\ or\ NAP}$, a_{ph} (data from the Sargasso Sea)

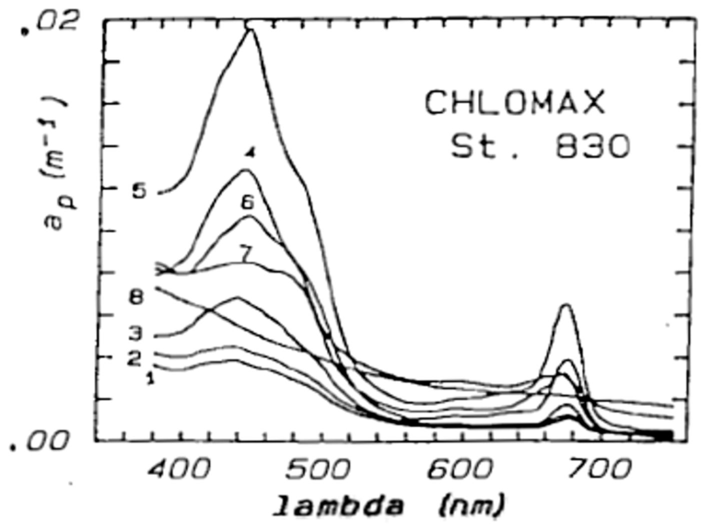

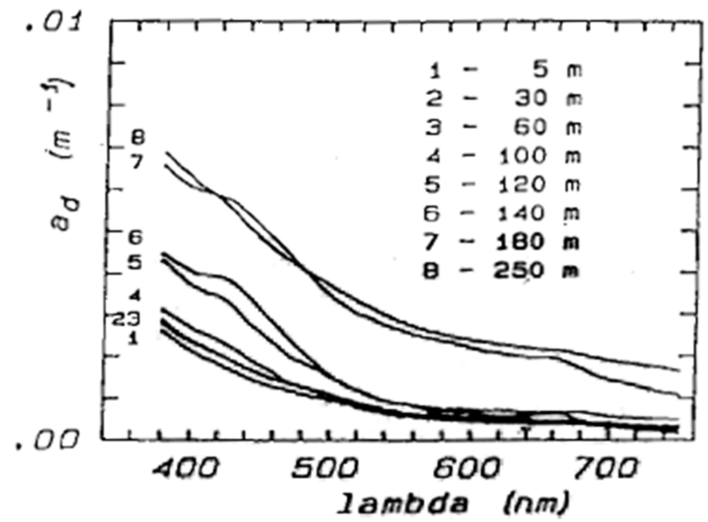

$a_{ph} = a_p - a_{d\ or\ NAP}$

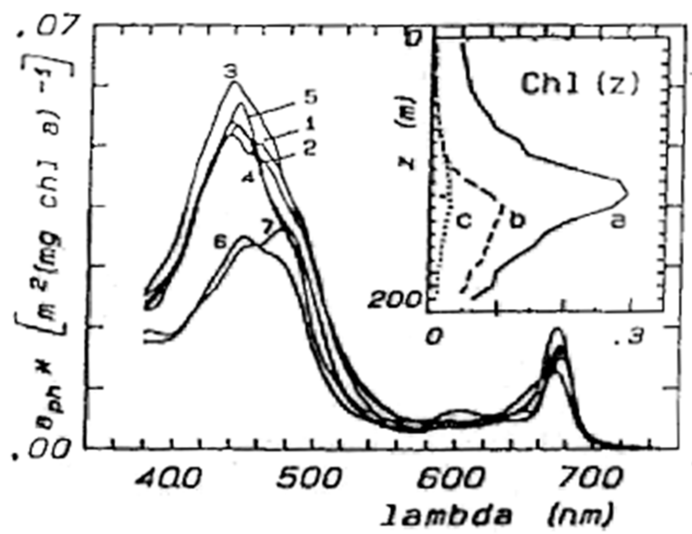

(Bricaud and Stramski 1990)

Example non-algal particle (NAP) absorption spectra and the corresponding exponential fits for different regions

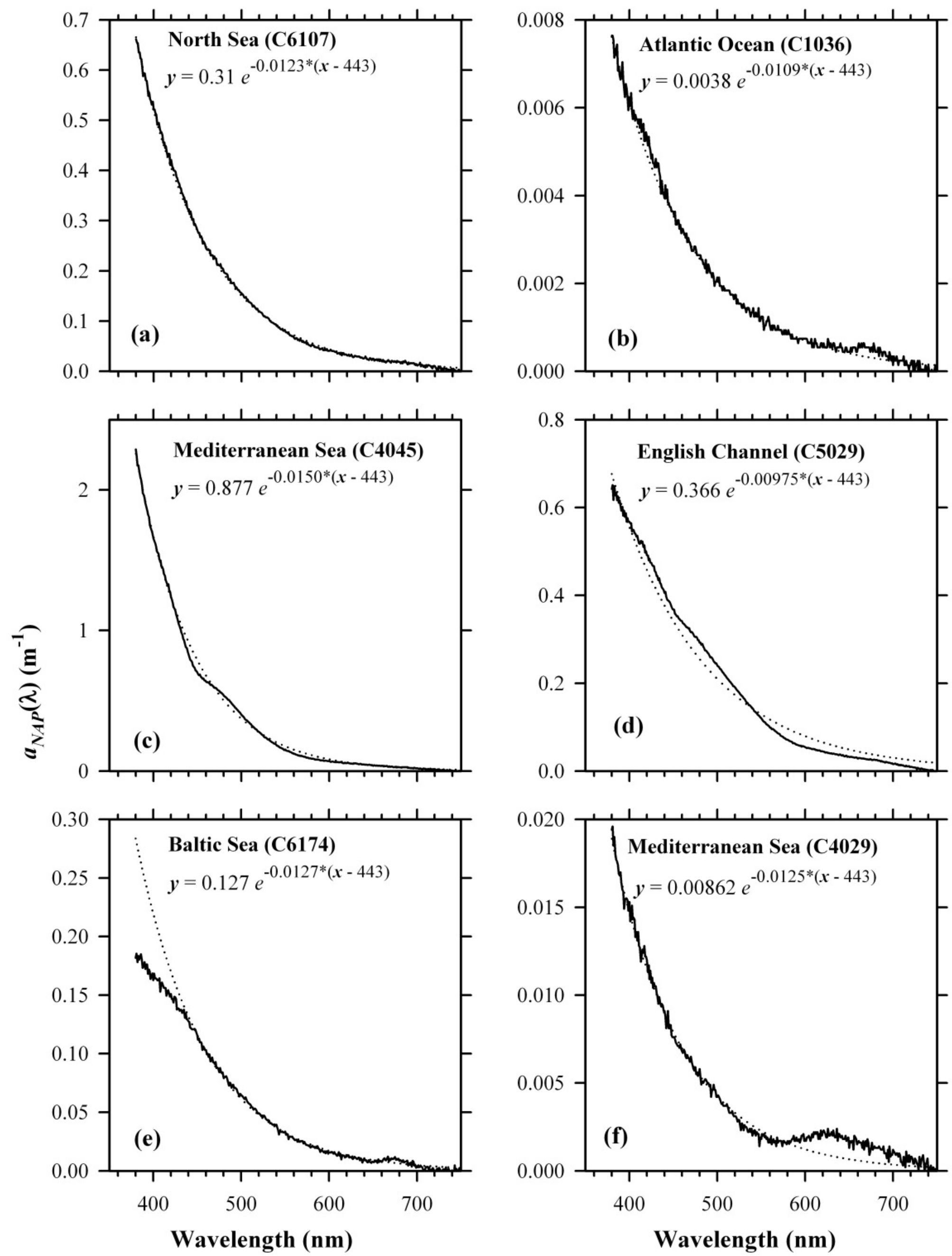

(Babin et al. 2003)

Frequency distribution of spectral slope of NAP absorption

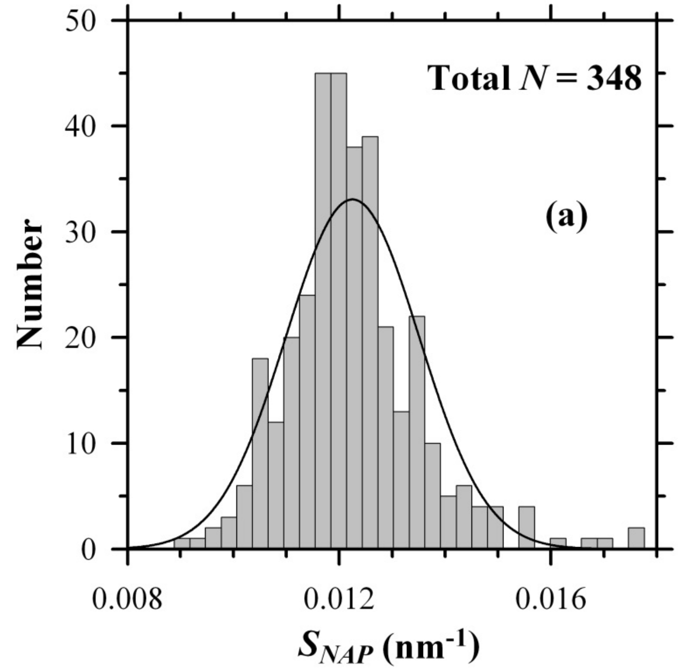

NAP absorption spectra calculated with $a_{NAP}(443)$=1 m^{-1} and S_{NAP} = 0.0123 nm^{-1} (±1.96 standard deviation, where SD=0.0013 nm^{-1})

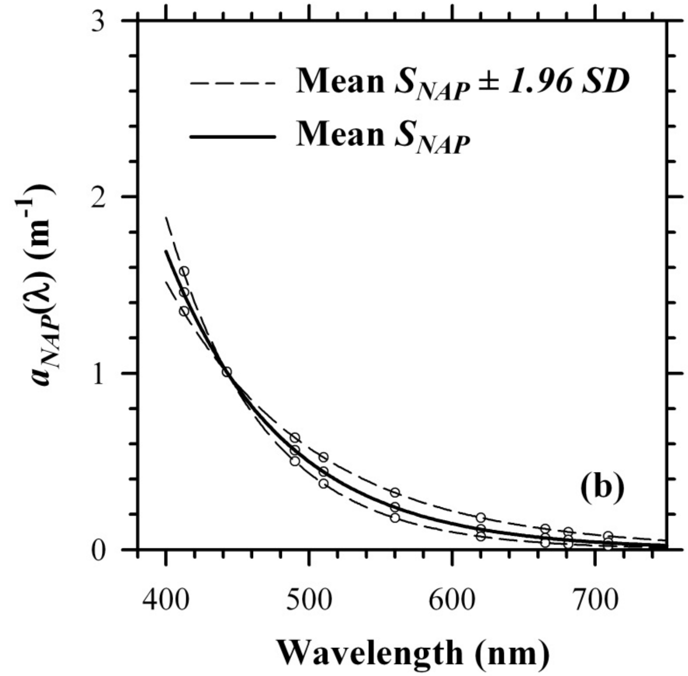

(Babin et al. 2003)

Chlorophyll-based approach

$$IOP(\lambda) = IOP_w(\lambda) + f\,[\,Chla\,]$$

for example $a_{ph}(\lambda) = f\,[\,Chla\,]$

$$a_p(\lambda) = f\,[\,Chla\,]$$

$AOP(\lambda)$ (*e.g.*, ocean reflectance) $= f\,[\,Chla\,]$

Case 1 and Case 2 Waters

CASE 1 WATERS

LIVING ALGAL CELLS
variable concentration

ASSOCIATED DEBRIS
Originating from grazing by zooplankton and natural decay

DISSOLVED ORGANIC MATTER
liberated by algae and their debris (yellow substance)

RESUSPENDED SEDIMENTS
from bottom along the coastline and in shallow areas

TERRIGENOUS PARTICLES
river and glacial runoff

DISSOLVED ORGANIC MATTER
land drainage (terrigenous yellow substance)

ANTHROPOGENIC INFLUX
particulate and dissolved materials

CASE 2 WATERS

Morel and Prieur (1977); Gordon and Morel (1983)

Absorption vs. chlorophyll-a

~ 4-fold variation

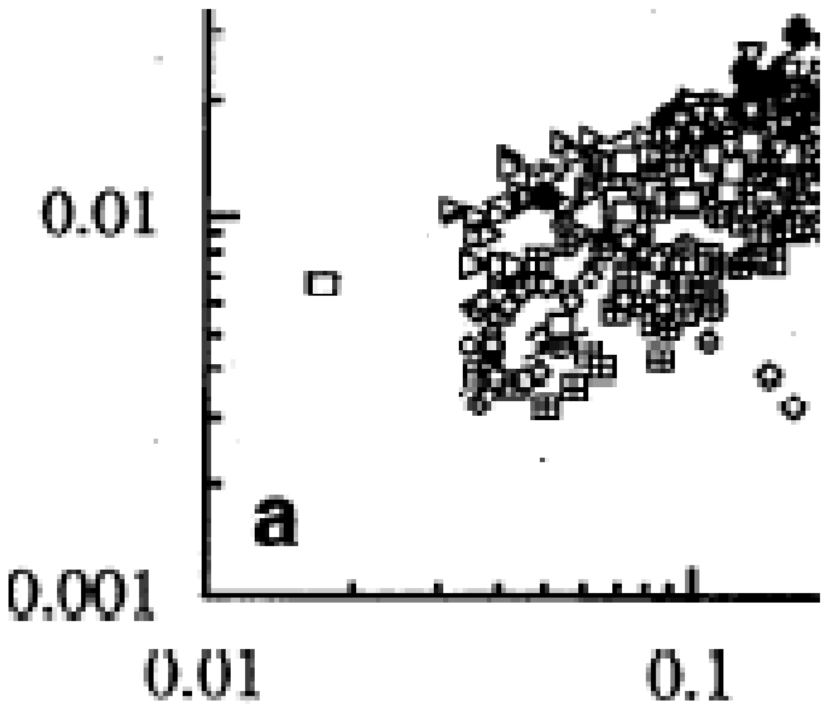

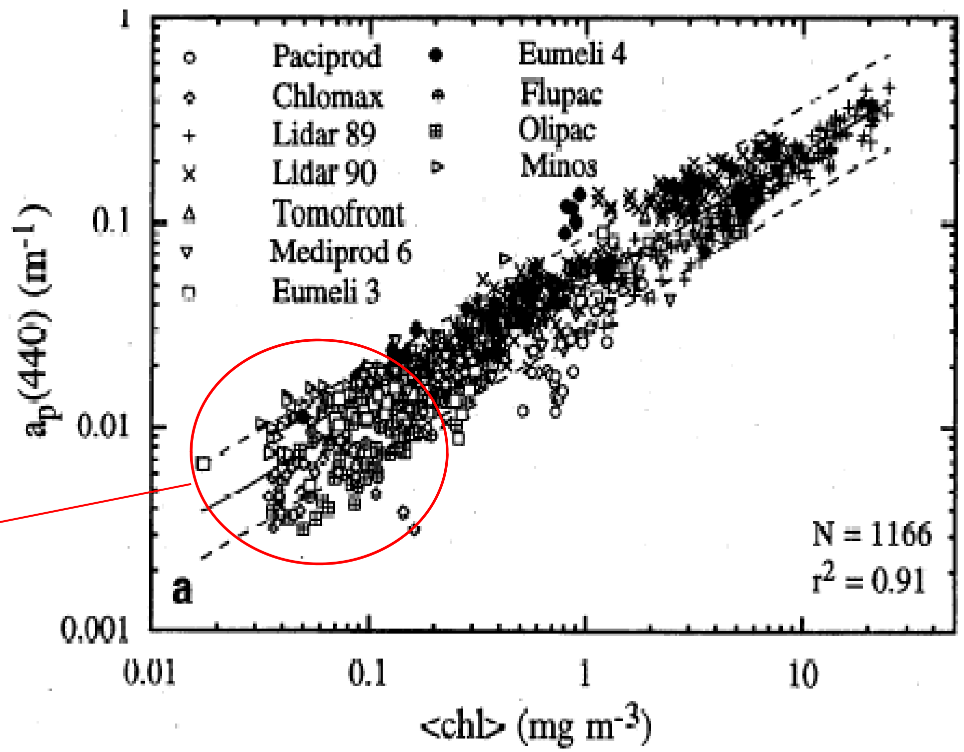

Cruise	Location
PACIPROD	Peru upwelling
CHLOMAX	Sargasso Sea
LIDAR 89	St. Lawrence estuary and gulf
LIDAR 90	St. Lawrence estuary and gulf
TOMOFRONT	northwestern Mediterranean
MEDIPROD 6	southwestern Mediterranean
EUMELI 3	tropical North Atlantic
EUMELI 4	tropical North Atlantic
FLUPAC	equatorial and subequatorial Pacific
OLIPAC	equatorial and subequatorial Pacific
MINOS	eastern and western Mediterranean

(Bricaud et al. 1998)

Beam attenuation vs. chlorophyll

> 10-fold variation

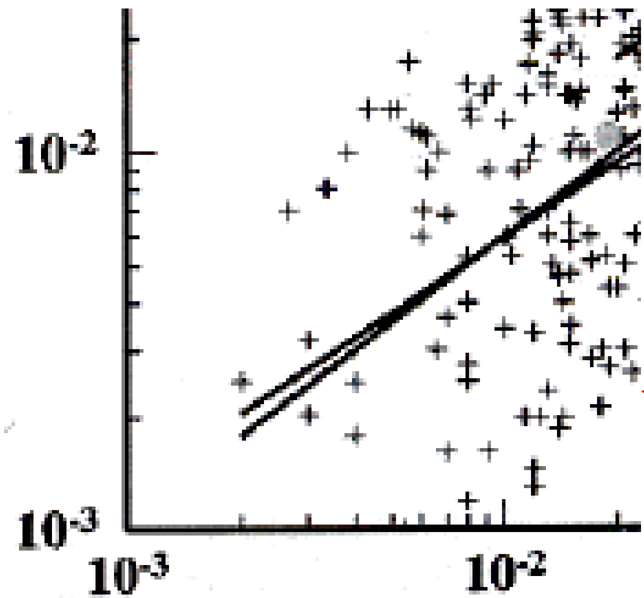

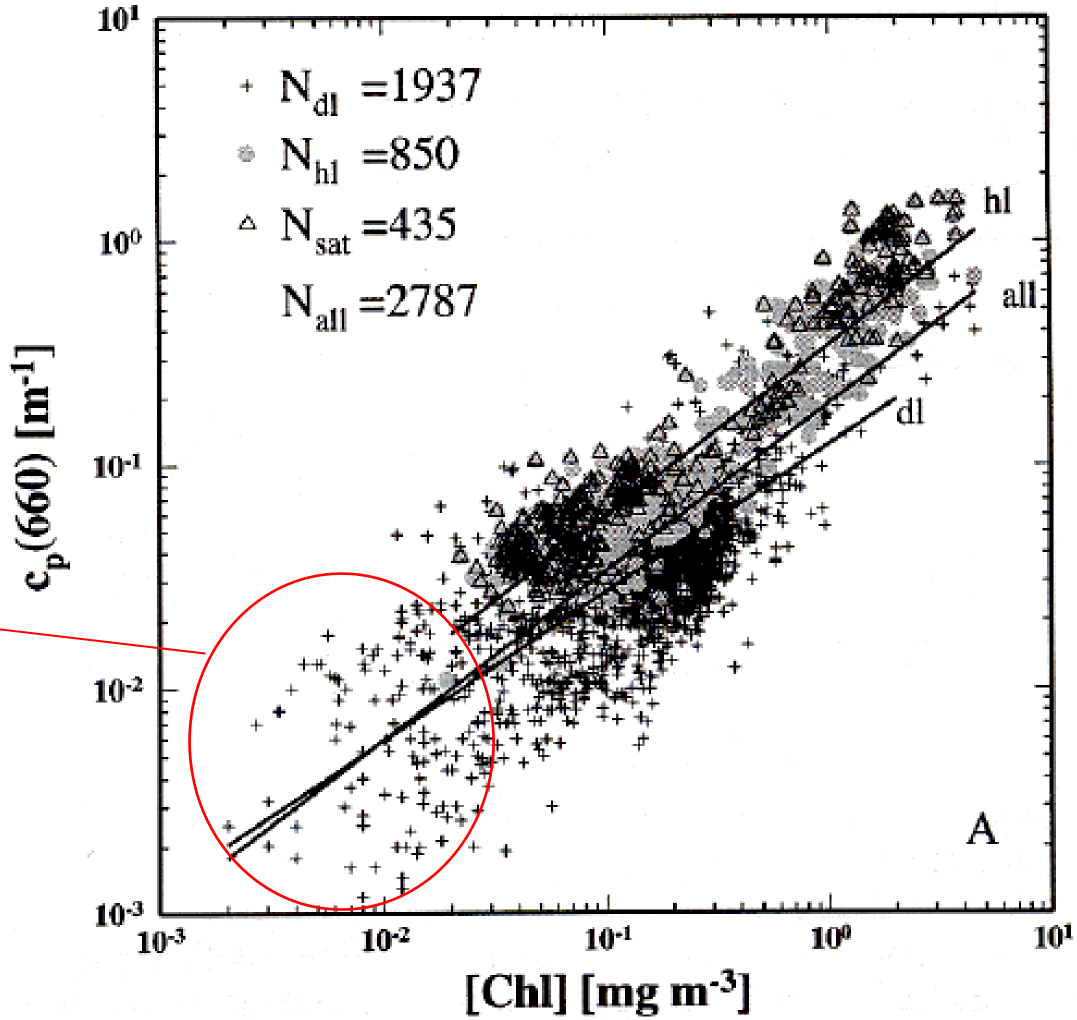

(Loisel and Morel 1998)

Chlorophyll-a algorithm

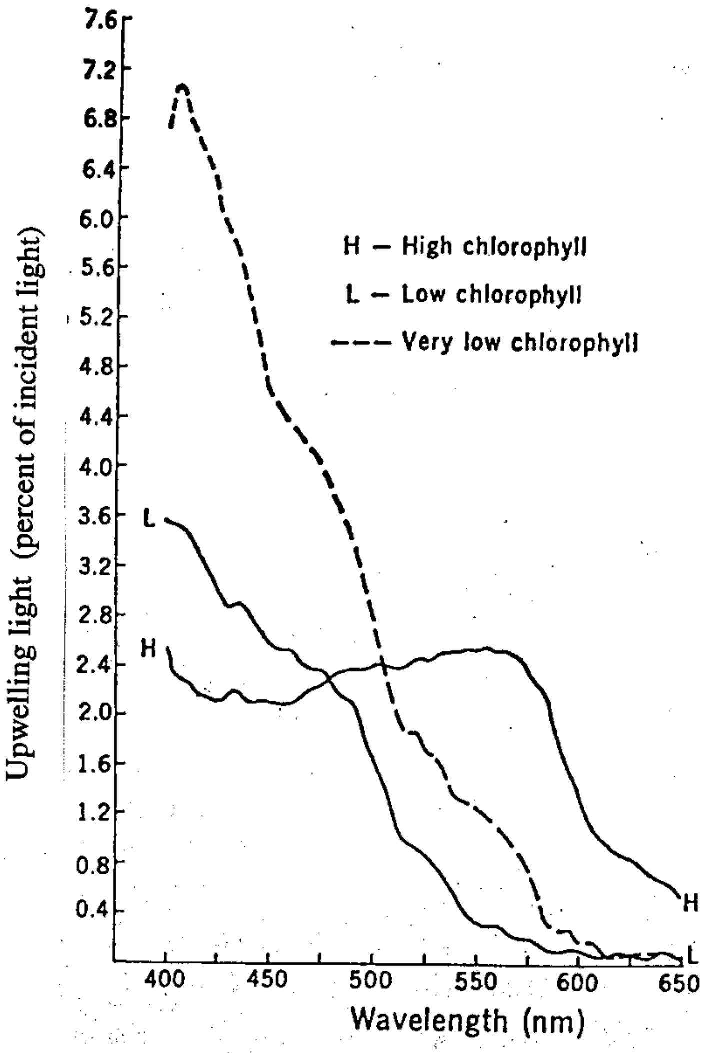

(Clarke, Ewing & Lorenzen 1970)

OC4 Algorithm

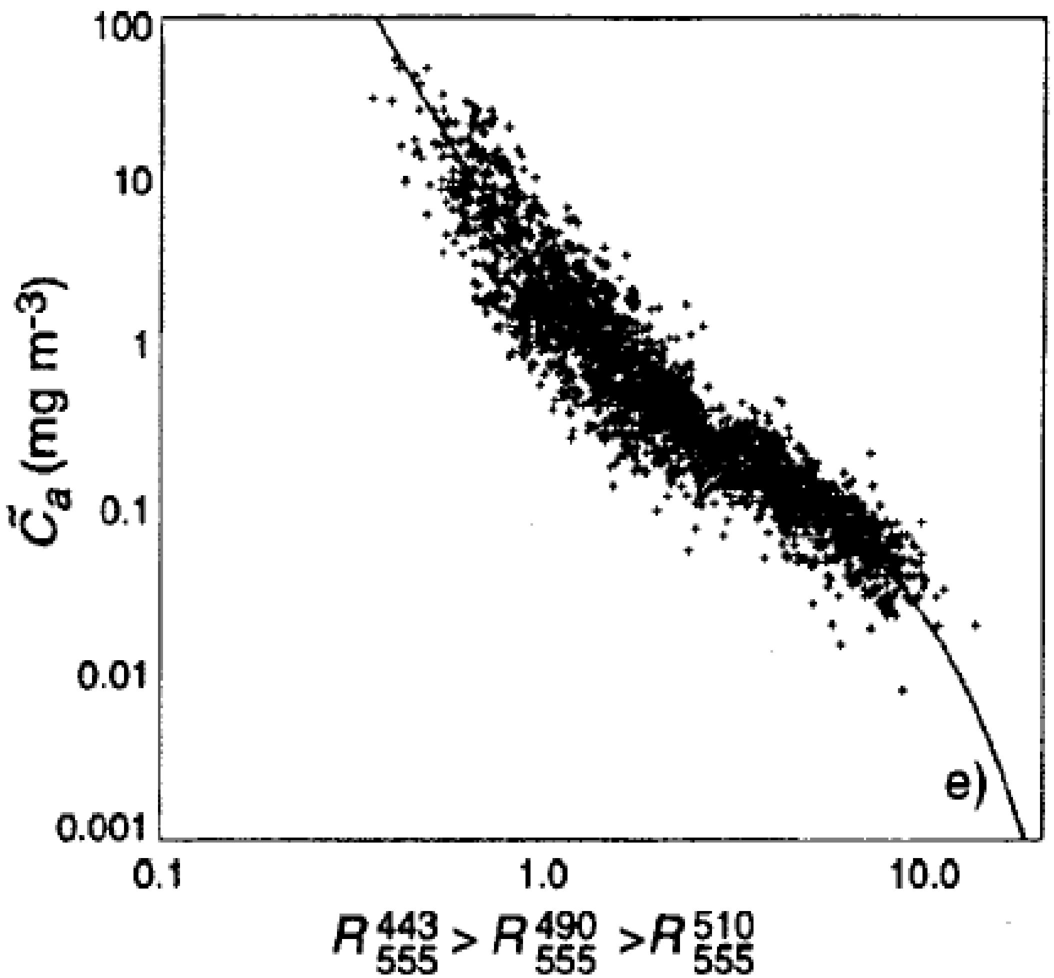

(O'Reilly et al. 2000)

Coastal Zone Color Scanner (CZCS)   1978 - 1985

First satellite image of global distribution of phytoplankton chlorophyll in the world's oceans from Coastal Zone Color Scanner

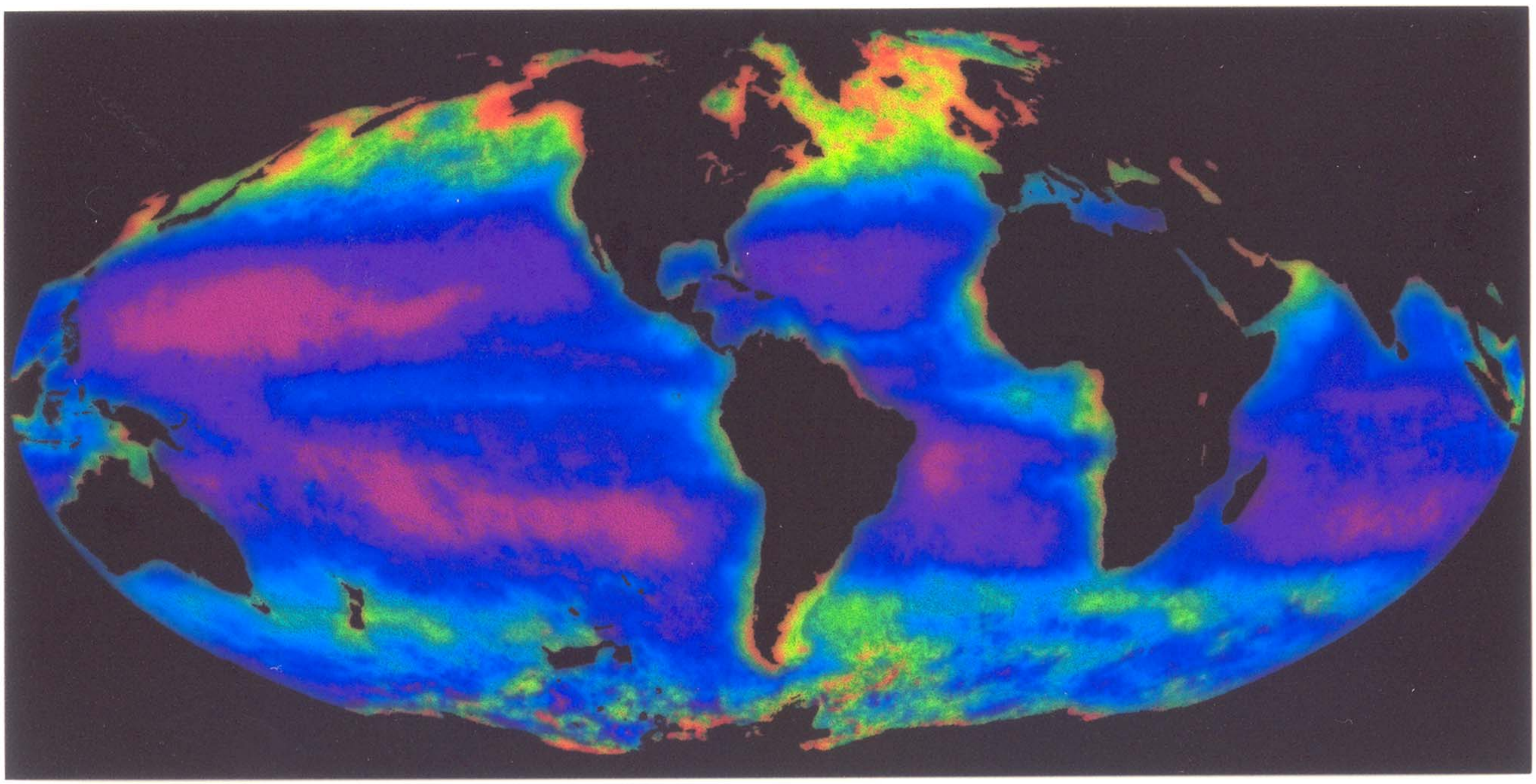

1997 - 2010

Sea-viewing Wide Field-of-view Sensor
(SeaWiFS)

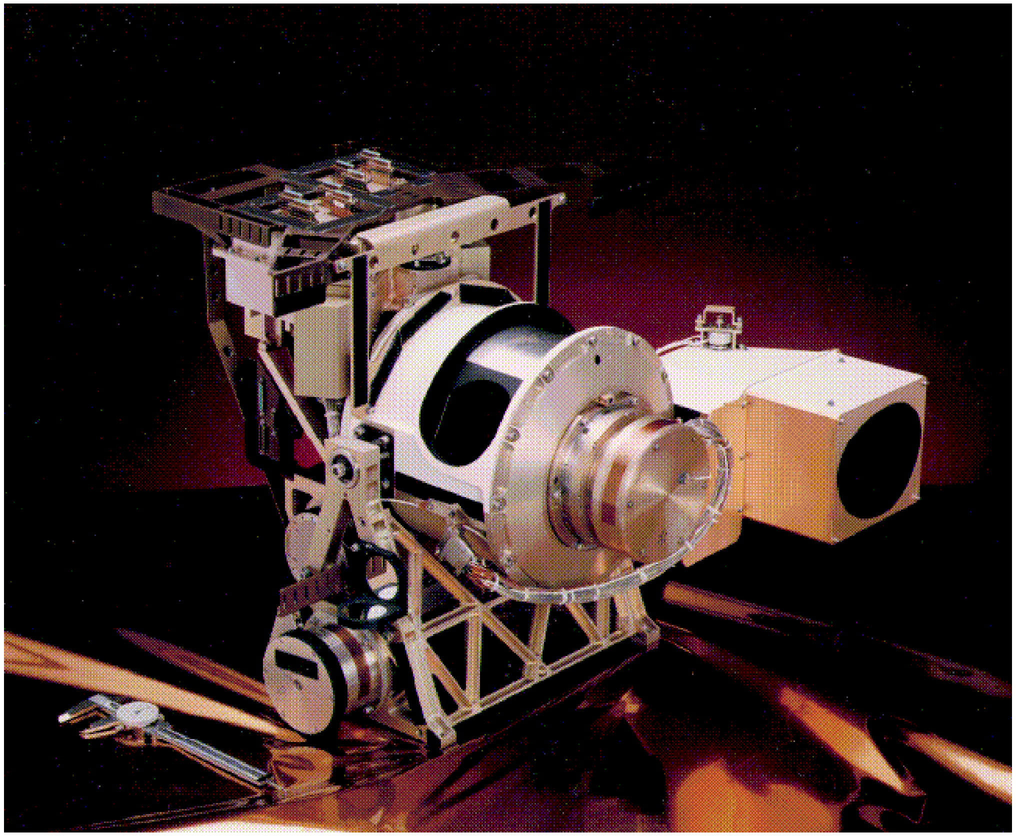

SeaStar spacecraft

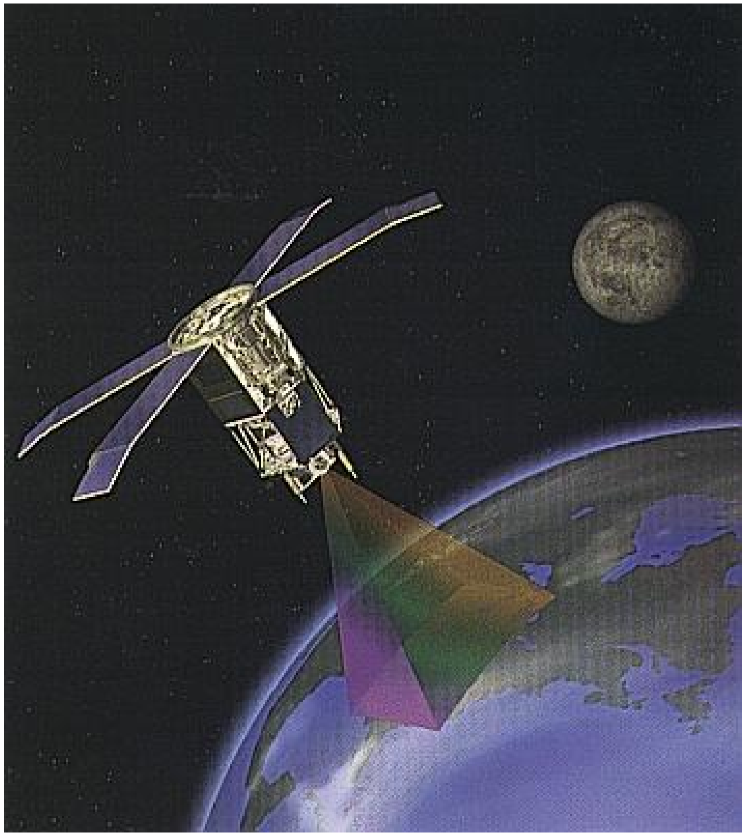

SeaStar orbits for remote sensing of ocean color

Global distribution of phytoplankton chlorophyll in the world's oceans from Sea-viewing Wide Field-of-view Sensor (SeaWiFS) based on Sep 1997 - Feb 2007 data

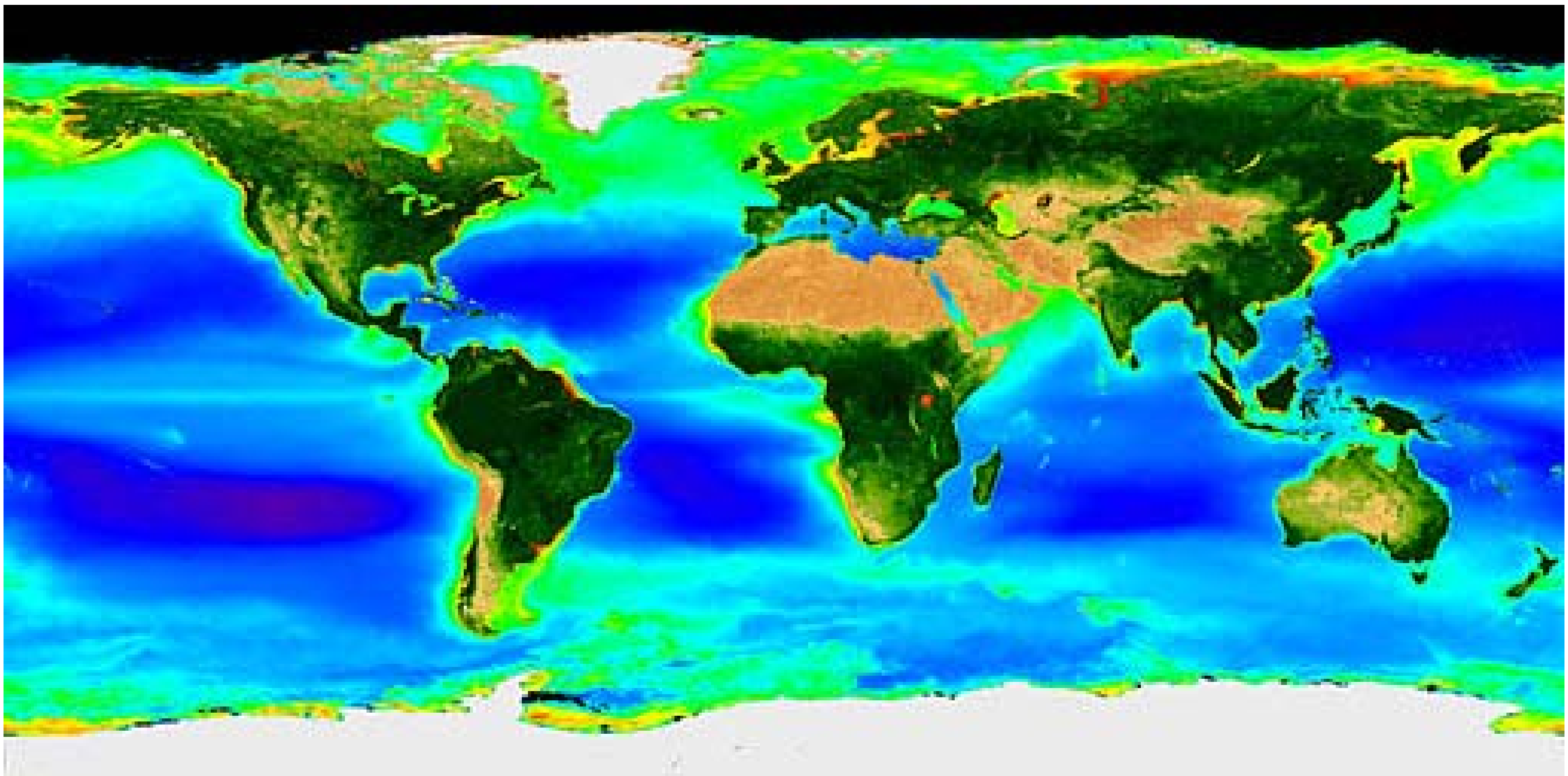

Courtesy of NASA

SeaWiFS July 2005

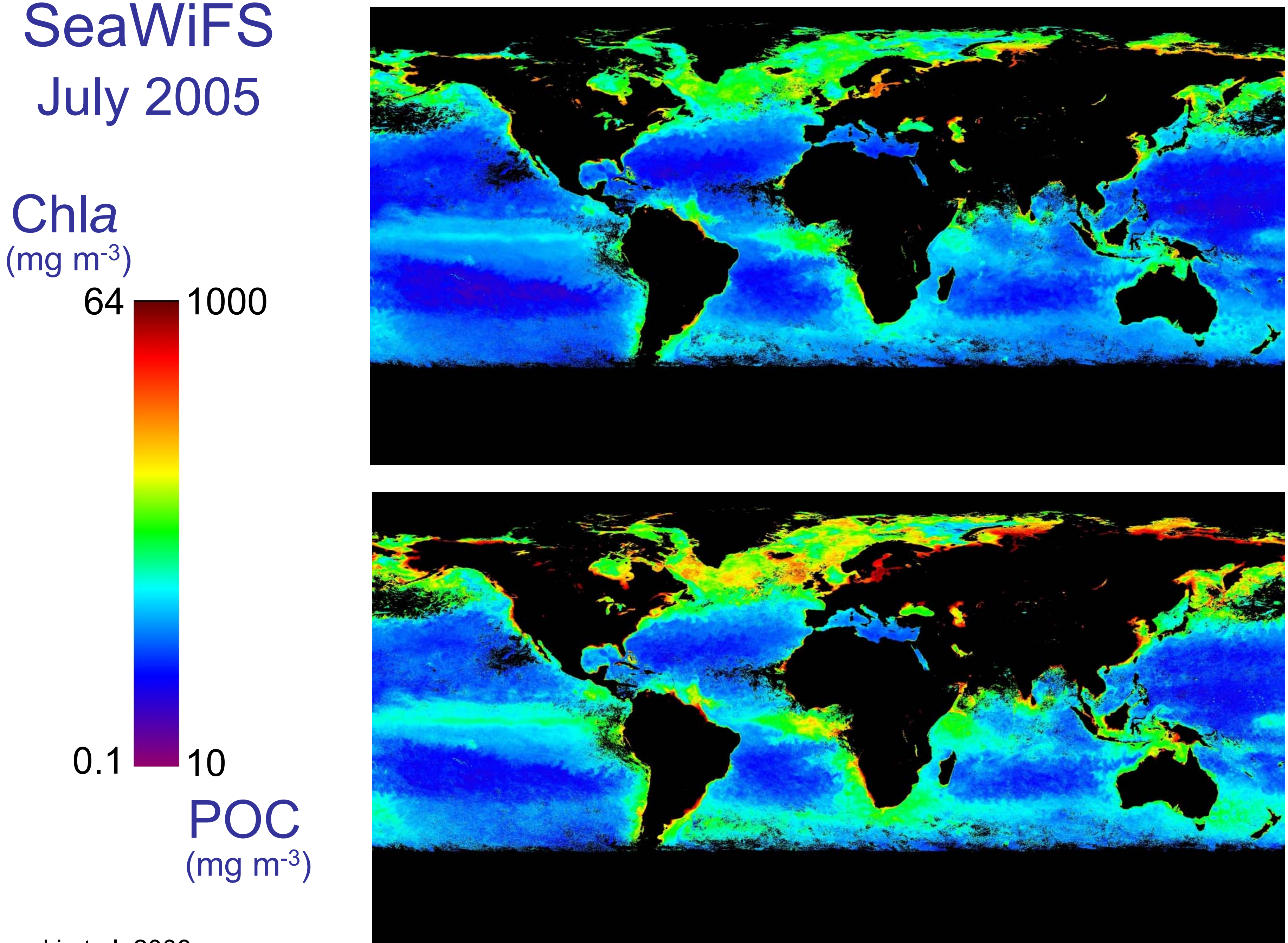

Stramski et al. 2008

Ocean color remote sensing of particulate inorganic carbon (PIC)

MODIS AQUA - 2014

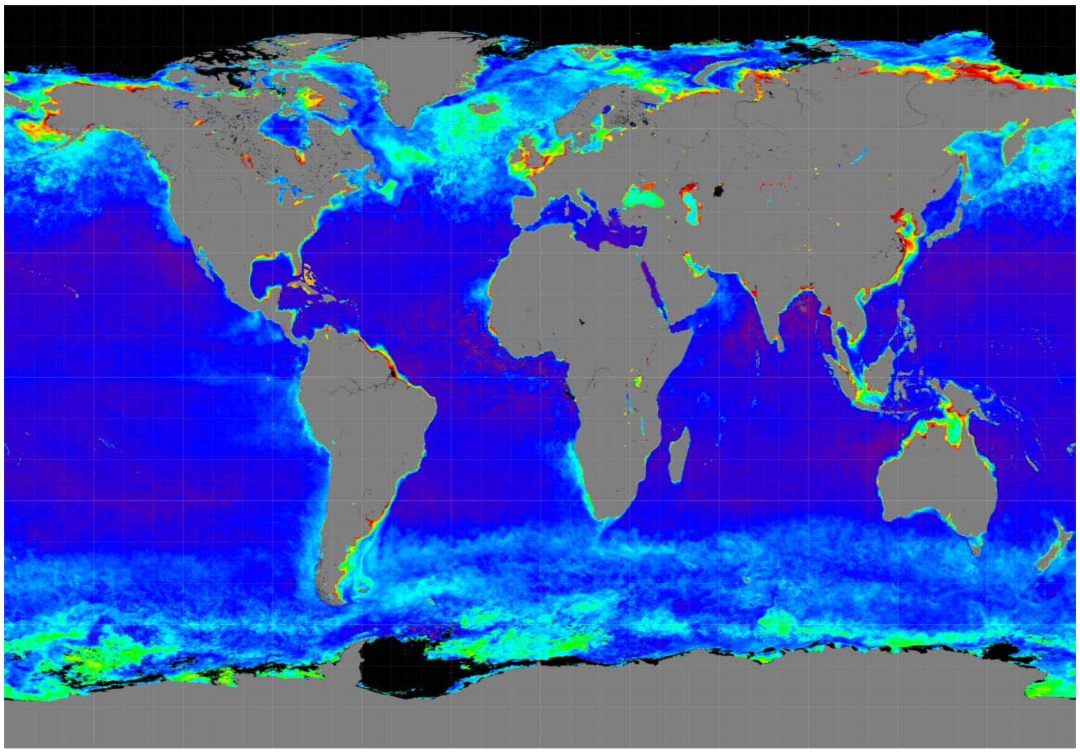

Emiliania huxleyi

Emiliania huxleyi
Ophiaster sp.

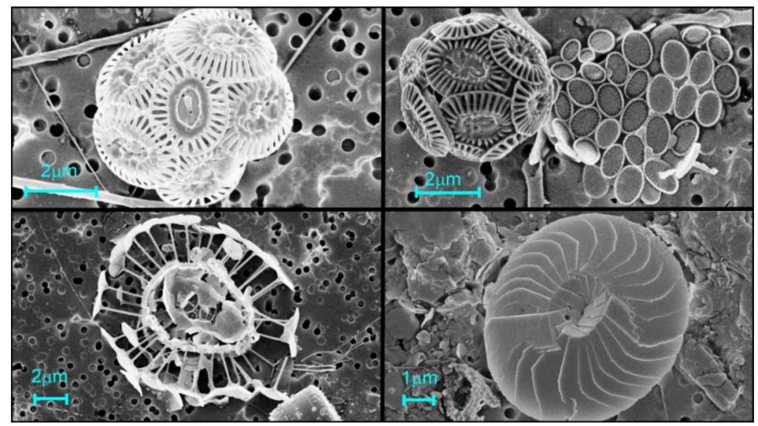

Papposphaera sp.

Calcidiscus leptoporous

Coccolithophores are strong drivers of ocean biogeochemistry and optics

Balch et al., Bigelow Laboratory

Chlorophyll-based approach: Summary

- Parameterization in terms of chlorophyll-a concentration alone
- Empirical regressions (statistically-derived models)
- Provide average trends but no information about variability
- Not valid for Case 2 waters
- Not necessarily satisfactory for Case 1 waters

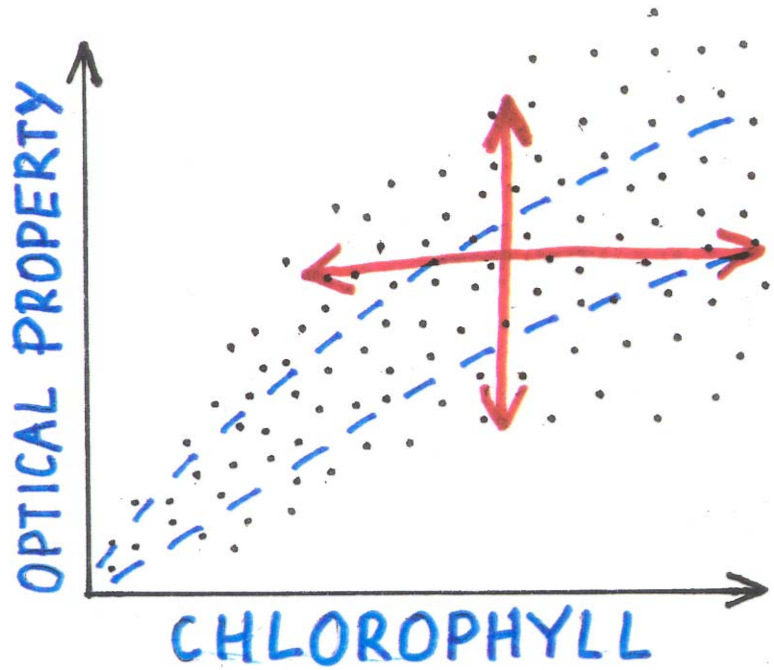

Reductionist approach

To develop an understanding and assemble a model of the whole, from the reductionist study of its parts

$$IOP_{\mathrm{p}}(\lambda) = \sum_{k} IOP_{k,\,pla}(\lambda) \quad \text{plankton}$$

$$+ \sum_{m} IOP_{m,\,min}(\lambda) \quad \text{minerals}$$

$$+ \sum_{n} IOP_{n,\,det}(\lambda) \quad \text{detritus}$$

Example IOP model with detailed description of plankton community

i	Component	Concentration [particles/m^3]	*Chl* [mg m^{-3}]
1	VIRU	$1.0 \cdot 10^{13}$	0
2	HBAC	$4.0 \cdot 10^{11}$	0
3	PROC	$7.0 \cdot 10^{10}$	0.1026
4	SYNE	$2.0 \cdot 10^{10}$	0.0403
5	SYMA	$8.0 \cdot 10^{9}$	0.0360
Σ	Picoplankton	$4.98 \cdot 10^{11}$	0.1789
6	PING	$4.5056 \cdot 10^{8}$	0.0540
7	PSEU	$0.9808 \cdot 10^{8}$	0.0303
8	LUTH	$0.9924 \cdot 10^{8}$	0.0107
9	GALB	$0.4839 \cdot 10^{8}$	0.0155
10	HUXL	$0.4339 \cdot 10^{8}$	0.0104
11	CRUE	$0.4496 \cdot 10^{8}$	0.0129
12	FRAG	$0.4768 \cdot 10^{8}$	0.0157
13	PARV	$0.6247 \cdot 10^{8}$	0.0181
14	BIOC	$0.3966 \cdot 10^{8}$	0.0900
15	TERT	$0.3570 \cdot 10^{8}$	0.0609
16	CURV	$0.2987 \cdot 10^{8}$	0.0099
Σ	Small Nanoplankton	$1.0 \cdot 10^{9}$	0.3284
17	ELON	$1.7 \cdot 10^{7}$	0.1595
18	MICA	$2.0 \cdot 10^{6}$	0.0508
Σ	Total Plankton	$1.0499019 \cdot 10^{13}$	0.7176
19	DET	$3.3 \cdot 10^{14}$	0
20	MIN	$1.1 \cdot 10^{14}$	0
Σ	Total Non-living Particles	$4.4 \cdot 10^{14}$	0
21	BUB	$7.1 \cdot 10^{6}$	0

(Stramski et al. 2001)

Size distribution

18 planktonic components
composite plankton
mineral particles
organic detritus
air bubbles

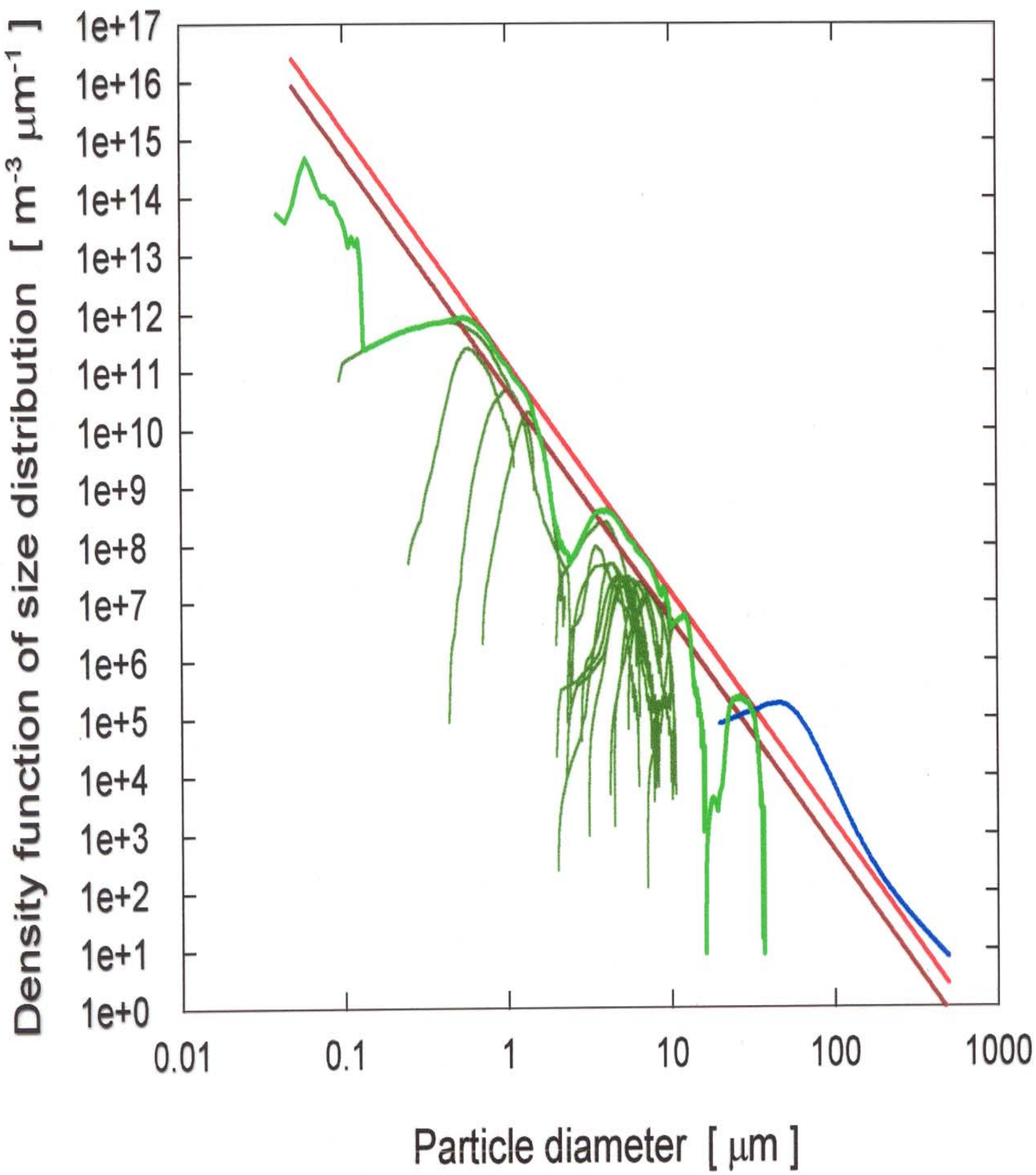

(Stramski et al. 2001)

Absorption

Scattering

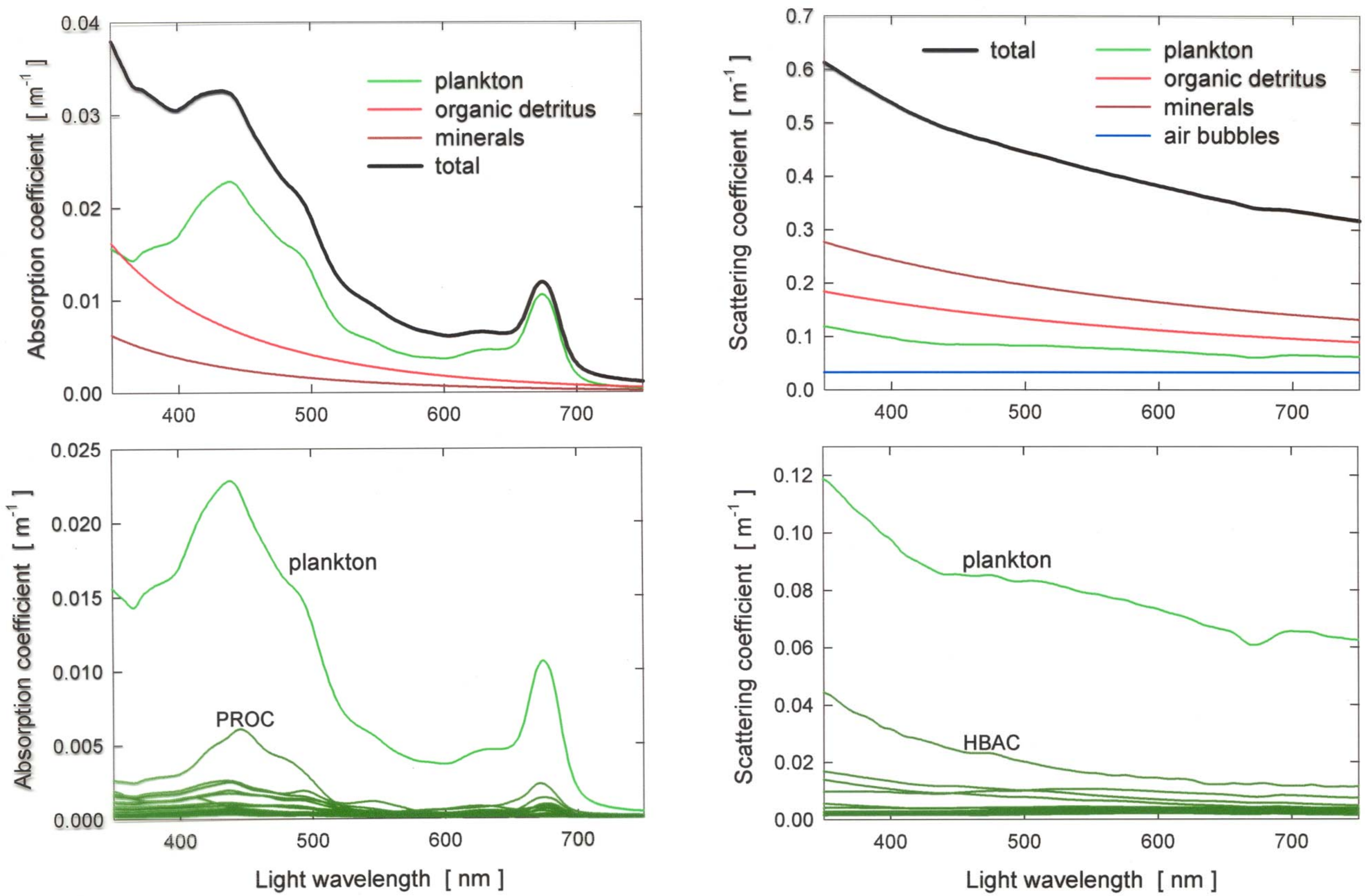

(Stramski et al. 2001)

Reductionist radiative transfer/reflectance model

Input to radiative transfer model

$$IOP(\lambda) = \sum_{i=1}^{j} IOP_i(\lambda) = \sum_{i=1}^{j} N_i \overline{\sigma_i}(\lambda)$$

Output, *e.g.* ocean reflectance

$$R(\lambda) = f\,[\sum_{i=1}^{j} N_{\mathrm{i}} \overline{\sigma}_{i,a}(\lambda), \sum_{i=1}^{j} N_{\mathrm{i}} \overline{\sigma}_{i,b}(\psi, \lambda)]$$

- In what ways does variability in detailed seawater composition determine variability in ocean reflectance?
- What information about water constituents and optical properties can we hope to extract from remotely sensed reflectance?

Example combination of reductionist IOP model and radiative transfer model for simulating ocean color

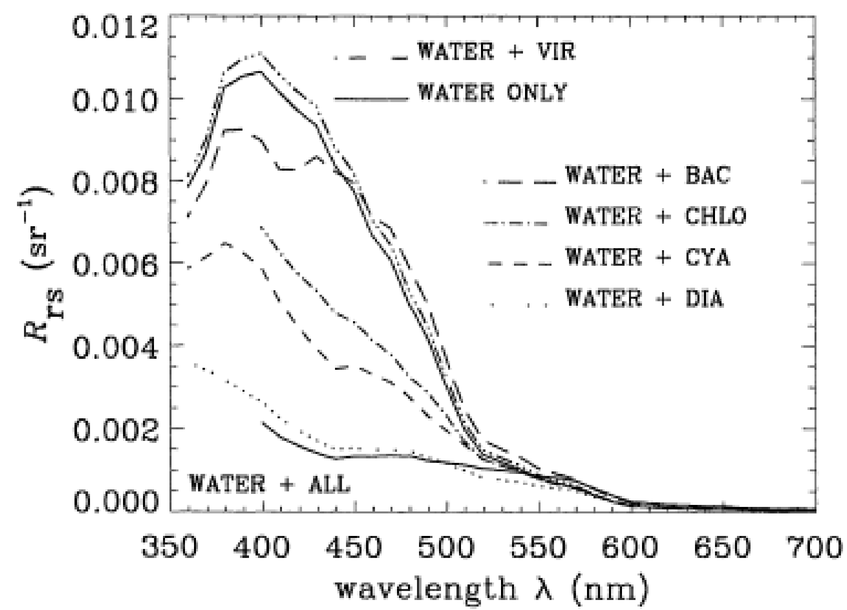

Viruses (~0.07 μm in size)
Heterotrophic bacteria (~0.5 μm)
Cyanobacteria (~1 μm)
Small diatoms (~4 μm)
Chlorophytes (~8 μm)
Detritus
CDOM

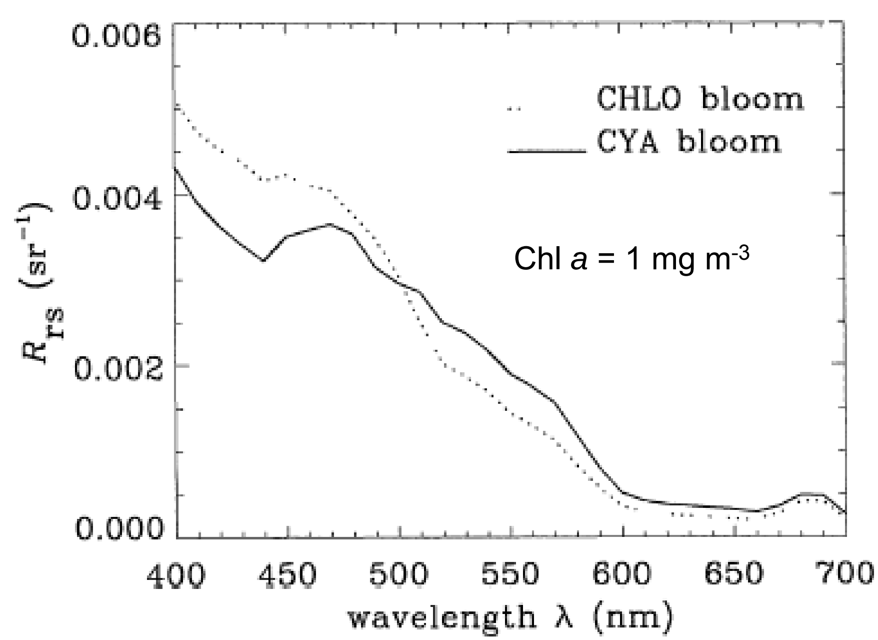

Stramski and Mobley (1997)
Mobley and Stramski (1997)

Particle Functional Types

Particle Class	Abbreviation
Small Organic Colloids	SCOL
Coarse Organic Colloids	LCOL
Small Minerals	SMIN
Heterotrophic Bacteria	HBAC
Prochlorophytes	PROC
Synechococcus	SYNE
Picoeukaryotes	PEUK
Small Nanophytoplankton	SNANO
Large Nanophytoplankton	LNANO
Microphytoplankton	MICRO
Organic Detritus	DET
Large Minerals	LMIN

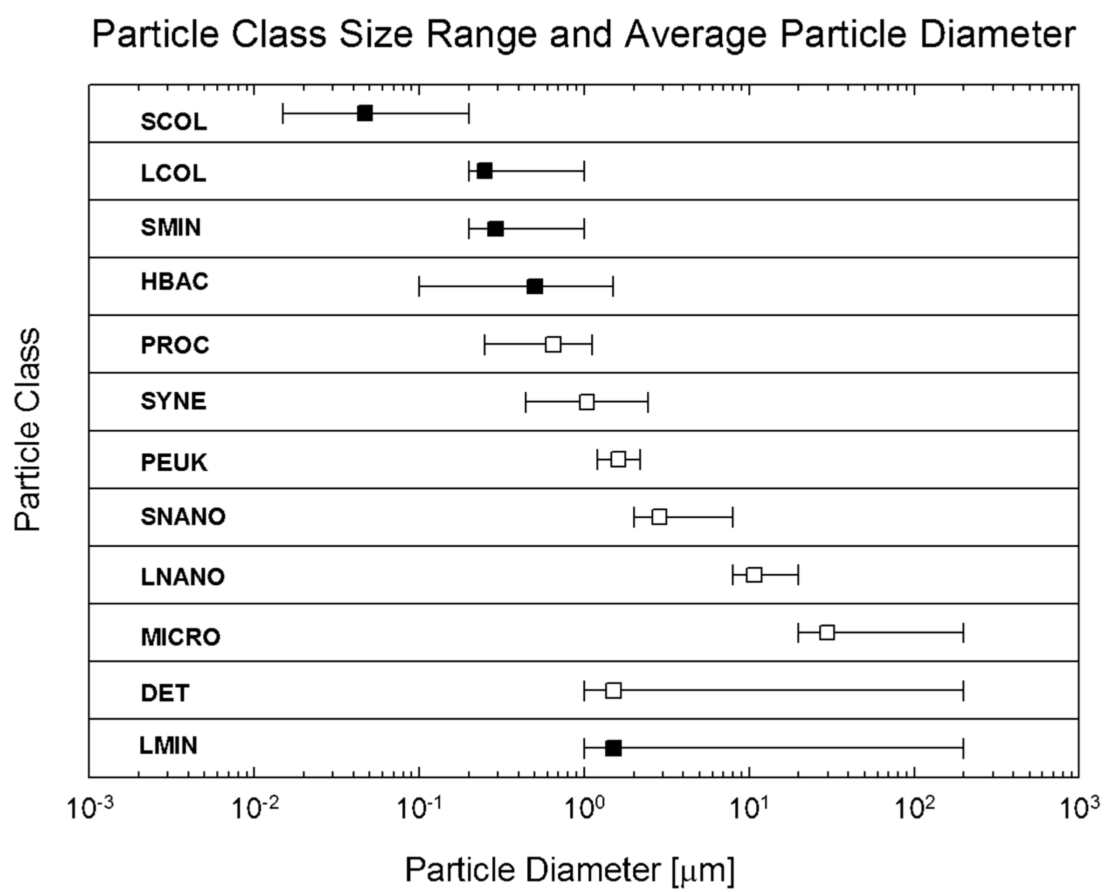

EXAMPLE MODELS

Base model

+ single class phytoplankton bloom

+ multiple class phytoplankton bloom

+ addition of organic colloids

+ addition of heterotrophic bacteria

+ addition of organic detritus

+ addition of minerals

+ phytoplankton bloom with the addition of detritus

+ phytoplankton bloom with the addition of detritus and minerals

Base model:
Chl$a$ = 0.3 mg m^{-3}
POC = 60 mg m^{-3}

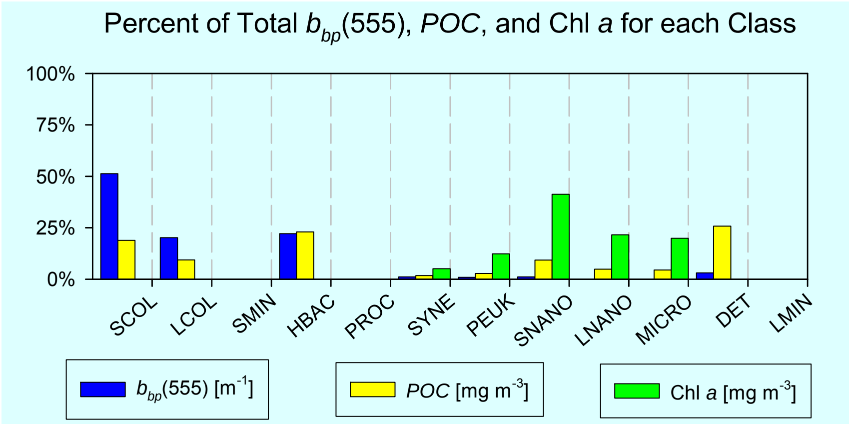

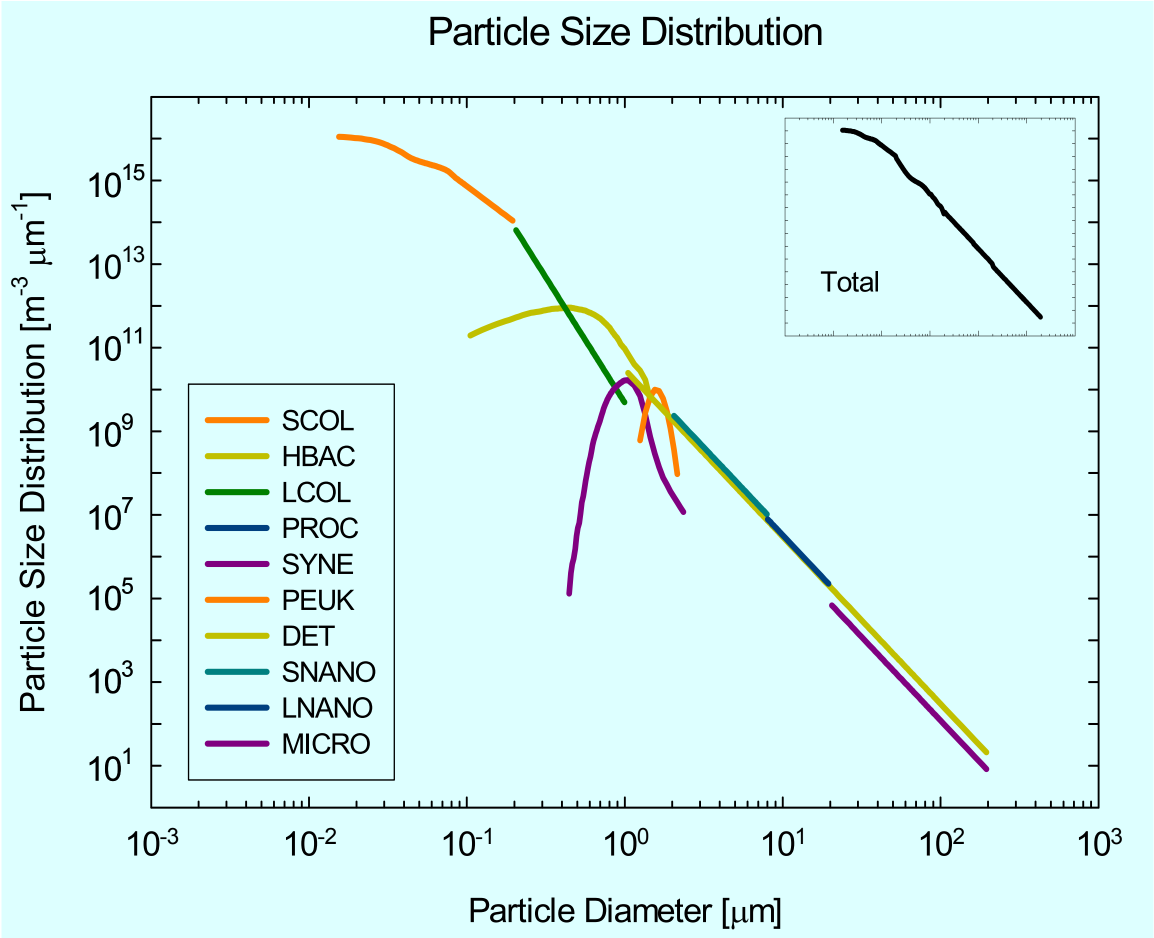

Multiple class phytoplankton bloom: Chl*a* = 1.77 mg m^{-3} POC = 125 mg m^{-3}

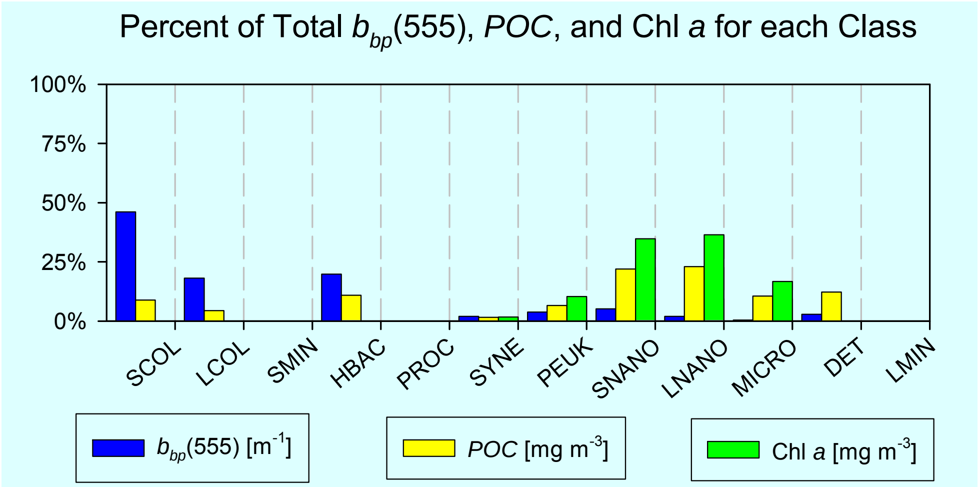

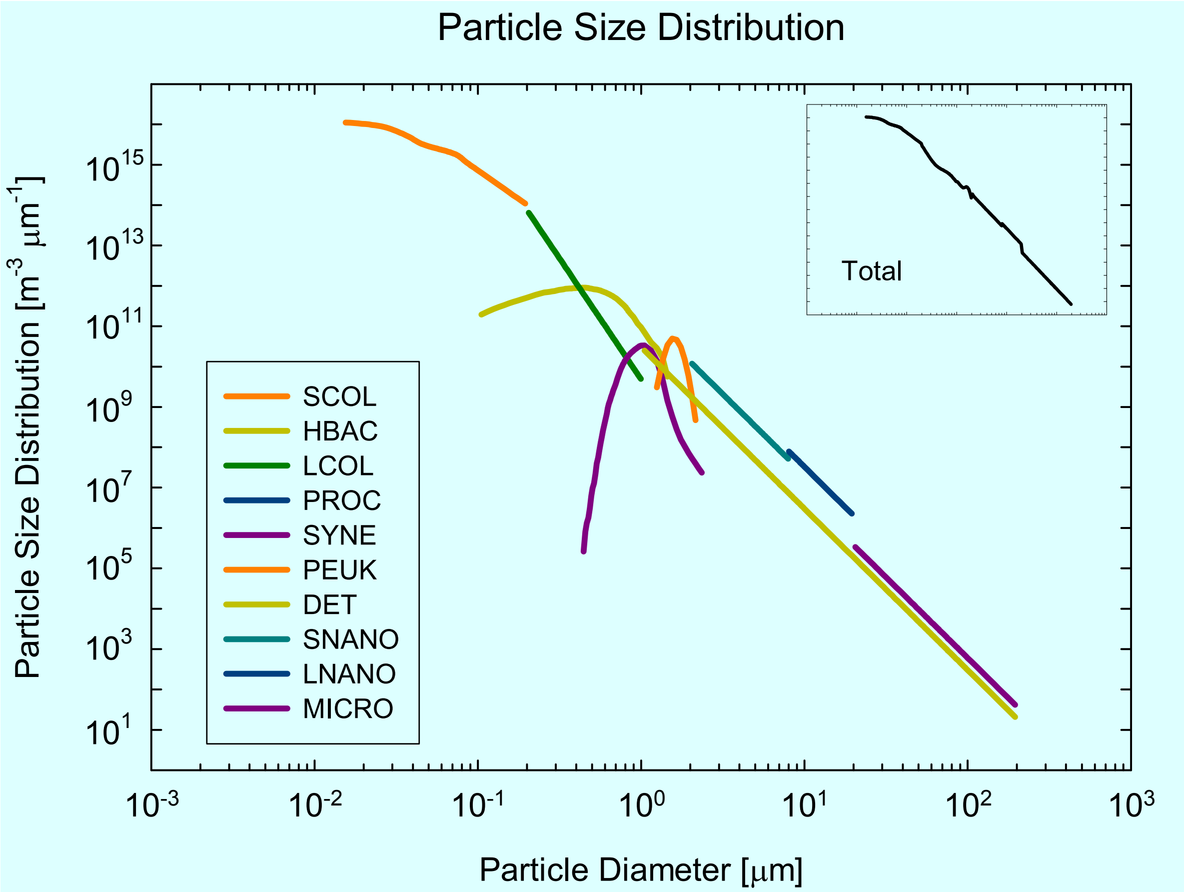

Comparison of model results to field data

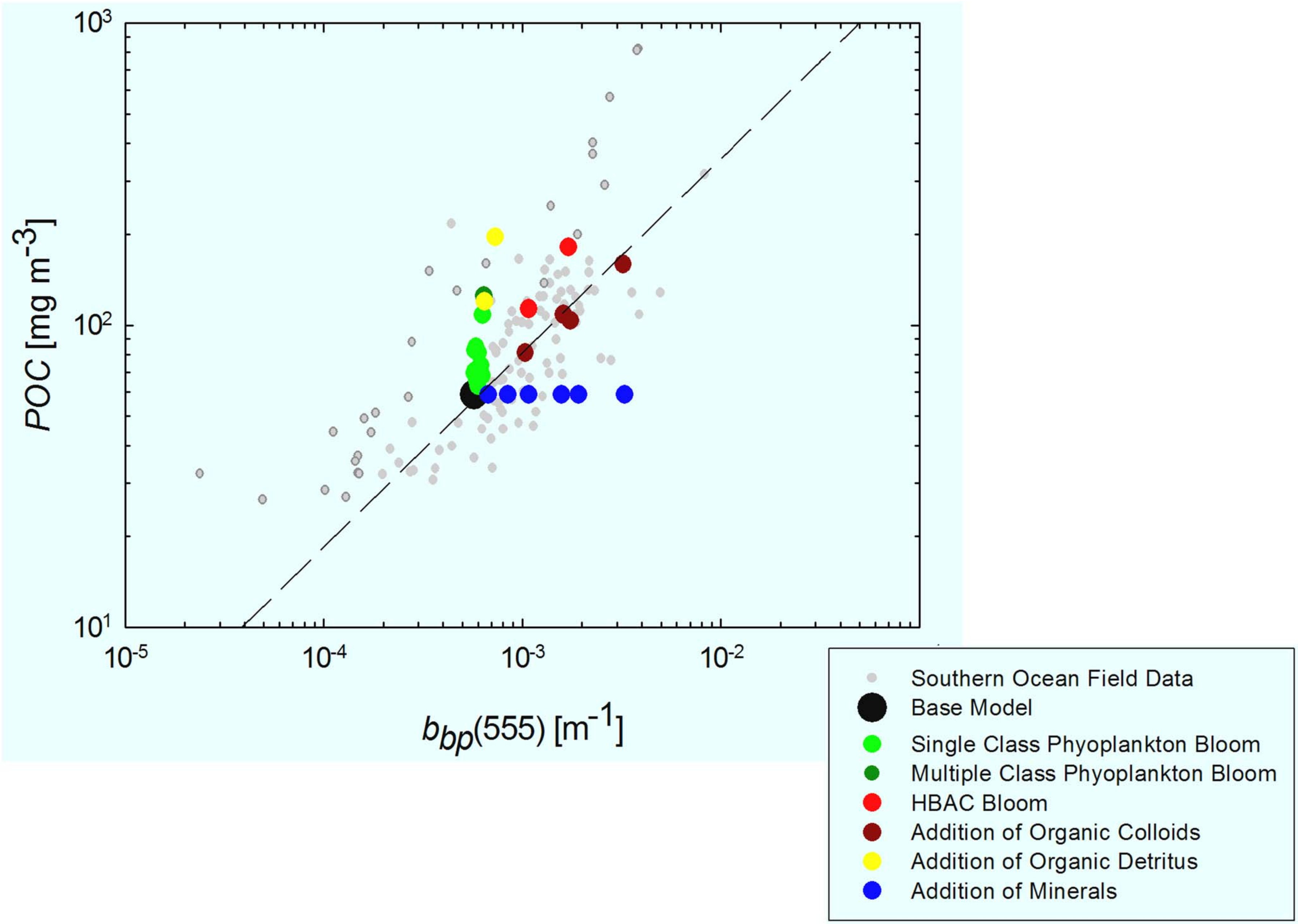

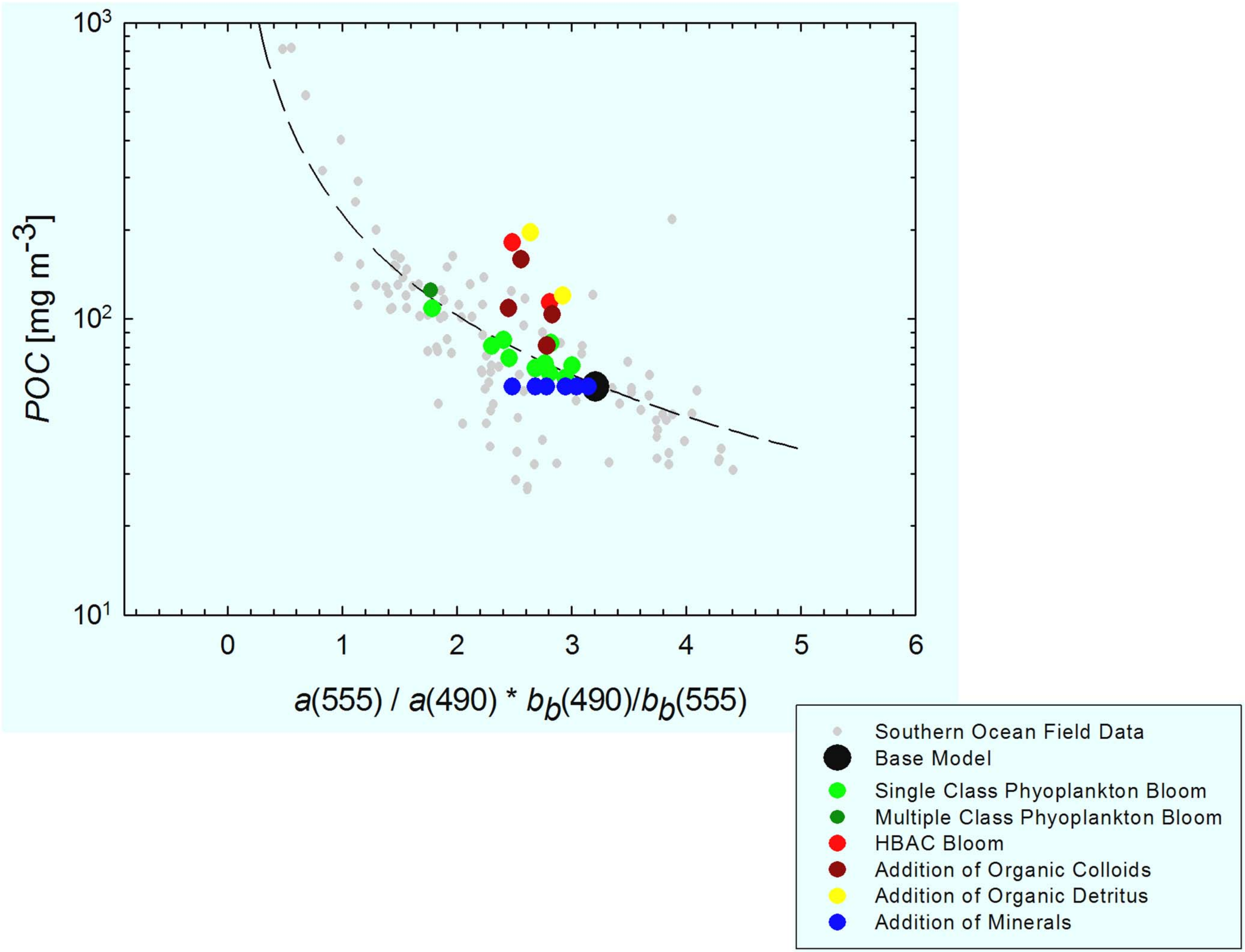

10^3
10^2
10^1
POC [mg m^-3]
0
1
2
3
4
5
6
a(555) / a(490) * b_b(490)/b_b(555)
Southern Ocean Field Data
Base Model
Single Class Phyoplankton Bloom
Multiple Class Phyoplankton Bloom
HBAC Bloom
Addition of Organic Colloids
Addition of Organic Detritus
Addition of Minerals

The complexity of seawater as an optical medium should not deter us from pursuing the proper course in future research

“The reductionist worldview has to be accepted as it is, not because we like it, but because that is the way the world works”

Steven Weinberg

1979 Nobel Prize in Physics